

Review

An Evaluation of the Biocatalyst for the Synthesis and Application of Zinc Oxide Nanoparticles for Water Remediation—A Review

Nkosingiphile E. Zikalala ^{1,2}, Shohreh Azizi ^{1,2,*}, Sithembela A. Zikalala ³ , Ilunga Kamika ³, Malik Maaza ^{1,2}, Ali Akbar Zinatizadeh ⁴ , Touhami Mokrani ⁵ and Kasinathan Kaviyarasu ^{1,2,*}

- ¹ UNESCO-UNISA Africa Chair in Nanosciences & Nanotechnology Laboratory, College of Graduate Studies, University of South Africa, Muckleneuk Ridge, P.O. Box 392, Pretoria 0002, South Africa
 - ² Nanosciences African Network (NANOAFNET)-Materials Research Department, iThemba LABS-National Research Foundation, Somerset West, P.O. Box 722, Cape Town 7129, South Africa
 - ³ Institute for Nanotechnology and Water Sustainability, College of Science, Engineering and Technology, University of South Africa, Florida, Johannesburg 1709, South Africa
 - ⁴ Environmental Research Center, Department of Applied Chemistry, Razi University, Kermanshah P.O. Box 67144-14971, Iran
 - ⁵ Department of Chemical Engineering, University of South Africa, Private Bag X6, Florida, Johannesburg 1709, South Africa
- * Correspondence: shohrehazizi1379@gmail.com or azizis@unisa.ac.za (S.A.); kaviloyolacollege@gmail.com (K.K.)



Citation: Zikalala, N.E.; Azizi, S.; Zikalala, S.A.; Kamika, I.; Maaza, M.; Zinatizadeh, A.A.; Mokrani, T.; Kaviyarasu, K. An Evaluation of the Biocatalyst for the Synthesis and Application of Zinc Oxide Nanoparticles for Water Remediation—A Review. *Catalysts* **2022**, *12*, 1442. <https://doi.org/10.3390/catal12111442>

Academic Editors: Farid Orudzhev and Irina A. Zvereva

Received: 30 September 2022

Accepted: 7 November 2022

Published: 15 November 2022

Publisher's Note: MDPI stays neutral with regard to jurisdictional claims in published maps and institutional affiliations.



Copyright: © 2022 by the authors. Licensee MDPI, Basel, Switzerland. This article is an open access article distributed under the terms and conditions of the Creative Commons Attribution (CC BY) license (<https://creativecommons.org/licenses/by/4.0/>).

Abstract: Global water scarcity is threatening the lives of humans, and it is exacerbated by the contamination of water, which occurs because of increased industrialization and soaring population density. The available conventional physical and chemical water treatment techniques are hazardous to living organisms and are not environmentally friendly, as toxic chemical elements are used during these processes. Nanotechnology has presented a possible way in which to solve these issues by using unique materials with desirable properties. Zinc oxide nanoparticles (ZnO NPs) can be used effectively and efficiently for water treatment, along with other nanotechnologies. Owing to rising concerns regarding the environmental unfriendliness and toxicity of nanomaterials, ZnO NPs have recently been synthesized through biologically available and replenishable sources using a green chemistry or green synthesis protocol. The green-synthesized ZnO NPs are less toxic, more eco-friendly, and more biocompatible than other chemically and physically synthesized materials. In this article, the biogenic synthesis and characterization techniques of ZnO NPs using plants, bacteria, fungi, algae, and biological derivatives are reviewed and discussed. The applications of the biologically prepared ZnO NPs, when used for water treatment, are outlined. Additionally, their mechanisms of action, such as the photocatalytic degradation of dyes, the production of reactive oxygen species (ROS), the generation of compounds such as hydrogen peroxide and superoxide, Zn²⁺ release to degrade microbes, as well as their adsorbent properties with regard to heavy metals and other contaminants in water bodies, are explained. Furthermore, challenges facing the green synthesis of these nanomaterials are outlined. Future research should focus on how nanomaterials should reach the commercialization stage, and suggestions as to how this ought to be achieved are presented.

Keywords: green synthesis; zinc oxide nanoparticles; antimicrobial approaches; photocatalytic activities; phytosynthesis; biosynthesis

1. Introduction

The concurrent occurrence of organic dyes and inorganic toxic pollutants, such as heavy metals (HMs), pharmaceuticals, and pathogenic microorganisms in wastewater is a

major worldwide concern [1]. Although the effects of each of the pollutants are well documented, the toxicity that arises from the co-occurrence of, and interactions between, these pollutants remains unknown; therefore, this presents a greater concern than the singular effects of each of the pollutants, with respect to the negative effect on the balance of the ecosystem, plants, and animals [2]. Synthetic dyes cause water to become unaesthetic, and they adversely compromise the health of humans and aquatic organisms by altering the biochemical oxygen demand (BOD), chemical oxygen demand (COD), salt concentration, light penetration, and rate of photosynthesis [3]. HMs are extremely poisonous due to the failure of living systems to remove them from the bodies of animals, thus leading to bioaccumulation. As such, HMs are responsible for neurological complications, carcinogenesis, mutations, and multiorgan failure in different organisms, even at low concentrations [4]. Pathogenic microorganisms comprise another class of public health concerns due to their short lifecycle, high reproductive rate per lifecycle, and ultrafast mutation rates that produce resistant strains. Around 500 waterborne microorganisms have been identified in wastewater treatment plants, including viral, bacterial, parasitic protozoan, and fungal pathogens [5]. These organisms invade a range of animal tissues, and they compromise the immune system through the release of toxins [6]; therefore, such detrimental pollutants must be efficiently eradicated from effluents before they are discharged into surface water bodies for the protection of ecological and biological systems.

Nanomaterials can address bottlenecks in conventional wastewater treatment systems because the nano-dimensions create a high surface area, quantum confinement, an attenuated surface charge, and other peculiar physical and chemical characteristics [7]. As such, various nanostructures have been synthesized for the purification of wastewater. Among the nanomaterials developed are: metallic nanoparticles such as Ag [8], Au [9], and Cu [10], and nanometal oxides such as TiO₂ [11], Fe₂O₃ [12], SnO [13], AgO [14], CuO [15], and ZnO [16].

ZnO is among one of the most used semiconductors because of its ease of synthesis and its photo-driven electronic response. ZnO is a crystalline n-type semiconductor, it is a member of the II–VI group, and it exhibits a wide bandgap (3.37 eV) in the near UV spectrum [17,18]. Moreover, it exhibits high exciton binding energy (60 meV) in standard atmospheric conditions [19]. With respect to its crystallographic structures, ZnO has three polymorphs, namely: zincblende, cubic rock salt, and the hexagonal wurtzite. Of these polymorphs, wurtzite is the most stable, hence its synthesis at room temperature (RT) under pressure. The rock salt polymorph is formed under high pressure which results in the close packing of the Zn and O atoms, as shown in Figure 1. The zincblende polymorph ZnO is metastable, and therefore, it cannot exist on its own in ambient conditions [20,21]. With respect to the morphology of ZnO, as seen under transmission electron microscopy (TEM) and scanning electron microscopy (SEM), there is a wide variety of nanoparticulate ZnO morphologies. These include nanorods [22], spheres [23], nanosheets [24], hexagons [25], tripods [26], nanowires [27], nanotubes [28], nanostars [29], nanoflowers [30], and nanocubes [31], as shown in Figure 2.

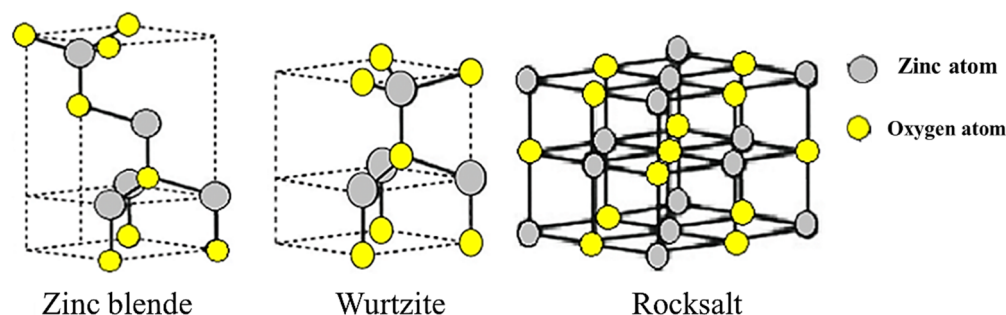


Figure 1. ZnO stable polymorphs (Reprinted with permission from Ref. [32]).

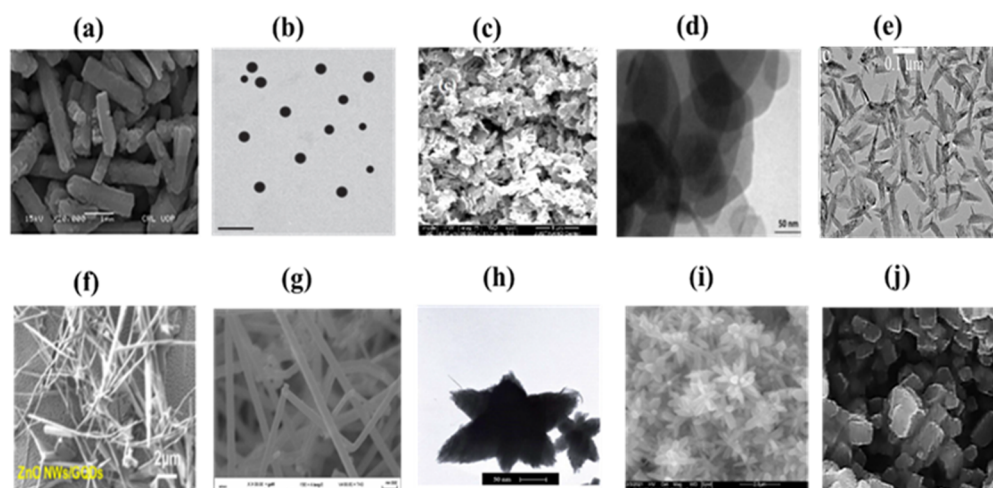


Figure 2. ZnO morphologies: (a) nanorods (Reprinted with permission from Ref. [33], © 2020, American Institute of Chemical Engineers) (b) spherical (Reprinted with permission from Ref. [34], © 2020, The Society for Applied Microbiology) (c) nanosheets [24], (d) hexagonal [35], (e) tripods (Reprinted with permission from Ref. [36], © 2015, American Chemical Society) (f) nanowires (Reprinted from Ref. [27], © 2020, American Chemical Society) (g) nanotubes, (Reprinted with permission from Ref. [28], © IOP Publishing Ltd) (h) nanostars [29], (i) nanoflowers [37], and (j) nanocubes (Reprinted with permission from Ref. [31], © 2016, Elsevier Inc).

Each morphology displays unique physical and chemical properties, and therefore, each one has a unique application or an added advantage over the other morphologies, with respect to a particular application [38]. These properties allow for the wide applicability of nanostructures in various fields, such as photocatalysis [39], antimicrobial action [40], adsorption [41], energy storage [42], gas sensors [43], cosmetics [44], cancer treatment [45], solar cells [46], agriculture [47], and wound healing [48], to name but a few. Owing to their multifunctional properties, such as better biocompatibility and the diverse applicability and solubility of ZnO in alkaline media, a wide range of physical and chemical synthesis procedures have been explored [49]. Regarding chemical synthesis, altering the precursor or the reaction parameters, such as temperature, pH, precursor concentration, type of precursor solvent, and the reaction pressure, produces a wide variety of morphologies, sizes, and geometries, with regard to the ZnO NPs. Jamkhande et al. [50] and Srujana et al. categorized chemical methods into the following groups: (i) liquid phase methods, which include sol-gel, hydrothermal, solvothermal, colloidal, and precipitation methods; and (ii) liquid-gas phase methods which include the spray pyrolysis and gas condensation methods [51]. Physical or mechanical synthesis techniques for ZnO include ball milling, physical/chemical/solid vapor deposition, laser ablation, sputter deposition, electric arc deposition, and ion implantation [52]. Some advantages of the chemical and physical methods include the high production rates, the fact that they produce controllable shapes, and they produce high purity levels [50]. Physical methods, however, suffer from non-uniformity in particle size and they have a high instrumentation cost. Moreover, chemical methods yield NPs that are agglomerated, unstable, as well as polydisperse. To counter these limitations, green synthesis routes have become the focus in current research that concerns the development of nanomaterials.

2. Green Synthesis

Over the last few decades, the “green synthesis” approach has received a lot of interest in the field of nanomaterial synthesis. Indeed, the green synthesis technique for nanomaterials is based on twelve green chemistry principles, namely: (i) to improve the reaction efficiency of atoms (atom economy); (ii) to improve the energy efficiency of reaction processes (i.e., avoidance of long synthesis times, high temperatures, and high pressure environments);

(iii) to use harmless chemicals in order to reduce the toxicity of the procedures and the synthesized nanomaterials; (iv) to reduce waste throughout the synthesis process; (v) to use easily available renewable precursors; (vi) to design non-toxic biodegradable products; (vii) to follow safer synthesis routes and replace hazardous substances with safe (or at least less toxic) reagents; (viii) to avoid the use of derivatives such as stabilizers; (ix) to avoid the release of toxic waste; (x) to employ eco-friendly solvents, such as water, instead of organic solvents; (xi) to accelerate reactions by including a catalyst, so as to reduce total energy demands in order to improve sustainability and efficiency; and (xii) to limit accidents during and after the synthesis process [53–55]. In traditional chemical synthesis, organic capping agents such as oleic acid, linolenic acid, oleylamine, hexadecylamine, and 2-mercaptoethanol need to be used to attain particles with the desired morphology and with a high degree of uniformity [56]. Biological synthesis, on the other hand, encourages the use of readily available resources, such as non-toxic solvents and auxiliaries, for a benign synthesis protocol [57]; therefore, it is in accordance with the principles of green synthesis. Biological synthesis promotes the development of nanoparticles using nature-derived materials such as plants [58], bacteria [59], fungi [60], algae [61], and biological derivatives [62]. These bio-sources (enzymes, polysaccharides, phytochemicals, biomolecules, vitamins, etc.) serve as green capping, stabilizing, or chelating agents [7]. During biosynthesis, a zinc salt such as chloride, acetate, sulfate, or nitrate is generally added to a previously prepared biological extract (from plants, bacteria, fungi, algae, yeast, etc.) to facilitate the complexation of metal ions with the available functional groups in the biological extract (Figure 3). This is achieved by heating and stirring the extract in an alkaline environment. The temperature, pH, and ratio of the precursors determine the growth phase, wherein the nucleated seeds grow either isotropically or anisotropically. Moreover, as is the case in conventional chemical synthesis processes, the synthesis parameters in green synthesis procedures determine the morphology, size, agglomeration, and size distribution of the resultant NPs [63]. After the metal oxide precipitates, it is washed, dried, and/or calcined to produce ZnO NPs, as indicated in Figure 3.



Figure 3. Schematic representation for the green synthesis of ZnO nanoparticles.

Several reviews point out the potential of biosynthesized ZnO NPs for various applications. These applications can be broadly grouped into medical, environmental remediation, and agricultural applications [7,57,64–66]. The interest in green-synthesized ZnO has increased due to its biocompatibility, photocatalytic capability, antimicrobial effectiveness, physical and chemical stability, and cost effectiveness. The current review discusses the biosynthesis of ZnO by focusing on the synthesis conditions, factors influencing the properties of the synthesized NPs, and the mechanisms of ZnO formation using various biological sources. The key characterization techniques for ZnO NPs are also discussed. Recent developments on the use of the ZnO NPs, regarding water remediation (photocatalysis, adsorption, and antimicrobial applications), are reviewed with an emphasis on the mechanisms of action. Lastly, the prospective outcomes of the green synthesis of ZnO are discussed.

2.1. Plant-Mediated/Phytosynthesis of ZnO NPs

2.1.1. Phytosynthesis Synthesis of Undoped ZnO NPs

In comparison with other ZnO green synthesis techniques, the utilization of plant extracts (*phytosynthesis*) has dominated scientific research, hence the large number of reports available for review [67–70]. Researchers prefer using parts of plants over microbes since the use of plants eliminates laborious and delicate procedures such as microbe isolation, growth, and maintenance. Furthermore, phytosynthesis is safer, as it eliminates the health risks associated with the use of hazardous microorganisms [65]. The phytosynthesis approach is preferred for large-scale production, as plant extracts can easily be obtained through the use of eco-friendly solvents such as distilled water or alcohols [71]. Additionally, plant sources are easily accessible, abundant, and hence more sustainable [72]. Since plant extracts naturally possess secondary metabolites, including amino acids, alkaloids, and flavonoids, among others, they are commonly employed as both chelating and reducing agents in the fabrication of nanoparticles [73]. Although the explicit mechanism of their formation cannot yet be explained, Bala et al. and Senthilkumar et al. concluded that phenols, flavonoids, and proteins are the main participants in the development of metallic and metal oxide NPs [74,75].

Various parts of a known plant species, including the leaves, seeds, pericarps, peels, roots, bark, or even the whole plant, have been used to synthesize ZnO NPs. Zinc salts are said to be oxidized by phenols and flavonoids into ZnO NPs with the help of the numerous functional groups that these molecules possess. These functional groups attach onto the surface of Zn^{2+} , and they oxidize the molecule into ZnO NPs [63,75]. Since the coordination chemistry of proteins is specific to that of zinc ions, they are the predominant chelating agents for Zn^{2+} . The H_2O molecules of the aqua complexes are exchanged when they bind to the protein ligands [76]. During their interaction with the acidic $[Zn(H_2O)_6]^{2+}$, an electron from the $-COO-$ initiates a nucleophilic reaction, which results in the formation of the $[Zn(OH)(H_2O)_5]^+$ complex [77]. The $[Zn(OH)(H_2O)_5]^+$ is then transmuted into ZnO NPs [78]. According to Singh et al., the $-OH$ and/or $-COO-$ of the flavonoids react with the ZnO precursor to generate a distinctive Zn flavonoid complex via the electrostatic interaction between negatively charged flavonoids and positively ZnO nuclei. This complex is then later converted to ZnO through thermal treatment [79]. An alkaline pH favors the formation of metal oxide nanoparticles that are stabilized by the phytochemicals in the plant extract [80]; thus, it follows that during the phytosynthesis of metal oxides such as ZnO, a combination of polyphenols, flavonoids, and proteins results in the creation of ZnO NPs [81]. Krol et al. [77] presented a probable reaction mechanism for a plant mediated ZnO, as shown in Figure 4.

Table 1 provides an overview of the plant-based synthesis of ZnO NPs. The use of the waste pericarp of *Ananas comosus* yielded spherical NPs, the sizes of which varied between 10 and 60 nm after sonicating for 1 h at 40 °C [82]. The seed extract of *Eriobotria japonica* produced hexagonal NPs when a mixture of the seed extract and $Zn(CH_3COO)_2 \cdot 2H_2O$ was heated at 60 °C for 1 h. Using Fourier-transform infrared spectroscopy (FTIR), the reducing and capping agents were revealed to be phenolic groups, alcohols, and aliphatic amines. Recently, fruit-derived aqueous extracts have been employed to prepare ZnO NPs [22,83–85]. Golmohammadi et al. [85] obtained spherical NPs with an average size of 29 nm when they refluxed *Zizyphus jujuba* fruit and $Zn(NO_3)_2 \cdot 6H_2O$ with water at 80 °C for 30 min prior to calcination. Recently, Faisal et al. [86] produced semi spherical NPs when synthesizing with the fruit extract of *Myristica fragrans*.

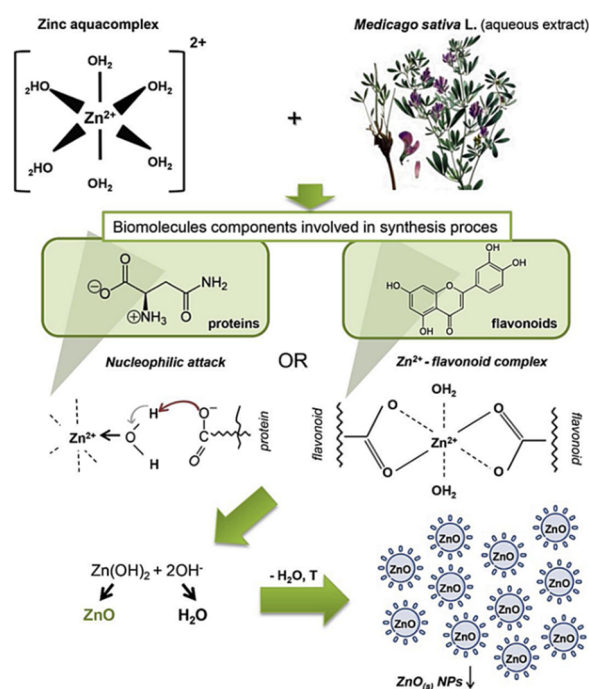


Figure 4. A proposed mechanism of ZnO formation via the phytosynthesis route. (Reprinted with permission from Ref. [77], © 2019, Elsevier Ltd.).

Biosynthesizing ZnO NPs using flower extracts have also been reported [87,88]. The extract of *Hibiscus sabdariffa* served as a reducing and stabilizing agent in order to produce wurtzite-phased NPs. The concentration of the employed extract determined the surface structure and size of the NP. The sizes ranged between 8.71 and 88.63 nm [83]. Khara et al. produced spherical and irregular ZnO NPs using *Peltophorum pterocarpum*, with a mean diameter of 69.45 nm [88]. This flower extract possesses phenolic compounds and flavonoids, among other properties, that potentially reduce and stabilize ZnO NPs. Moreover, Diallo and colleagues obtained very small (1–8.5 nm) quasi-spherical ZnO nanomaterials by applying the flower extract of *Aspalathus linearis* as a reducing/oxidizing chemical agent [89].

Regarding phytosynthesis, leaves are the most frequently used parts of a plant during extraction. This is likely due to their accessibility, abundance, and ease of grinding. Several authors have reported on the phytosynthesis of various nanomaterials through the use of leaf extracts from various species of plants [90–92]. Mostly, the attained NPs were spherical and irregularly shaped. Ekennia and colleagues, however, attained flower-shaped NPs (31 nm) when using an extract of *Euphorbia sanguinea* and ZnCl₂ as the salt precursor [93]. The appearance of the 1638 cm⁻¹ absorption band in the FTIR spectra was ascribed to the N–H bending of amines in alkaloids or C=O stretching in polyphenols, flavonoids, and reducing sugars, which were thought to be responsible for reducing and stabilizing the synthesized NPs. An extract of quince seed mucilage was kept for 4 h in the presence of Zn(NO₃)₂·6H₂O, before it was concurrently heated and stirred at 80 °C for 2 h to produce 25 nm spherical ZnO NPs [94]. Prior to this study, Prasad and colleagues [95] mixed *Abelmoschus esculentus* mucilage extract with Zn(OOCCH₃)₂·2(H₂O) salt and quince seed mucilage in water, and the mixture was stirred for 4 h, at RT, to obtain spherical ZnO NPs with an average diameter of 29 nm and 70 nm long nanorods. The reducing and capping agents for the NPs were carbohydrates, which are available in excess in plants. The heterogeneous sizes and shapes were ascribed to the method employed and the high calcination temperature (700 °C for 2 h); this poses a challenge with regard to controlling the morphology of the prepared particles.

There have also been reports on the utilization of the aqueous extracts in roots, regarding the biogenic preparation of ZnO NPs with various morphologies [96]. A methanolic extract was employed by Verma et al. [68] to obtain hexagonal and rod-shaped NPs after stirring $\text{Zn}(\text{CH}_3\text{COO})_2 \cdot 2\text{H}_2\text{O}$ in the presence of *Salvadora persica* root extract for 3 h at 80 °C; it was then heated at 400 °C for an appropriate length of time. Matinise et al. prepared ZnO NPs by capping the NPs with an aqueous solution of *Moringa oleifera* leaf. The extract completely dissolved the zinc salts at an ambient temperature; this was evidenced by the fact that the solution changed color, from clear to brown, after 18 h without any precipitation. Spherically shaped ZnO NPs were formed after drying the concentrated solution at 100 °C for 1 h [97]. Highly crystalline single phase zincite ZnO NPs were produced by adding an aqueous solution of *Agathosma betulina*, in order to reduce the presence of zinc nitrate hexahydrate salt; in this scenario, the temperature was set at 100 °C for 2 h. The resultant precipitate was further annealed at 500 °C for 2 h to obtain (15.8 nm) quasi-spherical NPs [98]. When Ngom et al. prepared the same nanoparticles by employing *Moringa oleifera* leaves as the chelating agent, wurtzite phased ZnO nanomaterials, with an average diameter of 10.81 nm, were produced [99].

Table 1. Plant-based synthesis of ZnO nanoparticles.

Serial No.	Plant Name	Plant Part	Extraction Solvent Temp (°C) Time	Zinc Precursor	Biosynthesis Time (h)/Temp (°C)	Calcination Temp (°C)/Time (h)	Shape	Size (nm)	Ref
1	<i>Pithecellobium dulce</i>	Peel	Water, 70 °C for 50 min	$\text{Zn}(\text{CH}_3\text{CO}_2)_2$		400/2	Spherical	30	[83]
2	<i>Ananas comosus</i>	Pericarp	Water, 80 °C for 20 min	$\text{Zn}(\text{CH}_3\text{COO})_2 \cdot 2\text{H}_2\text{O}$	Sonicated 1/40	–	Spherical	10–60	[82]
3	<i>Punica granatum</i>	Fruit peel	Water, 65 °C for 1 h	$\text{Zn}(\text{NO}_3)_2 \cdot 6\text{H}_2\text{O}$	–/90	600/1	Spherical and hexagonal	38.98	[84]
4	<i>Zizyphus jujuba</i>	Fruit	Refluxed with water, 80 °C for 30 min	$\text{Zn}(\text{NO}_3)_2 \cdot 6\text{H}_2\text{O}$	4/80	550/3	Spherical	29	[85]
5	<i>Myristica fragrans</i>	Fruit	Water, 150 °C for 20 min	$\text{Zn}(\text{NO}_3)_2 \cdot 2\text{H}_2\text{O}$	2/60	500/2	Semispherical	41.23	[86]
6	<i>Hibiscus sabdariffa</i>	Flower	Water, 60 °C, for 1 h after 2 h stirring at RT	$\text{Zn}(\text{NO}_3)_2$	1/RT.	400/1	Semi spherical	8.7–88.6	[87]
7	<i>Peltophorum pterocarpum</i>	Flower	Water, 80 °C for 1 h	$\text{Zn}(\text{NO}_3)_2$	–/80	400/2	Spherical and irregular	69.45	[88]
8	<i>Aspalathus linearis</i>	Flower	Water, 25 °C for 48 h	$\text{Zn}(\text{NO}_3)_2 \cdot 6\text{H}_2\text{O}$	–/–	300/2	Quasi-spherical	1–8.5	[89]
9	<i>Eucalyptus</i> spp.	Leaves	Water, 90 °C for 90 min	$\text{Zn}(\text{NO}_3)_2 \cdot 6\text{H}_2\text{O}$	2/110	250/6	Irregular shapes	32.71	[90]
10	<i>Capparis zeylanica</i>	Leaves	Water, 60 °C for 20 min	$\text{Zn}(\text{OOCCH}_3)_2 \cdot 2(\text{H}_2\text{O})$	2/80	400/2	Spherical	20–40	[91]
11	<i>Ocimum tenuiflorum</i>	Leaves	Powder	ZnSO_4	0.5/RT	600/0.5	Spherical and granular	50–63	[92]
12	<i>Euphorbia sanguinea</i>	Leaves	Water, 80 °C for 45 min	ZnCl_2	2/90	–	Flower-like	34	[93]
13	<i>Moringa oleifera</i>	Leaves	Water, 50 °C for 105 min	$\text{Zn}(\text{NO}_3)_2 \cdot 6\text{H}_2\text{O}$	18/RT then 100	500/1	Spherical	16–31.9	[97]
	<i>Gathosma betulina</i>	Leaves	Water, 100 °C for 60 min	$\text{Zn}(\text{NO}_3)_2 \cdot 6\text{H}_2\text{O}$	2/100	500/2	Quasi-spherical	15.8	[98]
14	Quince seeds	Mucilage	Water, 60 °C for 4 h	$\text{Zn}(\text{NO}_3)_2 \cdot 6\text{H}_2\text{O}$	2/80 after keeping for 4 h at RT	600/2	Spherical	25	[94]
15	<i>Abelmoschus esculentus</i>	Mucilage	Soaked for 24 h at RT	$\text{Zn}(\text{OOCCH}_3)_2 \cdot 2(\text{H}_2\text{O})$	4/RT	700/2	Spherical Rods	29 70	[95]

Table 1. Cont.

Serial No.	Plant Name	Plant Part	Extraction Solvent Temp (°C) Time	Zinc Precursor	Biosynthesis Time (h)/Temp (°C)	Calcination Temp (°C)/Time (h)	Shape	Size (nm)	Ref
16	<i>Panax</i> spp.	Roots and stems	Water, 85 °C for 8 h	Zn(NO ₃) ₂	2.5/85	500/2	Leafy flower	480	[96]
17	<i>Salvadora persica</i>	Roots	Water and methanol, 80 °C for 3 h	Zn(CH ₃ COO) ₂ ·2H ₂ O	2–3/80	400/2	Hexagonal and rods	24–25	[68]
18	<i>Rubus fairholmi-anus</i>	Roots	Acetone using Soxhlet apparatus	Zn(NO ₃) ₂	48/80	–	Spherical	1–100 clusters	[100]

2.1.2. Phytosynthesis of Doped ZnO Nanoparticles

Recently, the number of biogenically doped ZnO NPs has been increasing, which speaks to the efficiency of plant metabolites in nanomaterial synthesis. Doping occurs as a result of the wide band gap of ZnO, which causes ZnO to only absorb light that falls within the UV spectrum. Doping is a process wherein a point defect in a nanomaterial is formed by inserting a specific ion into the crystal lattice of a nanomaterial to modify its electronic band structure. The band structure is modified by the formation of shallow or deep energy level, known as mid-gap states, that extend the absorption range from shorter to longer wavelengths; this can even extend to the visible range of the electromagnetic spectrum [101,102]. The physicochemical properties of doped ZnO significantly depend on the dopant type and its concentration. p-type dopants tend to withdraw electrons from the ZnO, whereas n-type dopants increase the number of electrons. As the dopant concentration increases, the energy band gap E_g of ZnO decreases until an optimal dopant concentration is reached, beyond which, the dopant ions act as charge recombination centers and reduce the efficiency of ZnO in photocatalytic processes. The dopants also become active sites that are different from the ZnO active sites, thereby increasing the mass transfer of pollutants from the solution to the ZnO surface. This phenomenon is not only useful for increasing the adsorption efficiency in cases where ZnO is used as an adsorbent, but it also helps to increase the level of light that penetrates the polluted water, thereby increasing the photocatalytic efficiency; this will be discussed further in Section 4.1 [103]. As well as induced defects, ZnO exhibits intrinsic defects, which include zinc vacancy (V_{Zn}), oxygen vacancy (V_O), zinc interstitial (Zn_i), oxygen interstitial (O_i), or antisite oxygen (O_{Zn}) defects [104]. As with dopants, it is generally accepted that surface defects (i.e., surface V_O , V_{Zn} , O_i , and Zn_i , especially the anionic V_O) are beneficial to photocatalytic activity because they can serve as active sites for photocatalysis. These defects create mid-gap states that alter the electronic band structure of photocatalysts to facilitate charge separation with longer lifetimes [101]. Conversely, deep level defects (V_O and V_{Zn}), and other nonradiative defects, have negative impacts on photocatalysis because they create recombination centers for photogenerated charges; this causes electronic delocalization and low photocatalytic efficiency. These defects are repaired via annealing at appropriate temperatures [105].

The most used doping agents in the biogenetic synthesis of ZnO include Ag, Cu, Mg, Ce, Fe, and Co, though Ag doping is the most common [33,58,106]. Saeed et al. synthesized AgNO₃-ZnO NPs at an ambient temperature using different plant species and parts. Owing to its strong reduction potential, the extract of *Calotropis gigantea* resulted in the formation of rod-shaped NPs [33]. *Moringa olifera* seed extract yielded flower-like NPs [58], whereas *Ocimum tenuiflorum* seed extract produced hexagonal and spherical NPs ranging between 50 and 60 nm in diameter [106]. Mn-ZnO NPs were prepared by mixing a salt precursor with *Melastoma malabathricum*. The mixture was heated at 60 °C until a paste formed, and it was further heated at 400 °C to obtain spherical NPs with an average diameter of 222 nm [107]. Fe-ZnO NPs were produced by Jan et al. This was achieved by reducing

zinc ions with the flavonoids, phenolics, terpenoids, triterpenes, tannins, and fatty acids present in the leaf extract of *Myrtus communis* [108]. The NPs were produced after 3 h of stirring and heating at 60 °C, after which they were calcinated at 400 °C for 3 h. Their diameters were small, at 17 nm on average, with a pseudo-spherical shape. Okeke et al. prepared Mg-ZnO NPs by reacting $Zn(NO_3)_2$ and $Mg(NO_3)_2$ with *Piper guineense* leaf extract, which was then stirred and heated for 15 min at 80 °C before calcining the paste at 350 °C for 2 h [109]. A dual doping of ZnO NPs with Cu and Mg was successfully completed by Rahman et al. [110], who utilized a *Ziziphus mauritiana* solution to reduce $Zn(NO_3)_2 \cdot 6H_2O$, as depicted in Figure 5. The synthesized NPs were nearly spherical, but relatively large in size (0.1–1 μm), depending on the Cu/Mg dopant concentration. The FTIR suggests that the reduction of ions was controlled by tannins, flavonoids, saponins, and phenols. An eco-friendly fabrication of Nb-ZnO using *Vernonia amygdalina* leaf extract was reported by Nguyen et al., and the obtained Nb-ZnO NPs showed an improved photocatalytic degradation of tetracycline under natural light in comparison with pristine ZnO. The composite reached a 93.2% degradation efficiency after 3 h [111]. A summary of the synthetic procedures and the results of the doped-ZnO NPs are given in Table 2.

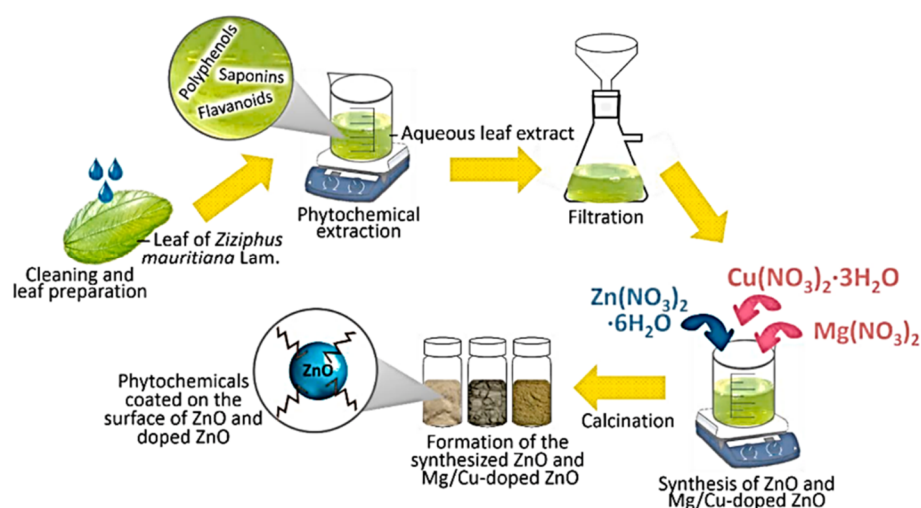


Figure 5. Schematic diagram of the synthesis of Mg/Cu dual-doped ZnO. (Reprinted with permission from Ref. [109], © 2021, Elsevier Ltd.).

Table 2. Phytosynthesis of the doped ZnO nanoparticles.

Serial No.	Plant Name	Dopant	Extraction Solvent, Temp and Time	Precursors	Biosynthesis Time (h) and Temp (°C)	Calcination Temp (°C)/Time (h)	Shape	Size (nm)	Ref
1	<i>Calotropis gigantea</i> (leaves)	Ag	Refluxing	$Zn(NO_3)_2 \cdot 6H_2O$ $AgNO_3$	3/RT	400/3	Rods	None	[33]
2	<i>Moringa oleifera</i> (seeds)	Ag	Aqueous powder, RT	$Zn(OOCCH_3)_2$ $AgNO_3$	50 min/RT	-	Flower-like	54.1	[58]
3	<i>Ocimum tenuiflorum</i> (seeds)	Ag	Water, boiled	$Zn(NO_3)_2 \cdot 6H_2O$ $AgNO_3$	2/RT	450/3	Hexagonal and spherical	50–60	[106]
4	<i>Melastoma malabathricum</i> (leaves)	Mn	Water, 60 °C	$Zn(NO_3)_2 \cdot 6H_2O$ $Mn(CH_3CO_2)_2 \cdot 4H_2O$	-/60	400/2	Spherical	222	[107]
5	<i>Myrtus communis</i> L.	Fe	Water, 40 °C for 1 h	$Zn(NO_3)_2 \cdot 6H_2O$ $Fe(NO_3)_3 \cdot 9H_2O$	3/60	400/3	Pseudo spherical	17	[108]
6	<i>Piper guineense</i> (leaves)	Mg	Water, 60 °C for 20 min	$Zn(NO_3)_2$ $Mg(NO_3)_2$	0.25/80	350/2	Spherical	364	[109]

Table 2. Cont.

Serial No.	Plant Name	Dopant	Extraction Solvent, Temp and Time	Precursors	Biosynthesis Time (h) and Temp (°C)	Calcination Temp (°C)/Time (h)	Shape	Size (nm)	Ref
7	<i>Ziziphus mauritiana</i> Lam. (leaves)	Mg and Cu	Water, RT for 1 h	Zn(NO ₃) ₂ ·6H ₂ O Cu(NO ₃) ₂ ·3H ₂ O Mg(NO ₃) ₂	–/60	400/2	Hexagonal disc shaped	100–1000	[110]
8	<i>Vernonia amygdalina</i>	Nb	Not available	Not mentioned	1/60	400/1	Spherical	1000	[111]

2.2. Microbial Synthesis of ZnO Nanoparticles

Microorganisms, or microbes comprising bacteria, fungus, and algae, have also been exploited for the biological synthesis of metal oxide NPs. Although many metal oxides have been synthesized biologically using microorganisms, the microbial production of ZnO has not been thoroughly investigated. An advantage of the microbial synthesis of NPs over phytosynthesis is the ease with which microorganisms can be reproduced, as they are easily grown in a laboratory. During microbial synthesis, metal reduction is made possible with the available enzymes, carbohydrates, proteins, and other metabolites that are intrinsically present in the microorganisms. The biomolecules that are secreted in the growth medium influence the shape, size, and dispersity of the produced NPs [112]. Under stressful conditions, or in the presence of heavy metals, microbes reduce these ions to metals in order to enable their own survival; thus, they act as natural nano-factories [113].

2.2.1. Bacterial Synthesis

Prokaryotic microorganisms, such as bacteria and algae, have been extensively studied because they are easy to handle and genetically modify [114]. Bacteria offer the advantage of being able to quickly multiply, thus creating a readily available source of secondary metabolites that are involved in the fabrication of ZnO. The most used microbes in the synthesis of NPs comprise *Actinobacter* sp., *Corynebacterium* sp., *Klebsiella pneumonia*, *Lactobacillus* sp., and *Pseudomonas* sp. [115]. The biological preparation of metal, and metal oxide nanomaterials, using bacterial cultures may occur in the intra- or extracellular environment [116]. The mechanism of formation during intracellular synthesis is challenging due to the intricacy of the bacterial cell make-up and its metabolic processes. The mechanism for the intracellular generation of ZnO in microbes is illustrated in Figure 6a. The cell walls of microbes have different types of polysaccharides and proteins that provide active sites for the binding of metal oxides through electrostatic interactions [117]. Then, reductases (NADH and NADPH) that are either present in the cell wall or secreted as soluble enzymes [118] reduce the trapped ions into elemental atoms [119]. Finally, the nuclei develop and assemble in the cytoplasm or cell wall, while the peptides and amino acids stabilize the NPs [120]. Bacteria-mediated nanoparticle synthesis creates less hazardous metal oxide nanoparticles, such as TiO₂, CuO, and ZnO; however, the downside to this is that it involves isolating, screening, and culturing potential microbes, which are time consuming processes. In addition, the process may involve the use of expensive chemicals, such as growth media [119]. The size distribution, shape, and crystallinity of microbe-synthesized NPs are not easy to monitor [121]. Moreover, the intracellularly formed nanomaterials can only be released by lysing the bacterial cells; thus, time consuming and laborious steps are unavoidable [122]. As a result, research on bacterial synthesis has, to date, focused on extracellular synthesis. Regarding extracellular synthesis, the enzymes that are released by microorganisms into the growth culture are responsible for the bio-reduction of metal ions into NPs. The bio-reduction of zinc ions occurs when an electron is transferred from NADH with NADH reductase [123]. The extracellular synthesis pathways are depicted diagrammatically in Figure 6b.

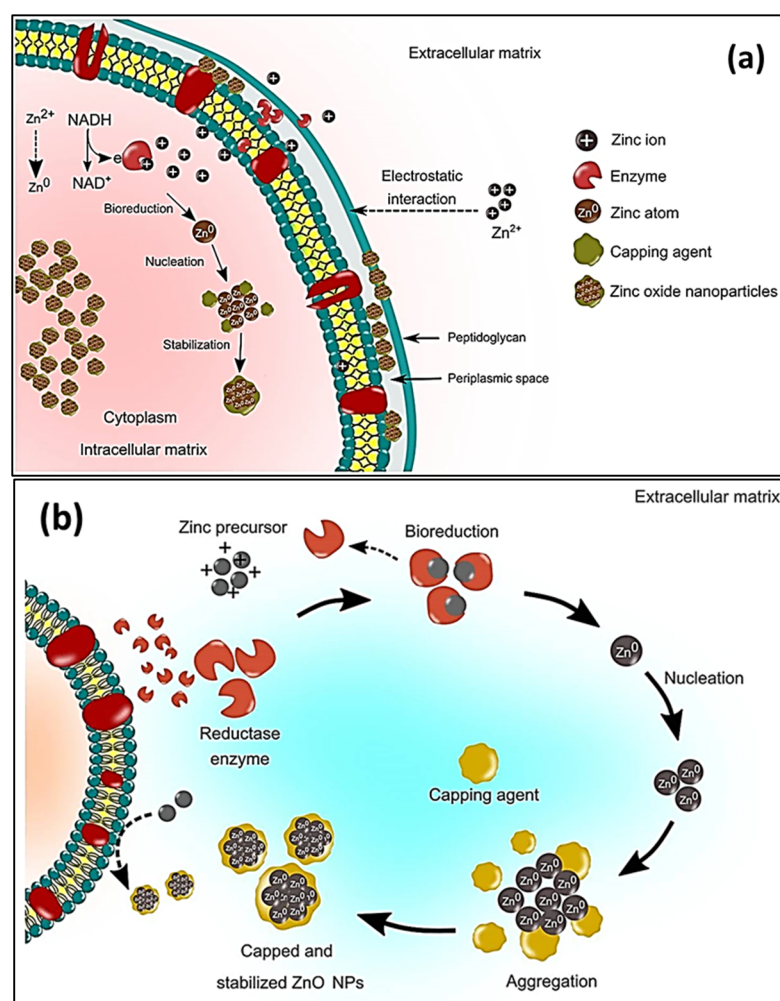


Figure 6. Schematic representation of the (a) microbial intracellular synthesis and (b) microbial extracellular synthesis of ZnO NPs [119].

Table 3 presents the current research on ZnO NP microbial synthesis. A variety of bacterial species are used in the green synthesis of ZnO NPs, including *Cyanobacterium Nostoc* sp. [29], *Aeromonas hydrophila* [59], *Serratia nematodiphila* [105], *Bacillus subtilis* [124], *Bacillus haynesii* [125], and *Alkalibacillus* sp. [126], to name but a few. Jayabalan et al. [127] reduced Zn (NO₃)₂ salt by incubating a mixture of the salt with a *Pseudomonas putida* cell culture solution at 37 °C for 24 h before calcining the resultant paste at 400 °C for 2 h. The resultant NPs were spherical agglomerates with diameters ranging between 25 and 45 nm. A green Taguchi method was employed to obtain optimum conditions in the extracellular bacterial-based production of ZnO NPs, using a *Halomonas elongate* extract, in order to reduce the presence of ZnCl₂ salt. Spherical NPs, with an average diameter of 18 nm, were obtained [128]. To produce ZnO NPs, a biomass of zinc-tolerant *Lactobacillus plantarum* TA4 was used as a nanofactory. The presence of protein, carboxyl, and hydroxyl on the surfaces of the resulting ZnO NPs was verified using FTIR analysis. Furthermore, TEM analysis of the generated NPs revealed a flower-like morphology for ZnO NP (supernatant) samples, and an irregular shape for ZnO NP (cell biomass) samples, with particle sizes of 291.1 and 191.8 nm, respectively. The presence of protein, carboxyl, and hydroxyl on the surfaces of the resulting ZnO NPs was verified using FTIR analysis. Furthermore, TEM analysis of the generated NPs revealed a flower-like morphology for ZnO NP (supernatant) samples, and an irregular shape for ZnO NP (cell biomass) samples, with particle sizes of 291.1 and 191.8 nm, respectively [129]. The presence of protein, carboxyl, and hydroxyl on the surfaces of the resulting ZnO NPs was verified using FTIR analysis. In addition, TEM

analysis of the generated NPs revealed a flower-like morphology for ZnO NP (supernatant) samples and an irregular shape for ZnO NP (cell biomass) samples, with particle sizes of 291.1 nm and 191.8 nm, respectively [129]. The biosynthesis of ZnO NPs was carried out using *Lactococcus lactis* NCDO1281(T) and *Bacillus* sp. PTCC 1538. A pure hexagonal crystalline structure of the particles was confirmed using XRD spectra. The SEM showed that ZnO NPs produced by *Bacillus* sp. were nanorods with an average size of 99 nm, whereas *L. lactis* produced NPs that were spherical, with diameter sizes ranging between 55 and 60.5 nm. The presence of amino and carbonyl groups in biosynthesized ZnO was confirmed using FTIR, and it was most likely related to residues of cell membrane proteins involved in NP biosynthesis [30].

Table 3. Microbial synthesis of ZnO nanoparticles.

Serial No.	Microbe Name	Extraction Method	Salt	Biosynthesis Time (h)/Temp (°C)	Calcination Temp (°C) Time (h)	Shape	Size (nm)	Ref
Bacteria								
1	<i>Cyanobacterium Nostoc</i> sp.	Water, 60 °C for 15 min	Zn(CH ₃ COO) ₂ ·2H ₂ O	2/RT	–	Star-shaped	60	[29]
2	<i>Aeromonas hydrophila</i>	Cell culture grew for 24 h and was diluted with water	ZnO	24/30	–			[59]
3	<i>Serratia nematodiphila</i> .	Inoculated in Luria-Bertani (LB) broth	ZnSO ₄	0.17/80 Then stored for 24 h	–	Near spherical	15–30	[105]
4	<i>Bacillus subtilis</i>	Cell culture in ammonium carbonate	Zn(CH ₃ COO) ₂	3/80	250/3	Spheres with hair-like appendages	10–15 and 1.2–1.3 um aggregates	[124]
5	<i>Bacillus haynesii</i>	Cell culture grown on agar Cell-free	ZnSO ₄	24/55	700/5	Spherical	20–200	[125]
6	<i>Alkalibacillus</i> sp.	supernatant collected by centrifugation	ZnSO ₄ ·7H ₂ O	48/35	–	Quasi-spherical	1–30	[126]
7	<i>Pseudomonas putida</i>	Cell culture solution	Zn (NO ₃) ₂	24/37	400/2	Spherical agglomerates	25–45	[127]
8	<i>Halomonas elongata</i>	Centrifugation	ZnCl ₂	Taguchi	–	Multiform shapes	18.11	[128]
9	<i>Lactobacillus plantarum</i>	Cell biomass collected by centrifugation	Zn(NO ₃) ₂ ·6H ₂ O,	24/37	–	Flower-like	152.8–613.5	[129]
10	<i>Streptomyces</i> spp.	Broth dilution then centrifugation	ZnSO ₄	0.25/40	400/8	Needle-like	12–35	[130]
Fungi								
11	<i>Aspergillus aeneus</i>	Cell-free filtrate	Zn (NO ₃) ₂	48/28	–	Spherical	100–140	[60]
12	<i>Aspergillus fumigatus</i>	Plating the inoculum on Martin Rose-Bengal agar medium	Zn (NO ₃) ₂	72/28	–	Oblate spherical	1.2–6.8	[131]
13	<i>Aspergillus fumigatus</i>	Cell biomass	ZnSO ₄	72/32	–	Spherical	60–80	[132]
14	<i>Aspergillus niger</i> .	Culture filtrate	Zn(NO ₃) ₂	48/32	–	Near spherical	53–69	[133]
15	<i>Agaricus bisporus</i>	Purchased	Zn(NO ₃) ₂ ·6H ₂ O	2/90	400/4	Spheroids	32	[134]
16	<i>Xylaria acuta</i>	Cultured then centrifuged	Zn(NO ₃) ₂ ·6H ₂ O	–/400	700/2	Hexagonal	34–55	[135]
17	<i>Pichia kudriavzevii</i>	Mycelia separated from the culture	Zn(CH ₃ COO) ₂ ·2H ₂ O	36/35	–	Hexagonal	10–61 (TEM, XRD)	[136]

Table 3. Cont.

Serial No.	Microbe Name	Extraction Method	Salt	Biosynthesis Time (h)/Temp (°C)	Calcination Temp (°C) Time (h)	Shape	Size (nm)	Ref
18	<i>Cochliobolus geniculatus</i>	Mycelial-free filtrate	Zn(CH ₃ COO) ₂	72/28	–	Quasi-spherical	2–6 (TEM)	[137]
19	<i>Saccharomyces cerevisiae</i>	Cell-free filtrate	Zn(CH ₃ COO) ₂ ·2H ₂ O	24/30	–	Spherical	20–30	[138]
20	<i>Cladosporium tenuissimum</i> FCBGr	Extracellular culture	Zn(NO ₃) ₂	36/RT	–	Bouquet-like	57	[139]
				Algae				
21	<i>Chlorella</i>	Soaking method	Zn(CH ₃ COO) ₂ ·2H ₂ O	1/58	–	Hexagonal	20	[140]
22	<i>Arthrospira platensis</i>	Biomass mixed with supernatant	Zn(CH ₃ COO) ₂ ·2H ₂ O	24/30	–	Spherical	30–55	[141]
23	<i>Padina gymnospora</i>	Millipore water stirred for 2 h at 100 °C	Zn(NO ₃) ₂ AgNO ₃	2/60	–	Spherical	20–40	[142]
24	<i>Sargassum</i> species	Ball-milled	Zn(NO ₃) ₂ ·6H ₂ O Co(NO ₃) ₂ ·6H ₂ O	2/RT	–	Nearly spherical	5.4–6.8	[143]

2.2.2. Fungal Synthesis

Fungi can release higher concentrations of secondary metabolites than bacteria. In addition, they exhibit a higher tolerance to metal concentrations, stronger binding capabilities, and better metal bioaccumulation than bacteria [144]. It is therefore possible that fungi have more potential than bacteria with regard to the upscaling of green-produced NPs. Moreover, fungal cells are more tolerant to intermediate products during the synthesis process; hence, they are more suitable for large-scale synthesis [145]. The mechanisms for generating metal and metal oxide NPs using fungal biomass or cultures are similar to the one discussed for green synthesis using bacteria in Section 2.2.1. Different *Aspergillus* species have already been employed in the green synthesis of ZnO NPs, such as *Aspergillus aeneus* [60], *Aspergillus fumigatus* [131], *Aspergillus fumigatus* [132], and *Aspergillus niger* [133], as shown in Table 3. The ability to reduce and cap the NPs is conferred by the alcohols, phenols, and the aromatic and primary amines that are present in the fungal extracts of the various *Aspergillus* species [132]. During extracellular synthesis, fungi secrete enzymes that produce pure and monodispersed NPs. These particles are free from the cellular components that are associated with organisms [131]. The biomass of *A. fumigatus* reduced ZnSO₄ and chelated the formed ZnO NPs after 72 h at 32 °C. The formed NPs were spherical with diameters ranging between 60 and 80 nm. The attained ZnO exhibited antimicrobial activities against *Klebsiella pneumoniae*, *P. aeruginosa*, *E. coli*, *S. aureus*, and *B. subtilis*, respectively, as indicated in Figure 7. The synthesis of ZnO NPs, using the aqueous extract of *Agaricus bisporus*, was carried out in [134]. According to the FTIR results, the phenol groups contained the prominent ingredients for reducing and capping ZnO NPs. The zeta potential (−20.5 mV) validated the NPs' stability, whereas the SEM and TEM revealed that the NPs were spheroids. ZnO NPs were produced with Zn(NO₃)₂·6H₂O and *Xylaria acuta* fungal filtrate using the combustion method at 400 °C. The resultant sample was then calcined for 2 h at 700 °C to obtain hexagonal shaped NPs with diameters ranging between 34 and 55 nm [135].

Moghaddam et al. [136] utilized *Pichia kudriavzevii* in the mycogenic synthesis of ZnO. The reaction proceeded for 36 h at 35 °C, the resultant NPs were hexagonal, and they exhibited diameters that ranged between 10 and 61 nm. Small, quasi-spherical particles (2–6 nm) were prepared in [137] using *Cochliobolus geniculatus*. Fluorescence spectroscopy confirmed the presence of proteins on the prepared ZnO in the form of tyrosine moieties, as per the emission peak at 350 nm. The FTIR absorption peaks confirmed the role of aromatic, aliphatic amines (amide I and amide II) in the fungal extract, and potentially in the stabilization of the ZnO NPs as well. Motazed et al. [138] prepared 20 nm to 30 nm spherical ZnO NPs using a cell-free extract of *Saccharomyces cerevisiae*. The FTIR results

suggested that the presence of alcohols, proteins, the phenolic group, fatty acids, and carbohydrates in the extracellular excretions of *S. cerevisiae* were potentially responsible for reducing the zinc ions so that ZnO NPs could be obtained. Mani et al. [139] prepared ZnO NPs at a pH of 7.2 using an endophytic fungus, *Cladosporium tenuissimum* FCBGr, which was isolated from a Vilva tree; bouquet-like NPs were obtained after 36 h of continuous stirring at RT.

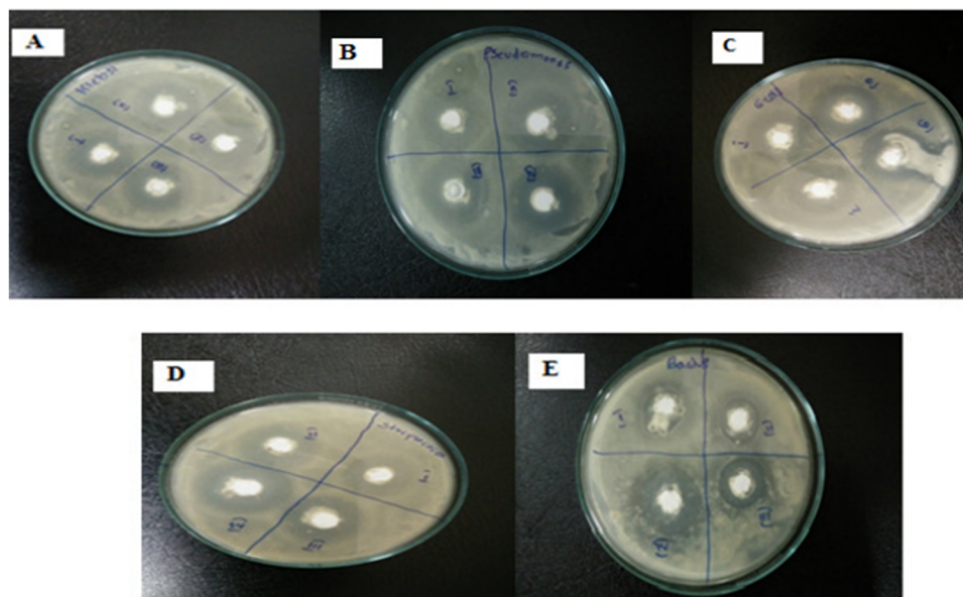


Figure 7. Antimicrobial activity of *Aspergillus fumigatus* synthesized ZnO NPs [132] working against (A) *Klebsiella pneumoniae*, (B) *P. aeruginosa*, (C) *E. coli*, (D) *S. aureus*, and (E) *B. subtilis* at different concentrations.

2.2.3. Algal Synthesis

Algae are mono and multicellular aquatic photosynthesizing organisms, but unlike plants, algae are without roots and leaves [115]; however, similarly to plants, macroalgae have active metabolites such as alkaloids, peptides, polysaccharides, proteins, tannins, quinones, lipids, and glycerol [146]. These metabolites have $-OH$ and $-COOH$ functional groups that can chelate and stabilize ZnO NPs [146]; therefore, the chemical formation route of ZnO NPs during algal synthesis is similar to that of plants [57], as discussed in Section 2.1.1. Khalafi et al. [140] propose a mechanism of ZnO NP formation using a *Chlorella* extract (Figure 8). Based on the assumption that *chlorella* contains a significant amount of carbohydrates (20%), it was presumed that carbohydrates predominantly served as Zn^{2+} reducing agents and as stabilizers of the prepared ZnO NPs. Moreover, the biosynthesis of green ZnO NPs was assumed to occur through a donor–acceptor mechanism that occurred between the oxygen atoms of functional moieties in *chlorella* and Zn^{2+} wherein the $-OH$ groups on the carbohydrates transfers an electron to the electrophilic Zn species, thus resulting in the oxidation of the $-OH$ group and Zn^{2+} reduction to Zn atoms.

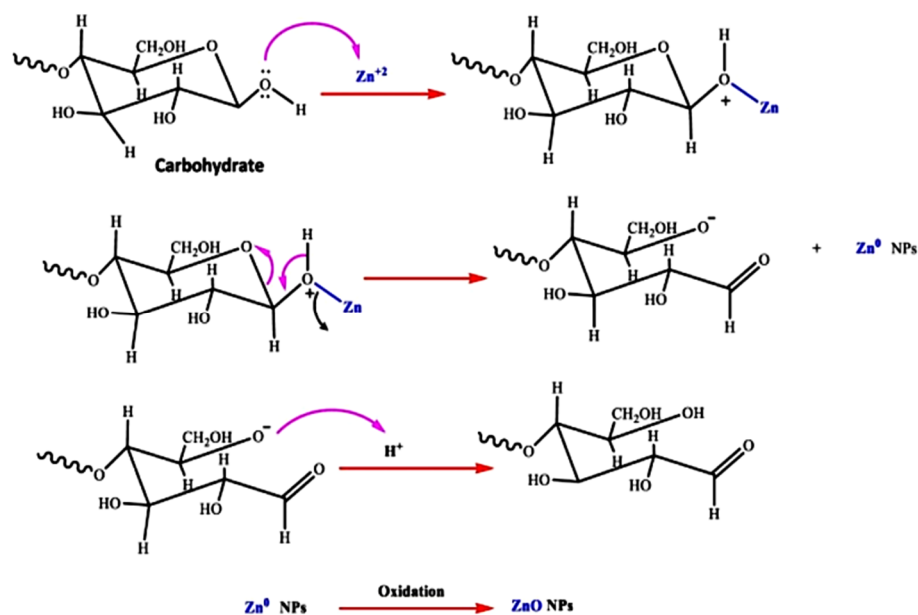


Figure 8. The probable method for the algal production of ZnO NPs, using aqueous *Chlorella* extract, is depicted schematically [140].

Algal species have been used to prepare ZnO NPs by reacting the extract with various zinc salts to obtain spheres, flower-like rods, and hexagonal shapes (Table 3). Recently, [141] produced 30 to 55 nm spherical NPs by reducing $Zn(CH_3COO)_2 \cdot 2H_2O$ with *Arthrospira platensis* extract at 30 °C for 24 h. The emergence of Zn–O characteristics, peaking at 503 cm^{-1} according to the FTIR results, confirmed the presence of ZnO particles. Algal extracts that were investigated for their ability to be synthesized with doped ZnO NPs have been successfully produced (Table 3). For instance, Rajaboopathi and Thambidurai prepared Ag–ZnO NPs by mixing separate solutions of $AgNO_3$ and $Zn(NO_3)_2$ salts with the leaf extract of *Padina gymnospora*. The solution was stirred at 60 °C for 30 min which led to a brown–white precipitate emerging from the light brown solution. The stretching and bending vibrations of water molecules ($-OH$) occurred at 3435 and 1638 cm^{-1} , respectively, whereas the stretching and bending vibrational bands of carbonate ions appeared at 1448 and 860 cm^{-1} , respectively. For the pristine ZnO NPs, the Zn–O band appeared at 420 cm^{-1} , whereas for Ag–ZnO, the Zn–O stretching vibrational bands appeared at 417 cm^{-1} [142]. *Sargassum* species extract was used to reduce the $Zn(NO_3)_2 \cdot 6H_2O$ and $Co(NO_3)_2 \cdot 6H_2O$ salts, and to stabilize the resultant Co–ZnO NPs with the aid of microwave radiation at pH 10.5. The obtained NPs were nearly spherical (5.4–6.8 nm). The interaction between Zn^{2+} , Co^{2+} , and the algae was ascertained as a result of the variation in the intensity of the FTIR spectra that corresponded with the Metal–O bond [143].

2.2.4. Preparation of ZnO NPs Using Biological Derivatives Synthesis

Apart from macro- and microorganisms, several biological derivatives have been used as precursors to synthesize NPs; however, only a handful reports discuss the use of biological derivatives for the green fabrication of ZnO, as shown in Table 4. Moreover, the polysaccharide pullulan was stirred together with $Zn(NO_3)_2 \cdot 6H_2O$ for 5 h at RT. This was followed by a 1 h heat treatment at 400 °C to yield spherical and hexagonal ZnO NPs with an average diameter of 58.13 nm [147]. El-Saied and Ibrahim, 2020, used chitosan to synthesize ZnO NPs, with average size of 55 to 70 nm [148]. Vijayakumar et al. [149] prepared egg albumen wrapped ZnO NPs, with diameters ranging between 20 and 60 nm, and with spherical and diagonal platelets. Additionally, artemia eggshells were used to hydrothermally produce ellipsoidal ZnO NPs. The prepared NPs had a 50 nm diameter on average, according to TEM [150]. Highly crystalline crustin-capped ZnO NPs were produced after the coprecipitation of the salt with an extract of crustin at RT for 2 h.

The average size of the resultant NPs were 50 nm [151]. Amino acid-capped NPs were produced via a wet chemical synthesis, prior to calcining at 550 °C for 3.5 h. The produced sheet-like NPs had diameters ranging between 22.46 and 40.29 nm [152]. Smaller ZnO NPs were produced with the aid of tannic acid, as both the size influencer and capping agent were treated at 70 °C for 1.5 h without further heat treatment. The particles had a spherical morphology, with diameters ranging between 26 and 34 nm [153]. A separate study reported that honey and cow urine, respectively, yielded spherical and hexagonal leaf-like ZnO NPs [154].

Table 4. ZnO nanoparticles prepared from biological derivatives.

Serial No.	Bio-Product	Precursors	Biosynthesis Temp (°C)/Duration	Thermal Treatment Temp (°C)/Time (h)	Shape	Size (nm)	Ref
1	Alginate	Purchased ZnO		—	Irregular spheres	20–90	[155]
2	Starch	Zn(NO ₃) ₂ ·6H ₂ O HAuCl ₄ ·3H ₂ O	Stirred at 90–100 °C	Oven dried at 80 °C Calcined at 600 °C for 4 h	Spherical	18.9	[156]
3	Lignin	Zn(NO ₃) ₂ ·6H ₂ O	Oven at 120 °C for 4 h	Oven dried at 120 °C for 4 h	Rods	5–10	[157]
4	Pullulan	Zn(NO ₃) ₂ ·6H ₂ O,	Stirred at RT for 5 h	Oven dried at 60 °C for 24 h Calcined at 400 °C for 1 h	Spherical and hexagonal	58.13	[130]
5	Chitosan	Zn(NO ₃) ₂ ·6H ₂ O	Stirred at 80 °C for 2 h	Oven dried at 80 °C for 24 h	Rods	50–70	[148]
6	Egg albumen	Zn(CH ₃ COO) ₂	Hydrothermal, at 85 °C for 3 h	—	Spherical and diagonal platelet	20–60	[149]
7	Artemia eggshell	Zn(CH ₃ COO) ₂	Hydrothermal, 180 °C for 20 h	—	Ellipsoidal	50	[150]
8	Crustin	Zn(CH ₃ COO) ₂	Co-precipitation, magnetically stirred for 2 h Stirred at 22 °C for 30 min prior to increasing the temperature to 150 °C	Vacuum dried at 30 °C		50	[151]
9	Amino acids	Zn(NO ₃) ₂ ·6H ₂ O		Calcined at 550 °C for 3 h 20 min	Sheet-like particles	22.46–40.29	[152]
10	Tannic acid	Zn powder	Stirred at 70 °C for 1 h and 30 min	—	Spherical	26–34	[153]
11	Honey and cow urine	Zn(NO ₃) ₂ ·6H ₂ O	Combustion method, further stirred at 100 °C	—	Hexagonal, leaf-like structure (cow urine) Spherical (honey)	27 44	[154]

2.3. Factors Influencing ZnO Nanoparticle Biosynthesis

To control the size distribution, shapes, and formation rate of NPs, the optimization of the reaction media and physical parameters is crucial. Biosynthesized NPs can be commercially considered if the NPs' yield is high and if they exhibit the desired size, size distribution, and morphology [119].

2.3.1. Temperature

The synthesis temperature influences the rate of crystallization in the wet synthesis procedures of semiconductor nanoparticles, and ZnO is no exception. The increased kinetic energy within the reaction vessel speeds up the rate at which nanoparticles collide, therefore forming crystalline nuclei. In cases of calcination, the calcination temperature influences the degree to which the amorphous ZnO matrix transforms into crystalline ZnO. The rate of nuclei formation increases with temperature, thus enhancing the degree of crystallinity, especially during biosynthetic processes involving ZnO [64]. In their investigation on the effect of temperature on the quality of the ZnO when using *Hibiscus subdariffa* leaf extract, Bala et al. [74] found that the UV-Vis spectra did not show the characteristic absorption band

at 355 nm for the ZnO that was synthesized at 30 °C, thus suggesting that the material was only an amorphous ZnO; however, for the ZnO synthesized at 60 and 100 °C, the presence of ZnO NPs was confirmed by the appearance of the absorption band and by the appearance of plasmonic bands at 377 nm. Moreover, the intensity of the bands became stronger as the synthesis temperature increased [74]. The effect of the synthesis temperature was further illustrated by the variation in ZnO morphology. The ZnO NPs that were synthesized at 30 °C were generally irregularly shaped, and they exhibited polydisperse-characteristics that are common in amorphous semiconductor matrices. As the temperature increased, the morphology became clearer, such that the ZnO NPs that synthesized at 60 °C were spherical, and those that synthesized at 100 °C were dumbbell shaped. Previously, Das et al. [158] noted that the effects of different temperatures could be observed through the degree to which the molecules associated with the synthesized biological media remained attached to the surface of the nanoparticles. The authors found that synthesis at 60 °C enabled numerous bio-compounds on gold to remain attached to the surface of NPs to a greater extent than synthesis at 100 °C. When Sukri et al. [84] prepared ZnO NPs using *Punica granatum* fruit peel, the TEM revealed mostly spherical and hexagonal ZnO NPs, and the mean sizes were dependent on calcination temperatures. The sizes were 32.98 nm and 81.84 nm when the samples were calcined at 600 °C and 700 °C, respectively.

2.3.2. Effect of pH

The metabolites that exist in biological extracts are pH sensitive; hence, variation in terms of medium tampers with their reducing and chelating capabilities, which directly affects the growth of the nanomaterials [159]. Furthermore, pH influences the redox activities of enzymes and other metabolites in the cell-free extract [123]. The changes in the acidity of the reaction medium also influences the NPs' yield and morphology. Al-Kordy et al. [126] reported that the average diameter of ZnO decreased gradually as the pH increased, but at higher pH levels, a slight increase in size was noticed when an extract of *Alkalibacillus* sp. W7 was used. This was due to the fact that the chelating/growth controlling compounds, that were present during the formation of the Alk-ZnO NPs, were denatured at an extreme pH [160]. Guan et al. [161] reported that a pH value of 8.5 encouraged the production of almost spherical hybrids, with an average diameter of 60 nm, because of the low OH⁻ ion concentration; however, at pH values of 10.5 and 11.0, sheet-like and flower-like hybrids were obtained because of the large quantity of OH⁻ ions. The hybrid nanomaterials exhibited a high degree of crystallinity and a high ZnO content, thus leading to higher thermal stability.

2.3.3. Effect of the Concentration of the Precursor

The concentration of biomass/extract and salt influences the morphology, and enhances the production, of nanoparticles [162]. When the zinc ion concentration increased from 0.005 M to 0.3 M, the formation of NPs occurred more quickly, but a lower yield of hexagonal ZnO NPs was obtained, with diameter sizes ranging between 20.7 and 96.5 nm. SEM images confirmed that the concentration of biosynthesized ZnO NPs occurred rapidly, and larger particles formed due to the competition between Zn²⁺ and the functional moieties found in the cherry extract, which served to accelerate the reduction [163]. This finding confirms the observations made by Jamdagni et al., who observed an increase in the absorbance of the UV-vis spectra as the precursor concentration increased [164]; however, further increases in concentration yielded a broad and low absorbance peak that signified a low yield of ZnO NPs. The sizes of the ZnO NPs obtained with 1% *Hibiscus sabdariffa* extracts ranged between 20 and 40 nm, whereas the 8% extract samples exhibited homogenous shapes and smaller NPs (5–12 nm) due to the abundant chelating compounds in the extract, thus resulting in very stable ZnO NPs [87].

2.3.4. Effect of Reaction Time

According to Fagier et al. [69], the biosynthesis of ZnO NPs is entirely determined by the temperature, pH, biological source, and zinc precursor, rather than the reaction time; however, Dhandapani et al. [165] observed that the heating duration at a particular temperature determines the formation of aggregates. For instance, upon increasing the heating duration for a reaction conducted at 50 °C, from 30 min to 90 min, the agglomeration of the particles increased. Prolonging the reaction time (36 h) during the fabrication of ZnO NPs using *Pichia kudriavzevii* resulted in aggregates with irregularly shaped NPs, whereas reaction times of 12 h and 24 h yielded smaller NPs [136]. These findings are consistent with observations of chemical methods, where extended nucleation times resulted in the generation of larger ZnO NPs [166].

2.3.5. Effect of Different Biological Species

Mahdi et al. prepared ZnO NPs using different bacteria, namely, *Lactococcus lactis* and *Bacillus* sp. [30]. The particles synthesized by *L. lactis* showed an absorption band at 444 cm⁻¹ with a distinct shoulder at 486 cm⁻¹, which is a typical ZnO absorption band, whereas the *Bacillus* sp. sample displayed absorption bands at 560 cm⁻¹ and 601 cm⁻¹. These changes in wavenumber, peak shape, and intensity indicate the changes in ZnO morphology and the size of particles. This finding was confirmed by the SEM, which revealed that the ZnO NPs synthesized by *L. lactis* were 55 nm spheres, whereas the ZnO NPs produced by *Bacillus* sp. exhibited diameters of 99 nm and they were rod shaped. In a separate study, Mohamed et al. [167] prepared ZnO NPs using extracts of two fungal strains, *Fusarium keratoplasticum* (A1–3) and *Aspergillus niger* (G3–1). The *F. keratoplasticum* strain (A1–3) yielded hexagonal (10–42 nm) NPs, whereas the *A. niger* strain (G3–1) resulted in nanorod-shaped (8–38 nm) NPs with –39 mV and –35 mV Zeta potential values for the hexagonal and nanorod ZnO NPs, respectively.

3. Characterization Techniques for ZnO

Having demonstrated the fact that a wide spectrum of morphological possibilities arises from the variation of synthesis parameters and plant extracts, it is necessary to study the ZnO NPs that are formed in greater detail. Although there are a wide variety of characterization techniques, only a few are needed to illustrate the story of ZnO green synthesis juxtaposed with the classical synthesis techniques. Among these techniques, the most important include the ultraviolet visible spectroscopy (UV-vis), X-ray diffraction (XRD), SEM, TEM, energy-dispersive X-ray spectroscopy (EDX), and FTIR. These are discussed in relation to the information that they provide regarding the uniqueness of green-synthesized ZnO NPs.

3.1. UV-Vis Spectroscopy

UV-Vis is a preliminary technique that is used to confirm the formation of the nanomaterial [140]. Ideal ZnO NPs display a characteristic absorbance peak between 320–390 nm which corresponds to the E_g (3.37 eV) of the material [133]. The inherent E_g absorption is attributable to the electron transitioning from the valence band to the conduction band ($O_{2p} \rightarrow Zn_{3d}$) [168]. The peak position, shape, and width is influenced by the structure and particle size, oxygen vacancies, E_g , and so on. [110]. The strong absorption of ZnO in the UV region warrants its applicability in the photocatalytic degradation of pollutants. Abdelhakim et al. [34] produced an absorbance peak of 369 nm with samples that were prepared using a culture filtrate of the endophytic fungus *Alternaria tenuissima*. The absorbance peak for *Phoenix dactylifera* waste-ZnO-NPs was found to be 381 nm. The red-shift was ascribable to the surface plasmonic resonance of the sample, which was determined by its morphology and size [39]. Doped ZnO samples also displayed the red-shifted position of the absorbance peak, as well as an improved intensity. This is a result of the decreased E_g , which is facilitated by the dopant, as observed when using Nb-ZnO that is prepared using the leaf extract of *Vernonia amygdalina* [111]. The same finding was reported in [110],

which mentioned that increasing the dopant concentration reduced the E_g in Mg and Cu co-doped ZnO NPs; this is because the dopants introduce dopant-induced states that provide additional pathways for electronic transitions. Although broad peaks indicate polydisperse NPs, narrow peaks suggest monodispersed ZnO NPs [110].

3.2. X-ray Diffraction (XRD)

XRD is used to ascertain crystallinity, confirm the respective crystallographic planes, and determine the purity of nanomaterials. Most ZnO diffraction peaks are indexed to the hexagonal phase in accordance with the wurtzite structure, which is the most stable phase in ambient conditions [169]. The wurtzite structure's peaks are approximately located at $2\theta \sim 31.7, 34.4, 36.3, 47.6, 56.7, 62.8, 63m$ and 69.5° , which are reflected in the lattice planes of (100), (002), (101), (102), (110), (103), (112), and (202), respectively [25,170,171]. In the case of bio-prepared samples, additional peaks are often located, and these arise from the crystallization of the biomolecules. As such, a peak was observed at 23° , which was due to crystallized chitosan [171]. In a separate study, Kaningini et al. [170] also identified extra peaks that were thought to have been reflected from excess crystallized extract. Moreover, ions such as K, S, and Cl, which were previously absorbed by the plant from the soil, were also identified; however, annealing at high temperatures (800°C) removes the additional diffraction peaks from the various ions. Doped ZnO samples display high intensity peaks compared with undoped ZnO. The enhanced intensity suggests an increase in the packing of atoms in their respective planes. Moreover, the doping of ZnO samples usually leads to a red shift in the 2θ position, as observed when doping ZnO with Ce [170]. The red shift is consistent with the reduction of E_g , as the dopants are incorporated into the lattice of ZnO. Annealing the obtained samples also improves the crystallinity, and thus, the intensity, of the Bragg's peaks since high temperatures repair the structural defects of the material [172]. Similarly, Hafiz et al. [173] observed that the (002) plane diffraction peak for Al-ZnO had a higher intensity compared with the unannealed sample.

The X-ray diffraction peaks of the biosynthesized ZnO samples displayed broadening, which can be attributed to the nano-scaled size of the samples; this was accompanied by fewer internal stresses within the sample [58]. In most of the green synthesis processes that were reported, the procedure ends with the calcination of amorphous ZnO in order to transform it into crystalline ZnO; as such, the high degree of crystallinity that was observed is more likely to be due to the high temperature than the use of green biosynthetic protocols. This is expected since annealing repairs the structural defects of synthesized ZnO; however, a few studies have developed highly crystalline ZnO without post synthesis calcination, or by just drying the amorphous ZnO at temperatures as low as 50°C . For example, Khalifu et al. synthesized ZnO NPs using a *Chlorella* microalgae extract, and they only dried the resultant ZnO at 50°C [140]. The XRD spectra showed intense peaks that were attributed to ZnO, and no traces of amorphous material, as indicated in Figure 9a. Another report showed that drying the amorphous ZnO at a low temperature (60°C), after being treated with zinc acetate and *Cyanobacteria* extract, produces ZnO with good crystallinity, albeit with some degree of amorphous composition [29] (Figure 9b). XRD spectra has also unearthed the dependence of the catalytic efficiency of ZnO on the ZnO facet that is most exposed. It has been shown that ZnO NPs with limited growth in the 0001 direction show a higher catalytic activity due to the facets on the 0001 plane that are rich with terminal oxygens [102,174,175] (Figure 9c). In the XRD spectra, the growth in the 0001 direction can be inferred from the intensity of the 002 peak, as when the 002 peak has a low intensity relative to the 101 peak, there is limited crystalline growth in the 0001 direction, and the ZnO has high catalytic activity.

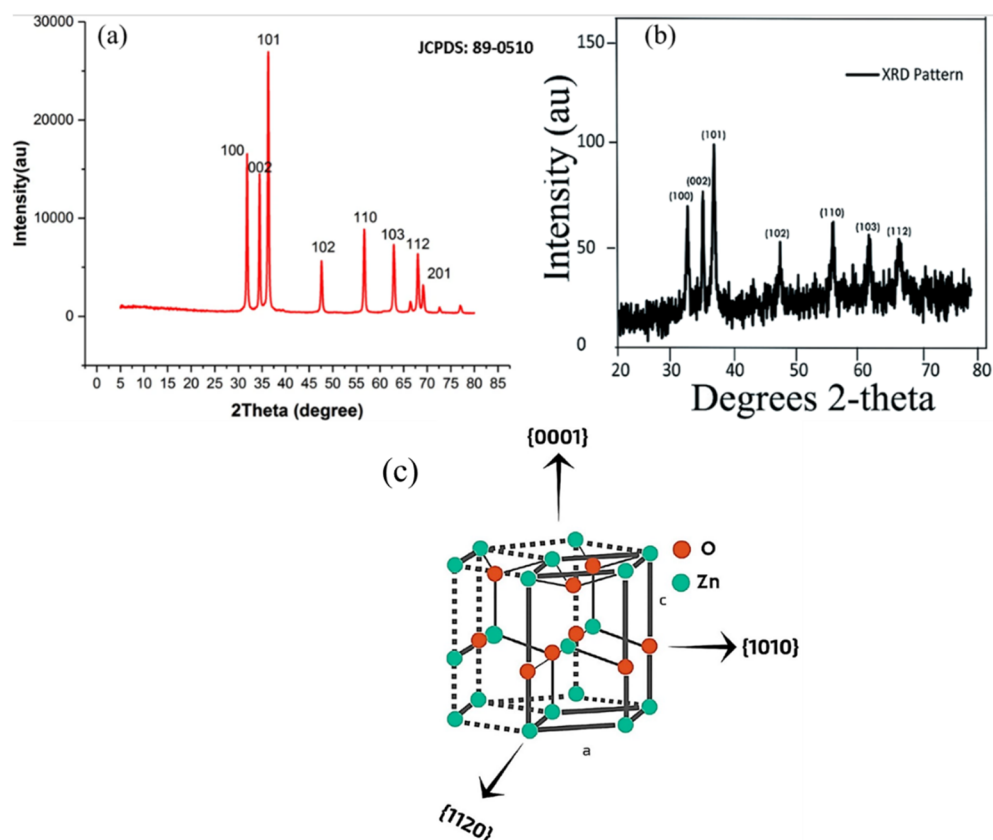


Figure 9. XRD spectra for ZnO (a) synthesized using *Chlorella* microalgae extract that was dried at 50 °C [140]; (b) synthesized using cyanobacteria extract and dried at 60 °C [29]; and (c) the possible growth directions for the ZnO Wurtzite crystals (lattice parameters $a = 0.325$ nm and $c = 0.521$ nm) [102].

3.3. Scanning Electron Microscopy (SEM) and Transmission Electron Microscopy (TEM)

SEM provides information on the topography and morphology of the NPs; however, currently, researchers prefer to use TEM because it offers greater magnification and resolution capabilities than SEM, and as a result, the information regarding the size, shape and crystallography of the nanoparticles from TEM is more accurate [64]. The size and morphology of ZnO NPs play crucial roles in terms of their properties and applications. Smaller NPs possess a higher surface area than larger ones; however, ZnO NPs form aggregates because smaller particles possess high surface energy that allows them to interact with each other, possibly via hydrogen, intermolecular Van der Waals, and electrostatic bonding during the synthesis and drying processes [25]. With respect to antimicrobial properties, small NPs penetrate microbial membranes with ease, thus enhancing their killing efficiency. Moreover, the release of the toxic Zn^{2+} and hydrogen peroxide is also enhanced by larger surface areas. The photocatalytic degradation of pollutants also relies on the size and uniformity of the nanomaterials. The morphology of the nanomaterials is affected by several factors, including the concentration of the salt precursor, as observed in the SEM analysis in [40], wherein small dispersed spherical NPs at 5 mmol/Kg, agglomerated sponge-like morphologies at 10 mmol/Kg, and nano capsules at 50 mmol/Kg were obtained, respectively. The TEM images were similar to those obtained using SEM, but using high resolution TEM (HRTEM), at 5 mmol/Kg, hexagonal crystalline ZnO NPs were attained; at 10 mmol/Kg, hexagonal ZnO NPs agglomerated to form short rods; and at 50 mmol/Kg, nanorods were formed. In retrospect, the precursor tunes the structure and morphology of ZnO NPs without altering the crystallite structure [40]. In another study, the SEM revealed uniformly dispersed spherical NPs. The diameters of the NPs decreased from 78 to 64 nm, with an increase in the concentration of *Syzygium cumini* leaf extract, from

10 to 25 mL. The size reduction occurred as a result of the capping efficiency of the extract during the formation of NPs [47]. Using the TEM technique [105], polydisperse ZnO NPs were obtained with sizes ranging between 15 and 30 nm. According to the surface area electron diffraction (SAED), the NPs exhibited a hexagonal crystalline structure. The high crystallinity of the ZnO NPs was confirmed by the presence of bright spots that formed a hexagonal pattern.

3.4. Energy-Dispersive X-ray Spectroscopy (EDX)

EDX is commonly used to analyze the elemental constituents and composition of NPs; therefore, in bio-prepared samples it is mainly used to confirm the sample's purity. In ultrapure ZnO samples, only the elements Zn and O are observed in the EDX spectrum; however, it is not uncommon for the EDX to detect the presence of Cu, which, in most cases, is due to the copper grid upon which the samples are often loaded. Additional C signals may originate from the carbon used to coat the grid, or alternatively, from the extra biocompounds that are adsorbed onto the ZnO NPs [169]. In samples synthesized with nitrogen-containing extracts such as chitosan and algae, it is common to observe the N signal arising from the (-NH₂) group [171]. If impurities and/or dopants are present, they are detected and shown in the spectra [108]. Samples that are annealed with oxygen reveal high levels of O compared with unannealed samples, or those annealed under controlled conditions [173].

3.5. Fourier-Transform Infrared Spectroscopy (FTIR)

FTIR provides information on the surface chemical functional groups, as well as bonding between the nanomaterials and biological extracts. The characteristic band for undoped and doped ZnO NPs lies between 400 and 700 cm⁻¹. This peak is due to the presence of the Zn-O stretching vibration [29]. The specific peak position and intensity of the absorption bands depends on the synthesis method and reducing agents. In the case of biosynthesized ZnO NPs, the position is influenced by the available biocompounds in the extract. Chemically prepared ZnO samples display a sharp absorption band at 536.86 cm⁻¹ [176], whereas this characteristic peak appeared at 547.38 cm⁻¹ for ZnO samples reduced with the extract of *Cyanobacterium Nostoc* sp. EA03 [29]; however, Shabaani et al. [25] prepared ZnO using the *Eriobotrya japonica* seed, and they observed the peak at 465.24 cm⁻¹, whereas it was positioned at 457 cm⁻¹ in the study presented in [177]. The other dominant absorption bands in the FTIR for bio-prepared ZnO NPs are found in the region of 800–1500 cm⁻¹; these are attributable to organic compounds (phenolic groups, alcohols, and aliphatic amines). The absorption peaks in the region of 1600–3400 cm⁻¹ are the result of the stretching bands of C=O in the amide group, and the presence of the -COOH and -OH groups, respectively [29]. If the extract predominantly contains proteins, bands at around 1650 cm⁻¹ (amide I, C=O stretching) and 1550 cm⁻¹ (amide II, C-N stretching and N-H deformation) become apparent. The N-O bands appear at 1380 cm⁻¹ [25]. Band shifts and changes in intensities indicate some form of chemical bonding between the NPs and the reducing agents.

3.6. Other Techniques for ZnO Analysis

The use of biomolecules to tailor ZnO also necessitates the determination of other aspects of ZnO NPs such as the chemical composition, bond order, surface area, interactions with liquids, and pollutants. X-ray photoelectron spectroscopy (XPS) is useful in determining the intrinsic chemical structure of ZnO NPs, and this is particularly the case regarding doped ZnOs. With XPS, the bond order of ZnO and the presence of defects can be determined with accuracy, and therefore, doping efficiency in green synthetic processes in comparison to conventional synthesis processes can be determined. The surface area of nanomaterials is determined using Brunauer-Emmett-Teller (BET) analysis with an inert gas such as N₂ to probe the available surface area [178]. The only limitation in terms of surface area, as represented by BET analysis, is that it is only representative of the surface

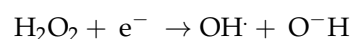
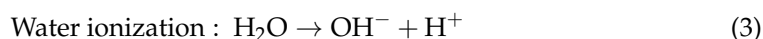
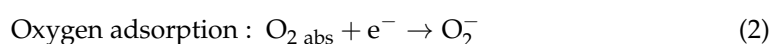
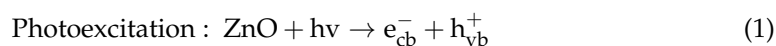
area of the dry sample yet ZnO is generally used in aqueous conditions in cases of water remediation. To counteract this limitation, the BET surface area is used in conjunction with the particle size and point of zero charge determination using dynamic light scattering (DLS) techniques. Although the DLS technique does not provide the size of the surface area, it does determine the size of the ZnO NP and the aggregation index in water. The BET technique also enables the prediction of the type of interaction between the ZnO and the pollutant (i.e., whether it is chemisorption or physisorption).

4. Application of Green ZnO NPs in Water Remediation

Traditional water treatment approaches such as chlorination, ultraviolet irradiation, and ozonation are undertaken in water treatment plants to reduce the pathogenic bacterial load. Although these techniques effectively decontaminate the water, the oxidizing agents typically react with natural organic matter to form disinfection by-products, especially halogenated organics which are renowned for their carcinogenicity [179]. Nanotechnology, on the other hand, can potentially enhance the treatment efficiency of wastewater and eliminate the threat of incurring toxic by-products, thereby nudging water treatment technologies a step closer to becoming green technologies. Since ZnO NPs exhibit salient physicochemical properties, they have been explored for water decontamination purposes, including the photocatalytic and adsorptive removal of pollutants such as dyes, heavy metals, pharmaceuticals, and microorganisms [180].

4.1. Photocatalytic Degradation of Pollutants

The decontamination of wastewater via the photocatalytic break down of microbes is superior to physical, chemical, and biological decontamination methods. This is because photocatalytic degradation is cost-effective and environmentally benign; it involves a rapid oxidation/reduction process and it can eliminate polycyclic products through mineralization [181]. In this sense, the catalytic process fulfils one of the twelve pillars of green synthesis and one of the green processes, specifically that which relates to the acceleration of a reaction using a catalyst and reduction of energy demands. ZnO nanostructures have been extensively applied as semiconductor photocatalysts owing to their high reactivity, abundant reactive sites, high yields of hydrogen peroxide, affordability, and non-toxicity [182]. The photocatalytic mechanism of action for ZnO is represented in Figure 10. Briefly, when irradiated by photons with an energy that is above the photo-threshold, the electrons (e^-) are excited from the valence band (VB) to the conduction band (CB). This forms positively charged holes (h^+) for every excited e^- [183] (Equation (1)). The newly formed electron-hole (e^-/h^+) pairs migrate to the surface of the semiconductor (ZnO) where the e^- reduces the adsorbed O_2 to generate superoxide anion (O_2^-) (Equation (2)). The h^+ reduces H_2O and OH^- to generate H_2O^\bullet and H_2O^\bullet radicals, respectively (Equations (3) and (4)). These radicals and the superoxide ions are known as reactive oxygen species (ROS) and they are responsible for the degradation of pollutants [47].



ZnO photocatalysts are mainly applied to decolorize water contaminated by synthetic, industrial dyes; this is because dyes cannot be completely degraded via aerobic approaches, thus rendering biotreatment ineffective [184]. ZnO-based photocatalysis has been shown to be capable of deactivating a wide variety of microbes and degrading or-

ganic pollutants, as depicted in Figure 10. Biosynthesized ZnO NPs have demonstrated photocatalytic efficiency matching that of conventionally synthesized ZnO, and reports concerning the photocatalytic degradation of pollutants using biosynthesized ZnO NPs are detailed in Table 5.

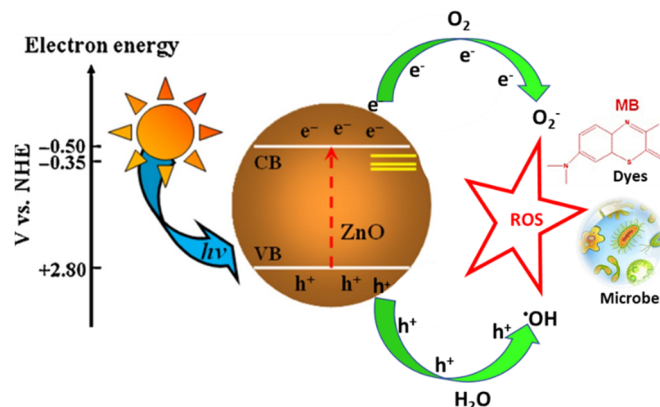


Figure 10. Mechanism of the degradation of pollutants by ZnO NPs. (Modified with permission from Ref. [185] © 2013, Elsevier B.V.).

ZnO nanoparticles generated by phytosynthesis, using plants such as *Lycopersicon esculentum* [186], *Calliandra haematocephala*-L. [187], and *Abelmoschus esculentus* L., have been applied in the photocatalytic decontamination of methylene blue (MB) [188]. Spherical ZnO NPs were synthesized by Nava et al. using *Camellia sinensis* extract and degraded MB at under a UV light after 120 min [189] with an 84.37% degradation efficiency. Other dyes that have been degraded by plant-based synthesized ZnO NPs include Congo red (CR), which was degraded by *Artocarpus heterophyllus*-reduced NPs [190], and Rhodamine 6 G (R6G), which was degraded by *Syzygium cumini*-stabilized ZnO NPs [47]. In addition to dye degradation, ZnO NPs that were synthesized using plant-mediated methods were used by Razanamahandry et al. [191] in order to break down free cyanide, a very toxic pollutant that is generated by metallurgical activities. When spherical ZnO NPs (9.8 nm) were synthesized using *Eucalyptus globulus* leaves, a 98% efficiency degradation of 3 g CN L1 under solar light was achieved, and a 45% efficiency degradation occurred under UV light within 20 min.

Table 5. Summary of the reported photocatalytic activities of ZnO (doped and undoped) nanoparticles synthesized from various biological sources.

Name of Biological Source	ZnO Morphology	Pollutant	Catalyst Concentration	Pollutant Concentration	Radiation	Exposure Time (min)	pH	Efficiency (%)	Ref
Plant based									
<i>Lycopersicon esculentum</i> ,	Polyhedral	Methylene blue (MB)	–	15 mg/L	10 W UV light	180	6	97	[186]
<i>Calliandra haematocephala</i> -L.	Nanoflower-like	MB	50 mg/100 mL	20 mg/L	Sunlight	270	6	88	[187]
<i>Abelmoschus esculentus</i> L.	Spherical	MB and methyl orange (MO)	15 mg/mL	10 mg/10 mL	UV light	270	4	96	[188]
<i>Camellia Sinensis</i>	Spherical	MB	15 mg/L	200 mg/L	10 W UV light	120	6	84.37	[189]
<i>Artocarpus Heterophyllus</i>	Spherical	Congo red (CR)	24 g/L	20 mg/L	30 W UV light = 2	60	9	>90	[190]

Table 5. Cont.

Name of Biological Source	ZnO Morphology	Pollutant	Catalyst Concentration	Pollutant Concentration	Radiation	Exposure Time (min)	pH	Efficiency (%)	Ref
<i>Eucalyptus globulus</i>	Spherical	Free cyanide	0.04 g/100 mL	0.3 g/L	UV light	20	unspecified	98	[191]
<i>Azadirachta indica</i>	Spherical and flower-like	MB	10 mg/mL	10 mg/L	Sunlight	120	6	97	[192]
<i>Rosmarinus officinalis</i>	Quasi-hexagonal	Industrial dye effluent MB	50 mg/50 mL TE	–	20 W Vis light	100	5.28	63	[193]
<i>Synadium grantii</i>	Spherical	Indigo carmine RhB	100 mg/L in 100 mL	25 mg/L	30 W UV light	75 75 75	unspecified	79.2% 80.8% 75%	[194]
Algae									
<i>Chlorella</i>	Spherical	DBT	0.01 g/20 mL	10 mgL/20 mL	UV light	180	7	97	[140]
<i>Sargassum specie</i>	Irregular	Malachite green (MG)	0.06 g	5 mg/L	150 W Vis light	60	8	92.5	[143]
Fungi									
<i>Cordyceps militaris</i>	Flower-like	MB	0.25 mg/mL	10 mg/L	UV light	180	6	97	[195]
<i>Saccharomyces cerevisiae</i>	Spherical	MB	12 mg/mL	5 mg/L	UV light	200	3	67	[138]
<i>Saccharomyces cerevisiae</i>	Spherical	4-nitrophenol	50 mg/L	1.5×10^{-4} M	UV-Vis light	100	6	78	[196]
<i>Aspergillus niger</i>	Near spherical	Bismarck Brown	–	1×10^{-4} M	Vis light	72 h	unspecified	89	[197]
Biological derivatives									
Pullulan	Spherical and hexagonal	Amoxicillin Paracetamol	50 mg/100 mL	30 mg/L	9 W Mercury lamp	120	9 5	85.7 96.8	[147]
Artemia eggshell	Spherical or ellipsoidal	RhB MB Neutral red	10 mg/100 mL	4 mg/10 mg/mL (10 mg/mL)	–	120	3–11	88.75 93.3 86.6	[150]
Chitosan	Flower-like	hexavalent chromium	25–100 mg	50 mg/L (50 mL)	32 W UV light 365	60	5.2	99.2	[198]
Cellulose Fibers	Flower-like	Methyl orange Phenol	0.3 g/15 mL	0.06 mmol/L (15 mL) 60 mg/L (15 mL)	6.6 W UV light 365	9 h	Dye	100	[199]

Co-doped ZnO supported in algae (*Sargassum* sp.) was synthesized for the photocatalytic decolorization of malachite green (MG) dye under visible light. The photocatalytic performances were enhanced by 58% for ZnO/algae, and by approximately 75% for Co-ZnO/algae, compared with pure ZnO without support, for 60 min. Rajaboopathi and Thambidurai [142] degraded MB and reactive blue 198 (RB-198) over 150 min using *Padina gymnospora* Ag-doped ZnO NPs, with 98.7% and 99.8% efficiency, respectively. Ag-doped ZnO NPs, developed with the aid of *Azadirachta indica* extract via a hydrothermal method, were obtained by Patil et al. [192]. The degradation efficiency of 10 mg/L MB dye and a 10 mg/mL catalyst concentration was 97% over 120 min under natural light, as shown in Figure 11a. The rate constant for degrading MB using the Ag-ZnO NPs was $5.9668 \times 10^{-2} \text{ min}^{-1}$, and it was higher compared with that of the undoped ZnO ($2.527 \times 10^{-2} \text{ min}^{-1}$) in Figure 11b. *Rosmarinus officinalis* yielded quasi-hexagonal Ag-doped ZnO NPs that were used to degrade an industrial dye under visible light at pH 5.28 with a 63% efficiency [193]. Cu-ZnO NPs were synthesized from *Synadium grantii* leaf extract. The resultant composites degraded MB, Indigo Carmine (IC) and RhB dyes with a 79.2%, 80.8%, and 75% efficiency, respectively [194].

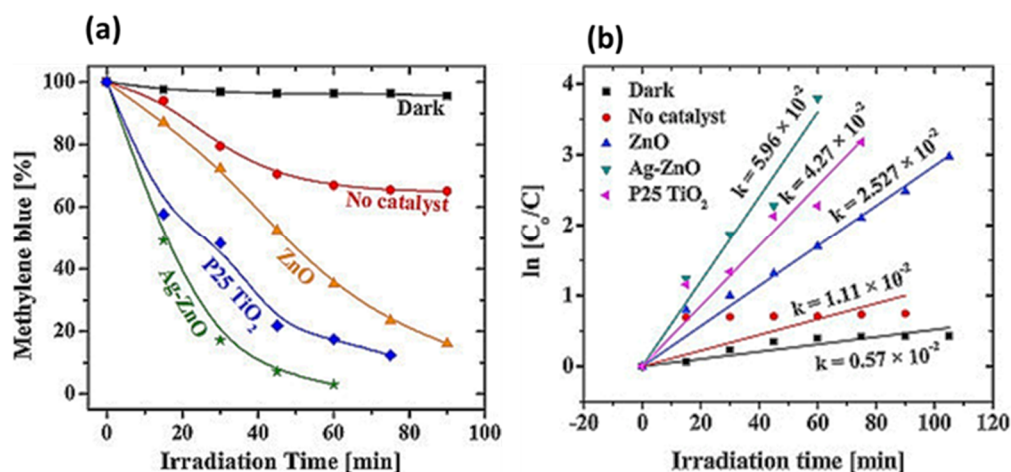


Figure 11. (a) Graph showing the amount of remaining MB according to irradiation time; (b) chemical kinetics for the photocatalytic degradation of MB using ZnO, Ag-ZnO, and P25 TiO₂ catalysts. Figure adapted with permission from Ref. [192], © 2015, Elsevier B.V.

ZnO NPs that are prepared with the aid of fungi are known to be viable for pollutant degradation. As such, *Cordyceps militaris* chelated flower-shaped ZnO NPs degraded 10 mg/L MB, with a 97% efficiency over 180 min, when irradiated with UV light [195], whereas *Saccharomyces cerevisiae*-stabilized NPs achieved only a 67% efficiency when degrading 5 mg/L MB under UV irradiation over 200 min [144]. Previously, Kumar et al. prepared 50 mg/L ZnO NPs using the biomass of *Saccharomyces cerevisiae* as a template to break down 1.5×10^{-4} M 4-nitrophenol (4-NP) [196]. The pollutant was degraded in 100 min under UV light with 78% efficiency. The precipitation process was used to prepare biogenic ZnO NPs utilizing pullulan as the biomaterial. The material photodegraded amoxicillin and paracetamol with 85.7% and 96.8% efficiency, respectively. The pharmaceuticals were destroyed with ring opening, oxidation, and/or the breaking down of molecules [147]. Biological chitosan was used to chelate ZnO NPs for the photocatalytic breakdown of Cr(VI) [198], whereas cellulose-stabilized ZnO NPs have been observed to completely degrade both phenol and MO after 9 h [188].

4.2. Adsorption of Heavy Metals and Organic Dyes

Adsorption is renowned for its simplicity and its versatility, and it can remove contaminants, whether in trace amounts or high concentrations, from wastewater [200]. Adsorption depends on the surface area and the type of adsorbate as well as the conditions under which adsorption is taking place [201]. The operation conditions (pH, temperature, contact time, and so on.) influence the surface charge of the adsorbent and the target pollutant, and as such, they provide a tailored adsorbent surface to target specific contaminants. During the adsorption process, the adhesion of adsorbates or pollutants to reactive sites on the adsorbent surface takes place through either physisorption or chemisorption [4]. ZnO nanoadsorbents are suitable candidates for removing pollutants from water because they are environmentally friendly, cost-efficient, and biocompatible [202]. Mahdavi et al. state that ZnO NPs are potential adsorbents due to their high adsorption capacity [203]. Non-functionalized wurtzite ZnO NPs bear a positive charge; however, the surface functionalization that takes place during biogenic synthesis results in NPs with negatively charged surfaces; this is due to the negatively charged functional groups [204]. Electrostatic attraction occurs between these negatively charged surfaces and positively charged pollutants, as indicated in Figure 12a. The mechanism of ZnO nanoadsorbents, with regard to dye removal, depends on the surface charge of the dye. It can be characterized using a point of zero charge (pH_{pzc}). For instance, [205] discovered that the pH_{pzc} of *Ocimum sanctum* which stabilized the ZnO nanoadsorbents was pH 6.2; therefore, if the pH was above 6.2, the surfaces of the ZnO NPs were negatively charged, thus resulting in electrostatic

repulsion with the anionic Congo Red dye molecules, but when the pH was below the pH_{pzc} , the surface of ZnO NPs was positively charged. The strong electrostatic interactions between ZnO NPs and anionic dye molecules are shown in Figure 12b. Nanostructure aggregates are superior nanoadsorbents to simple nanopowders because of their high porosity and ease of separation from a solution [206].

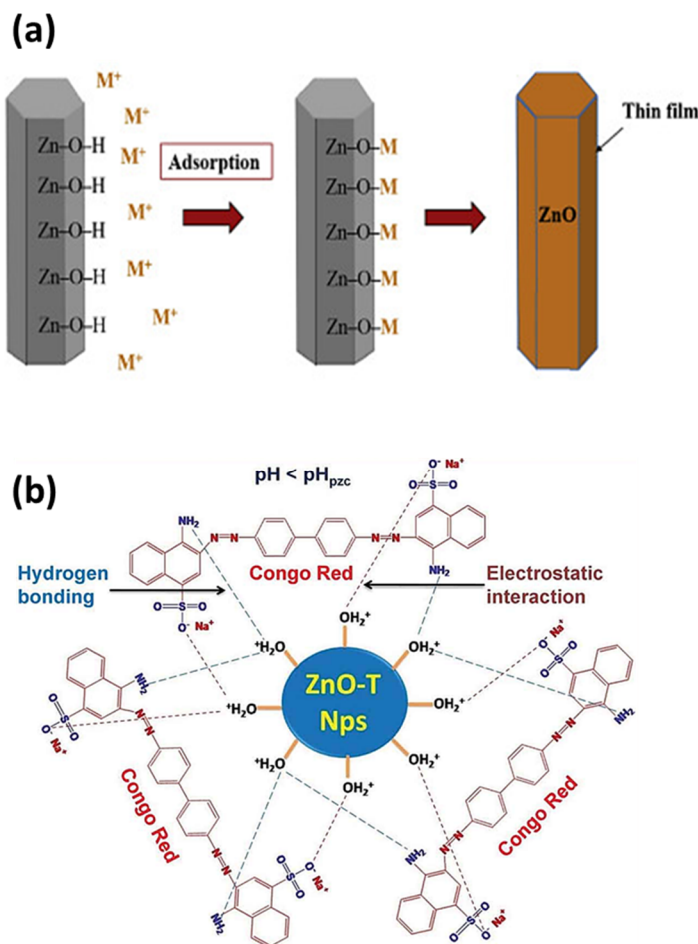


Figure 12. Mechanisms for HM ion adsorption with ZnO NPs: (a) adsorption (reprinted with permission from Ref. [207], © 2019 Elsevier Ltd); (b) schematic representation of the adsorption mechanism of Congo red onto ZnO-T nanoparticles (reprinted with permission from Ref. [205], © Taylor & Francis Ltd.).

Adsorption isotherms are crucial for explaining the process of distribution concerning the adsorbates between the solid and liquid phases. The parameters of isotherm models are generally used to determine the adsorption capacity of adsorbents, and the suitability of adsorption under a batch system [208]. The adsorption of HM ions such as Cr⁶⁺, Hg²⁺, Cd²⁺, Co²⁺, and Pb²⁺ using ZnO is best explained with the Langmuir isotherm. This suggests that the HM ions are distributed homogeneously on the ZnO adsorbent, which subsequently forms a monolayer. Modifying ZnO via doping and surface functionalization alters the isotherm model to Freundlich, Dubinin–Radushkevich (pore filling), and Redlich–Peterson (features of Langmuir and Freundlich) isotherms for Cd²⁺, Co²⁺, Cr⁶⁺, and Pb²⁺. In most cases, ZnO nanoadsorbents follow pseudo-second-order (PSO) kinetics, thus suggesting that chemical interactions between the contaminants and the ZnO adsorbent are favored [209].

4.2.1. Heavy Metal Adsorption Using ZnO NPs

Biosynthesized ZnO NPs have been applied in order to remove heavy metals. The natural occurrence of hexavalent chromium (Cr(VI)) is not common; therefore, the main contributors to Cr(VI) pollution are industrial processes [210]. An excess of the Cr(VI) ion in water causes respiratory tract irritation, different types of cancers, and even death; therefore, it is imperative to eradicate Cr(VI) from wastewater before it is discharged into the environment. When used with a 25 mg/L pollutant, guar gum biosynthesized ZnO NPs and removed Cr(VI) with a 98.63% removal efficiency (RE) and a 55.56 mg/g adsorption capacity. Most importantly, optimal adsorption occurred at pH 7, which is the natural pH of natural water in bodies [211]. *Parthenium hysterophorus* L. activated carbon-prepared ZnO NPs, and 1000 mg/L Cr(VI) at pH 4 was removed with a 98.8% removal efficiency over 180 min. MB was removed from industrial wastewater with the same nanoadsorbent over 150 min [212]. A lead ion (Pb^{2+}) is a very toxic HM. Pb^{2+} exposure has the potential to induce gastrointestinal, cardiovascular, neurological, hematological, and renal problems [213]. As a result, the World Health Organization (WHO) requires that the content of Pb^{2+} in industrial effluents is reduced to an acceptable level (0.01 mg/L) [214]. Somu and Paul prepared ZnO NPs, using casein as a reducing agent, and reported a 95.3% RE with (2 g/L) ZnO NPs in 100 mL water with 100 ppm Pd^{2+} at pH 8 over 120 min [215]. Based on the Langmuir model, the maximal adsorption capacity was 194.93 mg/g. This adsorption capacity was higher than the 3.41 mg/g reported by [216], wherein the NPs were reduced and stabilized with *Mangifera indica* leaves at pH 6 in 50 min. When *Shorea robusta* capped NPs were employed for the removal of Pb^{2+} , with 0.8 g adsorbed in 1000 mg/L pollutant at pH 6, the RE was 92.9% [208]. Table 6 presents a summary of the reported adsorption activities of ZnO nanoparticles synthesized from various biological sources.

Cd^{2+} is another extremely poisonous HM. The set maximum limit of Cd^{2+} in drinking water is 0.003 $\mu\text{g/L}$ [214]. Excess Cd^{2+} consumption causes high blood pressure, bone marrow malignancy, renal damage, gastrointestinal issues, and an increased chance of stillbirth, among other problems [217]. In a casein-based ZnO nanoadsorbent, the adsorptive capacity of Cd^{2+} was found to be 156.74 mg/g with an 85.63% RE [215]. Joshi and Singh [208] reported an RE of 84.6% within 50 min when removing Cd^{2+} from water containing 50 mg/L of the pollutant and 1 g of the nanoadsorbent at pH 6. The RE reported by [216] when the adsorbent was synthesized with *Shorea robusta* (leaf) was 89.9% at pH 6 with a pollutant concentration of 1000 mg/L.

4.2.2. Adsorption of Organic Dyes Using ZnO NPs

ZnO NPs synthesized with leaf extracts of *Hibiscus rosa-sinensis* were utilized in the removal of Congo red (CR) from water. The optimum adsorption occurred when 4 mg/L of the dye was used, the adsorbent dosage was 0.05 g, and at pH 4. [218]; however, *Ocimum sanctum* leaf extract prepared with ZnO removed CR at an adsorbent dosage of 0.2 g/L concentration and at pH 4, with a removal efficiency of 97% and a 74.07 mg/g adsorption capacity [205]. Curcumin-conjugated ZnO NPs were synthesized in [219] for CR removal, and it was discovered that the addition of KOH to the reaction media improved the stability of the formed nanoparticles. Moreover, the addition of chitosan further enhanced the NPs' stability with only a 10% loss in mass. The registered adsorption capacity of Zn(Cur)O was 89.85 mg/g, and the pseudo-second-order model was followed. *Aloe vera*-stabilized ZnO nanosheets removed 76.73% of the initial MG dye concentration after 180 min, whereas the adsorption kinetics fitted a pseudo-first-order model with an r^2 factor of 0.98984 [220]. Gum Arabic-grafted polyacrylamide (GA-cl-PAM) served as a self-template for the in-situ synthesis of ZnO NPs in order to remove MG from an aqueous solution. The nanocomposite adsorbed ~99% MG dye with a 0.4 g/L adsorbent dose at a neutral pH. A high adsorption capacity of 766.52 mg of dye per gram of adsorbent was attained at 25 °C [221]. An aqueous leaf extract of *Becium grandiflorum* was used in the friendly synthesis of ZnO NPs. The reported MB removal efficiency was 71.53% when both the adsorbent mass and dye concentration was 25 mg/L. The synthesized NPs showed an adsorption capacity

of 143.6 mg/g after 180 min [222]. Sawdust-derived cellulose nanocrystals, incorporated with ZnO NPs, were prepared in [223] at pH 4 in order to act as an adsorbent for MB removal. The MB adsorption was better characterized by the Langmuir isotherm which registered an adsorption capacity of 64.93 mg/g after 12 h. ZnO NPs were impregnated into *Ananas comosus* waste (Acp) for the adsorption of Celestine Blue (CEB), a dye that is used in the nuclear and textile industries. The adsorption process was best characterized by the Langmuir and pseudo-second-order models ($R^2 > 0.9518$). The biomass enhanced the process and exhibited endothermic characteristics. An RE of 70.2% was recorded at pH 9 after 120 min of reaction [224].

Table 6. Summary of the reported adsorption activities of ZnO nanoparticles synthesized from various biological sources.

Name of Biological Source	Morphology of ZnO	Pollutant	Concentration of Adsorbent	Concentration of Pollutant	Time (min)	pH	Removal Efficiency (%)	Isotherm Model	Adsorption Capacity (mg/g)	Ref.
Heavy metals										
Guar gum	Spherical	Cr (VI)	1.0 g	25 mg/L	50	7	98.63	Freundlich	55.56	[211]
<i>Parthenium hysterophorus</i> L.	Hexagonal and spherical	Cr (VI)	50 mg/L	100 mg/L	180	4	98.8		–	[212]
		MB			150	6				
Ceisen	Quasi-spherical	Cd	(2 g/L)/100 mL	50–500 mg/L	120	7	85.63	Langmuir	156.74	[215]
		Co					71.23		67.93	
		Pb					95.33		194.93	
<i>Mangifera indica</i> (leaves)	Semi-spherical	Cu ²⁺	1.0 g	50 mg/L	50	6	89.1	Freundlich	2.35	[208]
		Pb ²⁺					92.1		3.41	
		Cd ²⁺					84.6		2.65	
<i>Shorea robusta</i> (Leaf)	Smaller clusters	Pb ²⁺	0.8 g	1000 mg/L	50	6	92.9			[216]
		Cd ²⁺					89.9			
Organic dyes										
<i>Hibiscus rosa-sinensis</i> .	Spherical, cubic, and hexagonal	CR	0.05 g	4 mg/L	20	4	95.55	Langmuir		[218]
<i>Ocimum sanctum</i> (leaf)	Spherical	CR	0.2 g	40 mg/l	30	4	97	Langmuir	74.07	[205]
Cucumin	Spherical	CR	0.15 g	11.15 mg/L	24 h	–	–		89.85	[219]
<i>Aloe vera</i> (Leaf)	Nanosheets	MG	10 mg/500 mL	10 mg/L	180	–	76.23			[220]
Gum Arabic	Flower-like	MG	0.4 g/L	50–800 mg/L	60	7	99		766.52	[221]
<i>Becium grandiflorum</i> (Leaf)	Spherical	MB	25 mg/L	25 mg/L,	180	–	71.53		143.6	[222]
Cellulose	Spherical	MB	0.15	100 mg/L	1440	4	97.5	Langmuir	64.93	[223]
<i>Ananas comosus</i>	Irregular	Celestine blue (CEB)	0.15	50 mg/L	120	9	70.2	Langmuir	6.52	[224]

4.3. Antimicrobial Activity of ZnO NPs

Microorganism-infested bodies of water are the main sources of infectious diseases affecting people and animals. The infectious microorganisms are bacteria, fungi, algae, viruses, and parasitic protozoans. Antimicrobial activity refers to the ability of a material to either kill microbes or inhibit the growth of infectious agents and antimicrobial agents [7]. Green-synthesized antimicrobial nanomaterials meet this criterion, and they have the added advantage of being non-toxic to living organisms. These green synthesized nanomaterials, such as ZnO, owe their non-toxicity to their small size, which favors internalization into the cells of microorganisms [225]. In addition, the residual surface functional groups comprising the biological capping agents may imbue the ZnO with enhanced capabilities to attach onto the cell walls/cell membranes of the disease-causing microorganisms.

The reaction mechanisms of ZnO NPs, regarding their function as antimicrobial agents, are broadly classified into three types: (1) the generation of ROS via photocatalysis, as

discussed in Section 4.1; (2) the dissolution of ZnO NPs into Zn^{2+} ; and (3) the direct interaction between ZnO NPs and cell membranes. Generation of ROS within and in the periphery of the bacterial cell is arguably the main contributor to antibacterial activities as shown in Figure 13a. In addition, the H_2O_2 generated during photocatalysis penetrates the bacterial cell membrane and damages organelles through the hydrolysis of the constituent molecules such as lipids, proteins, and DNA, thus causing cell lysis [49] (Figure 13b). With respect to the dissolution of ZnO, studies suggest that the dissolution of Zn^{2+} is caused by size and morphology; indeed, morphologies that offer a large surface area, such as nanosheets and nanorods, have a greater surface area that is in contact with the water, and therefore, they can release the Zn^{2+} ion more quickly (Figure 13c). The better morphologies for use as bactericides therefore tend to be smaller nanoparticles. Secondly, the ZnO NPs with a large, exposed surface area easily penetrate bacterial cells and tamper with active transport and enzyme activity, thereby inhibiting the growth of the bacteria [226] (Figure 13a). Moreover, a large number of NPs is required to envelope a bacterial colony, which leads to innumerable ROSs [227]. With respect to the direct interactions between ZnO NPs and cell membranes, Stoimenov et al. [228] concluded that Gram-negative bacteria are more susceptible to inactivation by ZnO NPs because they harbor an overall negative charge due to the presence of the $-COOH$ and $-OH$ groups on their cell walls. ZnO NPs, on the other hand, have a positive charge when placed in an aqueous medium due to the fact that they become partially dissolved. These opposite charges encourage electrostatic interactions (Figure 13d) that damage the plasma membrane and cause a leakage of organelles. Furthermore, the build-up of ZnO NPs in the cytoplasm disrupt bacterial metabolic activities, thus leading to their inactivation.

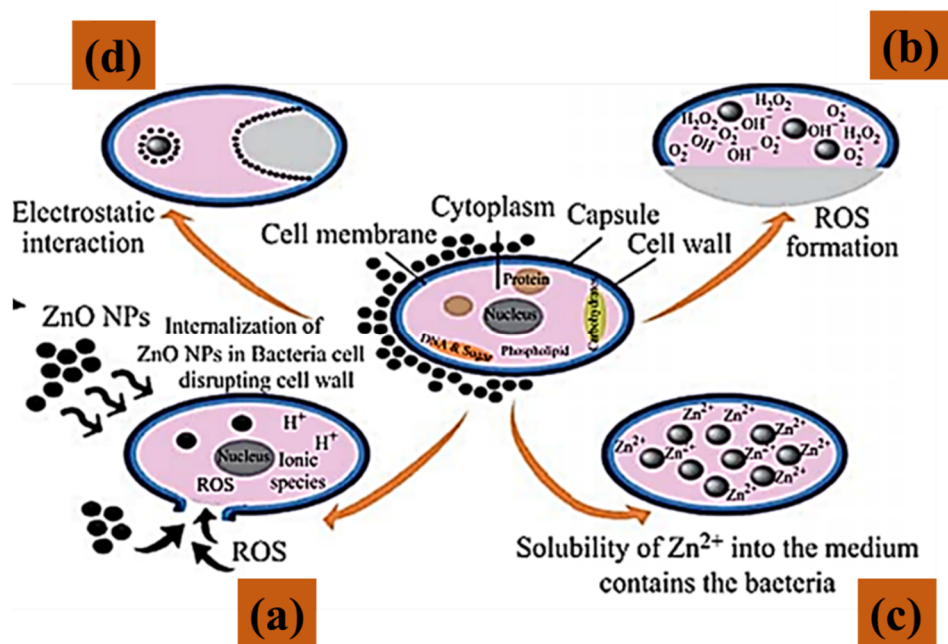


Figure 13. A schematic representation of the ZnO NPs' antimicrobial mechanism against bacteria [49].

4.3.1. Antibacterial Activity of Biologically Prepared ZnO NPs

The antibacterial activity of biogenic ZnO NPs is not exempt from the selectivity of conventionally synthesized ZnO NPs with regard to its use in Gram-negative bacteria. This is because Gram-positive bacteria are more resistant due to their thick peptidoglycan layer around the cell walls. Moreover, the electrostatic interactions that exist between the positively charged Zn^{2+} and the negatively charged surfaces of the Gram-negative bacteria promote the penetration of Zn^{2+} NPs into Gram-negative bacteria [169] (Figure 13c). Sharma et al. [73] prepared spherical ZnO NPs that inhibited the growth of *B. subtilis* (21.3 mm), *E. coli* (18.6 mm), *S. typhi* (20.6 mm), *Klebsiella pneumoniae* (21.6 mm), and *S.*

aureus. Rajendran et al. [100] recorded a minimum inhibitory concentration (MIC) of 157.2 µg/mL against *S. aureus* when the bacterial concentration was 1×10^5 CFU/mL and the root extract of *Rubus fairholmianus* synthesized with ZnO NPs (100 µL) was employed. The production of H₂O₂ that disturbed the lipid and protein bilayers was largely responsible for the inactivation of the bacterial cells [70,229,230] (Figure 13b). An extract from *Phoenix roebelenii* leaves was used to chelate ZnO NPs during their synthesis, the inhibition zones for which were 21.4 mm for *S. typhi*, 15.8 mm for *E. coli*, 15.1 mm for *S. pneumoniae*, and 15 mm for *S. aureus*. The prepared samples exhibited a greater antibacterial performance against Gram-negative bacteria than against Gram-positive bacteria. The extract of *Prunus dulcis* was employed by Anand and colleagues for the synthesis of ZnO NPs. The high-resolution SEM (HRSEM) showed aggregated, but homogeneous, ZnO NPs with a mean size of 25 nm. The antibacterial activity of the produced nanoparticles was evaluated using the agar diffusion technique. The green prepared ZnO NPs showed bactericidal effects on *S. aureus*, *E. coli*, and *S. paratyphi*, with zone diameters of 18 mm, 32 mm, and 25 mm, respectively. Interestingly, there was no zone of inhibition (ZOI) observed on the Gram-negative bacteria, *Klebsiella pneumoniae*, and *P. mirabilis* [231]. Table 7 summarizes recent findings on the plant-mediated production of ZnO NPs which aimed to inactivate both Gram-positive and Gram-negative bacteria.

Table 7. Summary of the reported antimicrobial activities of ZnO nanoparticles that were synthesized from various biological sources.

Source	Name/Part	ZnO Morphology	Method	Concentration of ZnO NP and Microbe	MIC (µg/mL)	Test Organism and Efficiency	Ref.
Antibacterial							
Plant	<i>Rubus fairholmianus</i> root	Spherical	Agar well diffusion	N/A 1×10^5 CFU/mL bacteria	157.22	<i>S. aureus</i>	[100]
	<i>Ficus palmata</i> .	Spherical	Agar well diffusion	N/A/ N/A	390.6	<i>S. aureus</i> (19.6 mm) <i>B. subtilis</i> (21.3 mm) <i>E. coli</i> (18.6 mm) <i>S. typhi</i> (20.6 mm) <i>K. pneumoniae</i> (21.6 mm)	[73]
	<i>Cochlospermum religiosum</i> (L.)	Hexagonal	Disc diffusion	50 µL of (100 µg) N/A N/A/ 100 µL of 1.5×10^8 CFU/mL bacteria	4.8 to 625	<i>B. subtilis</i> <i>S. aureus</i> <i>E. coli</i> <i>P. aeruginosa</i>	[229]
	<i>Vitex trifolia</i> L.	Spherical	Disc diffusion	200 µg/mL N/A	6.25–50	ZOI= <i>S. aureus</i> (22.5 mm) <i>B. subtilis</i> (21.5 mm) <i>P. aeruginosa</i> (19.8 mm) <i>P. mirabilis</i> (19.3 mm) <i>E. coli</i> (20.1 mm)	[70]
	<i>Mucuna pruriens</i>	Nano-flower-like	Broth dilution assay	100 µg/mL/ N/A	20	<i>B. subtilis</i>	[230]
	<i>Phoenix roebelenii</i>	Spherical	Agar well diffusion	0.4 mg/mL/ N/A	-	<i>S. typhi</i> (21.4 mm) <i>E. coli</i> (15.8 mm) <i>S. pneumoniae</i> (15.1 mm) <i>S. aureus</i> (15 mm)	[169]
	<i>Prunus dulcis</i>	Near spherical	Well diffusion method	N/A/ Standard inoculum	25	<i>S. aureus</i> (18 mm) <i>E. coli</i> (32 mm) <i>S. paratyphi</i> (25 mm) <i>K. pneumoniae</i> (0 nm) <i>P. mirabilis</i> (0 nm)	[231]
Algae	<i>Hypnea musciformis</i>	Spherical	Serial dilution	32 mg/mL		<i>S. aureus</i> <i>E. coli</i>	[232]

Table 7. Cont.

Source	Name/Part	ZnO Morphology	Method	Concentration of ZnO NP and Microbe	MIC ($\mu\text{g/mL}$)	Test Organism and Efficiency	Ref.
	<i>Phormidium</i> , <i>Viridiplanta</i> , and <i>Cosmarium</i> sp.	Varying shapes	Well diffusion	60 μL of	–	<i>E. coli</i> (20 mm) <i>S. aureus</i> (14.5 mm) <i>K. pneumoniae</i> (11 mm), <i>C. freundii</i> (20 mm) <i>M. luteus</i> (12 mm)	[233]
	<i>Sargassum muticum</i>		Agar well diffusion	1.5×10^8 CFU/mL	200 mg/mL	<i>P. stutzeri</i> <i>A. baumannii</i> (18 mm) <i>B. filamentous</i> <i>Bacillus flexus</i> (12 mm)	[234]
Fungi	<i>Aspergillus fumigatus</i>		Well diffusion	1000 $\mu\text{g/mL}$	–	<i>K. pneumoniae</i> (30 mm) <i>P. aeruginosa</i> (27 mm) <i>E. coli</i> (25 mm) <i>S. aureus</i> (30 mm) <i>B. subtilis</i> (20 mm)	[132]
	<i>Pichia kudriavzevii</i>	Hexagonal	Disc diffusion	100 $\mu\text{g/mL}$	–	<i>B. subtilis</i> (19 mm) <i>S. epidermidis</i> (9 mm) <i>S. aureus</i> (10 mm) <i>E. coli</i> (10 mm) <i>S. marcescens</i> (mm)	[136]
	<i>Saccharomyces cerevisiae</i>	Spherical	Colony forming units	100 $\mu\text{g/mL}$ 10^8 CFU/mL <i>E. coli</i>		<i>E. coli</i>	[196]
Biological derivatives	Lignin	Litchi-like	Optical density	200 $\mu\text{g/mL}$	100 lg/mL	Inactivation of <i>E. coli</i> (97.54%) <i>S. aureus</i> (99.55%)	[157]
	Crustin	Spherical	Agar well diffusion	50 $\mu\text{g/mL}$	–	The inhibition zone for <i>S. mutans</i> (9.5 mm) <i>L. fusiformis</i> (4.5 mm) <i>Proteus vulgaris</i> 6.1 mm, <i>A. hydrophila</i> (7.2 mm)	[151]
	Honey and cow urine	Hexagonal and leaf-like	Dilution and plate count	1×10^8 CFU/mL	–	<i>E. coli</i> <i>B. subtilis</i>	[154]
	Chitosan	Rods	Disc diffusion	40 $\mu\text{g/mL}$ 10^5 CFU/mL bacteria	–	<i>E. coli</i> (25.5 mm) <i>K.pneumoniae</i> (24.5 mm) <i>S. aureus</i> (22.5 mm) <i>B. subtilis</i> (21 mm)	[171]
Antifungal							
	<i>Pithecellobium dulce</i> (peel)	Spherical	Broth dilution	1000 mg/L ZnO 10 mL of nutrient potato dextrose agar/1 mL of fungal stains.	–	Growth inhibition <i>A. flavus</i> (63.57%) <i>A. niger</i> (57.17)	[83]
Plant	<i>Capparis zeylanica</i>	Spherical	Well diffusion	100 $\mu\text{g/mL}$	–	ZOI= <i>C. albicans</i> (30 mm) <i>A. niger</i> (12 mm)	[91]
	<i>Bixa orellana</i>	Spherical Almond-shaped	Well diffusion	10 mg/mL 10^4 – 10^5 CFU/mL (100 μL fungal spores)	–	<i>Penicillium</i> sp. <i>Aspergillus flavus</i> <i>Fusarium oxysporum</i> , <i>Rhizoctonia solani</i>	[235]
	Gelatin	Spherical	Light microscopy	50 $\mu\text{g/mL}$	–	<i>C. albicans</i>	[62]
	Bacterial cellulose with propolis	Irregular	Disc diffusion	0.4987/143 mL	0.438 mg/mL	<i>C. albicans</i>	[236]

Bacteria have also been inactivated by algae-synthesized ZnO NPs [232,233]. When Debnath et al. [218] prepared spherical *Hypnea musciformis*-capped ZnO NPs, the growth of *S. aureus* and *E. coli* was inhibited via ROS generation on the surface of the NPs and the interactions between zinc and the cell membranes of bacteria through the adhesion of ZnO NPs. Jamil et al. [233] inhibited the growth of *E. coli* (20 mm), *S. aureus* (14.5 mm),

Klebsiella pneumoniae (11 mm), *C. freundii* (20 mm), and *M. luteus* (12 mm) by capping the NPs with *Phormidium* sp., *Viridiplantae* sp., and *Cosmarium* sp. When an aqueous extract from *Sargassum muticum* was used as a bioreducing reagent for the preparation of ZnO NPs, the obtained NPs showed enhanced antibacterial activity against Gram-negative, drug-resistant *Pseudomonas stutzeri* and *Acinetobacter baumannii*, when compared with the antibacterial activity against Gram-positive *Bacillus filamentosus* and *Bacillus flexus*. This is because the cell walls of the Gram-positive bacteria are complex and they have a very thick peptidoglycan that restricts the NPs from entering the bacterial cells [234].

The fungal-mediated synthesis of ZnO NPs that are active against bacteria has been reported, and the findings are summarized in Table 7. *Aspergillus fumigatus* synthesized ZnO NPs are used for eradicating *Klebsiella pneumoniae* (30 mm), *P. aeruginosa* (27 mm), *E. coli* (25 mm), *S. aureus* (30 mm), and *B. subtilis* (20 mm) when following a well diffusion method [126]. The bactericidal activity of *Pichia kudriavzevii*-capped ZnO NPs on both Gram-positive bacteria (*B. subtilis*, *S. epidermidis* and *S. aureus*) and Gram-negative bacteria (*E. coli* and *Serratia marcescens*) was reported. A zone of inhibition (~19 mm) was observed for *S. epidermidis* at a concentration of 100 µg/mL (ZnO NPs) for a sample prepared at RT for over 4 h [130]. Spherical ZnO NPs, stabilized with *Saccharomyces cerevisiae*, were reported to kill *E. coli* [196]. Results on the bactericidal activity of biological derivatives that mediated ZnO have been amply reported [151,157,171] and are summarized in Table 7.

4.3.2. Antifungal Activity of ZnO NPs

Phyto-mediated ZnO NPs that exhibited antifungal activity were reported by Madhumitha, who prepared ZnO NPs from the peels of *Pithecellobium dulce*, using a broth dilution procedure in order to inhibit the growth of *A. flavus* and *A. niger* with 63.57% and 57.17% efficiency, respectively, when the NP concentration was 1000 mg/L [83]. Nilavukkarasi et al. [91] used a *Capparis zeylanica* leaf extract to cap NPs, and they incorporated 100 µg/mL ZnO NPs using a well diffusion method to inactivate *C. albicans* and *A. niger*. Moreover, they realized that the zone of inhibition was 30 mm and 12 mm for *C. albicans* and *A. niger* after 24 h, respectively. The fungi were killed by oxidative stress, which resulted in cell death by apoptosis. Spherical and almond shaped ZnO NPs were attained by using different parts of *Bixa orellana*. These ZnO NPs demonstrated antifungal activity against *Penicillium* sp., *Aspergillus flavus*, *Fusarium oxysporum*, and *Rhizoctonia solani* [235]. Gelatin-coated ZnO NPs were synthesized via co-precipitation, which effectively inhibited the biofilm growth of the fungus *Candida albicans* at 50 µg/mL [62]. ZnO NPs were produced on the surface of bacterial cellulose (BC) films with the aid of an ultrasound. These were later impregnated with the extracts of ethanolic propolis (EEP). The BC-ZnO-100US film exhibited an MIC value of 1.3 mg/mL against *C. albicans*. Propolis' antibacterial efficacy was shown to be reliant on the presence of phenolic chemicals, such as flavonoids, which allow the nanomaterial to break down fungal cell membranes, thus resulting in a loss of K⁺ and subsequent cell autolysis [236].

5. Conclusions

The attainment of ZnO NPs via the green protocol has been a focal point for research in recent times. Green sources, such as plants, bacteria, fungi, and algae, operate as both reducing and stabilizing agents to regulate the morphologies of the NPs. This review has provided insights on green synthesis and its advantages over traditional synthesis techniques. Recent advances in the biosynthesis of ZnO NPs, which uses plants, bacteria, fungus, and algae, show the ability of biosynthesis protocols to produce nanoparticles in the same size range as ZnO NPs that are synthesized using conventional chemical synthesis procedures. The morphology and particle size are shown to depend on factors such as reaction time, pH, temperature, and the biogenic precursor used. The key characterization techniques investigate the structural and chemical properties of the biosynthesized ZnO NPs and most importantly, the crystallinity. Furthermore, the use of the produced ZnO NPs for water treatment and disinfection were also explored. In retrospect, green, synthetic

approaches for ZnO NPs have, so far, managed to satisfactorily meet five of the twelve pillars of green synthesis. These pillars include the use of readily available precursors; the avoidance of the use of derivatives such as stabilizers; the employment of ecofriendly solvents; and the use of harmless chemicals to evade toxicity. In place of chemical stabilizers and solvents, it is evident that natural metabolites (plant, bacterial, and fungal) are able to satisfactorily be used as stabilizers, capping agents, and reducing agents. Indeed, the particle sizes for the ZnO NPs that are manufactured using green, synthetic approaches are comparable to the ZnO NPs that are synthesized using conventional approaches. There is still a great deal of research that needs to be undertaken in order to create greener ZnO green synthesis approaches with respect to the atom economy and reducing energy expenditure during synthesis. A great deal of progress has been made with regard to the reduction of energy requirements when formulating microbe-mediated, greener approaches, as shown by the elimination of post-synthesis calcination, albeit with less crystalline ZnO; however, this progress is unsatisfactory.

6. Future Perspectives

- The likelihood of integrating cheap, readily available biological sources with one another, and gaining control of the parameters concerning environmentally benign syntheses, justifies a future focus on the sustainable and scalable production of ZnO NPs; however, to completely maximize and make use of the advantages that biogenic ZnONPs provide, several areas need more research to enable a better understanding of the topic.
- As there are few studies on ZnO nanomaterial synthesis using microorganisms, biopolymers, marine fungi, algae, and waste materials, there exists a need for further exploration into biogenic synthesis protocols, largely because it offers more advantages over conventional chemical and physical synthesis.
- It is difficult to use ZnO NPs for biosynthesis on an industrial level as the underlying reaction mechanisms and kinetics of the process are not yet fully understood, especially microbial synthesis processes. Currently, reproducing bio-prepared NPs is difficult and may be time consuming because the mechanisms are insufficiently understood. The development of predictable synthesis protocols thus remains a challenge.
- A thorough understanding of the manner in which the most active of the bioprecursors that cap and reduce the nanomaterials are isolated and traced, in addition to an understanding of their structure, is necessary. Understanding the structure and chemistry of the reducing agents will speed up the commercialization of the green synthesis protocol. Moreover, the green protocol method must be explored in greater depth in order to understand the effects of the various biological extracts on the surface of ZnO, and to understand the deep level defects that occur, especially with respect to the photocatalytic break down of pollutants. Understanding this critical information may assist in eliminating the need to anneal the resultant samples, which consumes a great deal of energy.
- The manner in which the yield of the ZnO NPs corresponds with the precursors has not been reported, and process cost comparisons between biologically synthesized NPs and traditionally produced NPs have not been reported on as the former has not yet been upscaled. Understanding how the yield corresponds with the precursors should be a priority in order to obtain realistic expectations regarding this synthesis protocol. This requires a full understanding of the life cycle of specific bioprecursors in order to ensure continuous availability. This should prevent the production of the material from stopping or from being significantly reduced once the commercialization of green synthesis has been fully adopted. Such studies would also enable biosynthesis protocols to improve the atom economy in synthetic processes, thus meeting another pillar of green synthesis.

The eventual release of a high concentration of the green synthesized ZnO NPs into bodies of water would likely be toxic; therefore, it is imperative that these NPs are embed-

ded onto solid substrates that can easily be separated from bodies of water. Furthermore, the toxicity of the NPs should not only be studied *in vitro*, but also *in vivo*, in order to obtain a comprehensible idea of the material's toxicity on living things. Lastly, ZnO, being an amphoteric oxide, is soluble in water at extreme pH levels, thus the Zn²⁺ ion can be placed in water. There is a need to investigate the influence of biosynthetic approaches on the stabilization of ZnO NPs with a range of pH levels.

Author Contributions: All the listed authors contributed to the writing of the review manuscript. N.E.Z.—wrote prepared the original draft, reviewed, and edited the manuscript as advised; S.A.Z.—contributed on the manuscript drafting, reviewed, and edited the whole document; S.A.—Supervised the work, sourced the funding, I.K.—Read, reviewed, and edited the manuscript; A.A.Z.—Reviewed and edited the document; M.M.—Supervised, provided funding, and reviewed the document; K.K.—Visualization and Validation, and edited the manuscript, T.M.—Visualization and edited the manuscript. All authors have read and agreed to the published version of the manuscript.

Funding: This work is supported by the SASOL-NRF University Collaborative Research Grant (No. 138626).

Data Availability Statement: Not applicable.

Acknowledgments: The authors are grateful to SASOL-NRF University Collaborative Research Grants (Grant No. 138626) and to the Unesco-Unisa Africa Chair for Nanoscience and nanotechnology for their support.

Conflicts of Interest: The authors declare no conflict of interests.

References

1. Herrmann, S.; De Matteis, L.; de la Fuente, J.M.; Mitchell, S.G.; Streb, C. Removal of Multiple Contaminants from Water by Polyoxometalate Supported Ionic Liquid Phases (POM-SILPs). *Angew. Chem.-Int. Ed.* **2017**, *56*, 1667–1670. [[CrossRef](#)]
2. Sun, H.; Cao, L.; Lu, L. Magnetite/Reduced Graphene Oxide Nanocomposites: One Step Solvothermal Synthesis and Use as a Novel Platform for Removal of Dye Pollutants. *Nano Res.* **2011**, *4*, 550–562. [[CrossRef](#)]
3. Mok, C.F.; Ching, Y.C.; Muhamad, F.; Abu Osman, N.A.; Hai, N.D.; Che Hassan, C.R. Adsorption of Dyes Using Poly(Vinyl Alcohol) (PVA) and PVA-Based Polymer Composite Adsorbents: A Review. *J. Polym. Environ.* **2020**, *28*, 775–793. [[CrossRef](#)]
4. Dhiman, V.; Kondal, N. ZnO Nano-adsorbents: A Potent Material for Removal of Heavy Metal Ions from Wastewater. *Colloids Interface Sci. Commun.* **2021**, *41*, 100380. [[CrossRef](#)]
5. Ashbolt, N.J. Microbial Contamination of Drinking Water and Human Health from Community Water Systems. *Curr. Environ. Heal. Rep.* **2015**, *2*, 95–106. [[CrossRef](#)] [[PubMed](#)]
6. Roberts, K.; Alberts, B.; Johnson, A.; Lewis, J.; Raff, M.; Walter, P.; Edition, F.; Roberts, K.; Alberts, B.; Johnson, A.; et al. *Molecular Biology of the Cell, Fourth Edition Description*, 6th ed.; W.W. Norton & Company: Boca Raton, FL, USA, 2017; ISBN 9781315735368.
7. Prasad, A.R.; Williams, L.; Garvasis, J.; Shamsheera, K.O.; Basheer, S.M.; Kuruvilla, M.; Joseph, A. Applications of Phyto-genic ZnO Nanoparticles: A Review on Recent Advancements. *J. Mol. Liq.* **2021**, *331*, 115805. [[CrossRef](#)]
8. Oluwafemi, O.S.; Anyik, J.L.; Zikalala, N.E.; Sakho, E.H.M. Biosynthesis of Silver Nanoparticles from Water Hyacinth Plant Leaves Extract for Colourimetric Sensing of Heavy Metals. *Nano-Struct. Nano-Objects* **2019**, *20*, 7–9. [[CrossRef](#)]
9. Singh, A.K.; Srivastava, O.N. One-Step Green Synthesis of Gold Nanoparticles Using Black Cardamom and Effect of pH on Its Synthesis. *Nanoscale Res. Lett.* **2015**, *10*, 1–12. [[CrossRef](#)]
10. Akintelu, S.A.; Folorunso, A.S.; Folorunso, F.A.; Oyebamiji, A.K. Green Synthesis of Copper Oxide Nanoparticles for Biomedical Application and Environmental Remediation. *Heliyon* **2020**, *6*, e04508. [[CrossRef](#)]
11. Zikalala, S.A.; Kuvarega, A.T.; Mamba, B.B.; Mhlanga, S.D.; Nxumalo, E.N. The Effect of Synthetic Routes on the Physicochemical Properties and Optical Response of N-Doped Titania–Oxidized Carbon Nanotube Nanohybrids. *Mater. Today Chem.* **2018**, *10*, 1–18. [[CrossRef](#)]
12. Ling, D.; Lee, N.; Hyeon, T. Chemical Synthesis and Assembly of Uniformly Sized Iron Oxide Nanoparticles for Medical Applications. *Acc. Chem. Res.* **2015**, *48*, 1276–1285. [[CrossRef](#)] [[PubMed](#)]
13. Kuriganova, A.B.; Vlaic, C.A.; Ivanov, S.; Leontyeva, D.V.; Bund, A.; Smirnova, N.V. Electrochemical Dispersion Method for the Synthesis of SnO₂ as Anode Material for Lithium Ion Batteries. *J. Appl. Electrochem.* **2016**, *46*, 527–538. [[CrossRef](#)]
14. Sobhani-Nasab, A.; Behpour, M. Synthesis and Characterization of AgO Nanostructures by Precipitation Method and Its Photocatalyst Application. *J. Mater. Sci. Mater. Electron.* **2016**, *27*, 1191–1196. [[CrossRef](#)]
15. Siddiqui, H.; Qureshi, M.S.; Haque, F.Z. Surfactant Assisted Wet Chemical Synthesis of Copper Oxide (CuO) Nanostructures and Their Spectroscopic Analysis. *Optik* **2016**, *127*, 2740–2747. [[CrossRef](#)]

16. Sahu, K.; Choudhary, S.; Singh, J.; Kuriakose, S.; Singhal, R.; Mohapatra, S. Facile Wet Chemical Synthesis of ZnO Nanosheets: Effects of Counter Ions on the Morphological, Structural, Optical and Photocatalytic Properties. *Ceram. Int.* **2018**, *44*, 23094–23101. [[CrossRef](#)]
17. Champi, A.; Marques, F.C. Structural Changes in Amorphous Carbon Nitride Films Due to Bias Voltage. *Thin Solid Film.* **2006**, *501*, 362–365. [[CrossRef](#)]
18. Aminuzzaman, M.; Ying, L.P.; Goh, W.S.; Watanabe, A. Green Synthesis of Zinc Oxide Nanoparticles Using Aqueous Extract of *Garcinia mangostana* Fruit Pericarp and Their Photocatalytic Activity. *Bull. Mater. Sci.* **2018**, *41*, 1–10. [[CrossRef](#)]
19. Janotti, A.; Van De Walle, C.G. Fundamentals of Zinc Oxide as a Semiconductor. *Rep. Prog. Phys.* **2009**, *72*, 12–15. [[CrossRef](#)]
20. Xu, S.; Weintraub, B.; Wang, Z.L. *Zinc Oxide Nanowire Arrays on Flexible Substrates. Wet Chemical Growth and Applications in Energy Conversion*, 1st ed.; Elsevier Ltd.: Amsterdam, The Netherlands, 2010; ISBN 9781437778236.
21. Ayoub, I.; Kumar, V.; Abolhassani, R.; Sehgal, R.; Sharma, V.; Sehgal, R.; Swart, H.C.; Mishra, Y.K. Advances in ZnO: Manipulation of Defects for Enhancing Their Technological Potentials. *Nanotechnol. Rev.* **2022**, *11*, 575–619. [[CrossRef](#)]
22. Adeyemi, J.O.; Elemike, E.E.; Onwudiwe, D.C. ZnO Nanoparticles Mediated by Aqueous Extracts of *Dovyalis Caffra* Fruits and the Photocatalytic Evaluations. *Mater. Res. Express* **2019**, *6*, 11–14. [[CrossRef](#)]
23. Narendra Kumar, H.K.; Chandra Mohana, N.; Nuthan, B.R.; Ramesha, K.P.; Rakshith, D.; Geetha, N.; Satish, S. Phyto-Mediated Synthesis of Zinc Oxide Nanoparticles Using Aqueous Plant Extract of *Ocimum americanum* and Evaluation of Its Bioactivity. *SN Appl. Sci.* **2019**, *1*, 1–9. [[CrossRef](#)]
24. Awwad, A.M.; Albiss, B.; Ahmad, A.L. Green Synthesis, Characterization and Optical Properties of Zinc Oxide Nanosheets Using *Olea europea* Leaf Extract. *Adv. Mater. Lett.* **2014**, *5*, 520–524. [[CrossRef](#)]
25. Shabaani, M.; Rahaiee, S.; Zare, M.; Jafari, S.M. Green Synthesis of ZnO Nanoparticles Using Loquat Seed Extract; Biological Functions and Photocatalytic Degradation Properties. *LWT* **2020**, *134*, 110133. [[CrossRef](#)]
26. Rajabairavi, N.; Raju, C.S.; Karthikeyan, C.; Varutharaju, K.; Nethaji, S.; Hameed, A.S.H.; Shajahan, A. Biosynthesis of Novel Zinc Oxide Nanoparticles (ZnO NPs) Using Endophytic Bacteria *Sphingobacterium thalpophilum*. *Springer Proc. Phys.* **2017**, *189*, 245–254. [[CrossRef](#)]
27. Wu, J.; Yin, C.; Zhou, J.; Li, H.; Liu, Y.; Shen, Y.; Garner, S.; Fu, Y.; Duan, H. Ultrathin Glass-Based Flexible, Transparent, and Ultrasensitive Surface Acoustic Wave Humidity Sensor with ZnO Nanowires and Graphene Quantum Dots. *ACS Appl. Mater. Interfaces* **2020**, *12*, 39817–39825. [[CrossRef](#)]
28. Timerkaev, B.A.; Felsing, V.S.; Kaleeva, A.A.; Erlingayte, E.A.; Uktamov, J.A.; Nuriddinov, H.S. Plasma-Chemical Synthesis of Zinc Oxide Nanotubes. *J. Phys. Conf. Ser.* **2021**, *1870*, 012003. [[CrossRef](#)]
29. Ebadi, M.; Zolfaghari, M.R.; Aghaei, S.S.; Zargar, M.; Shafiei, M.; Zahiri, H.S.; Noghabi, K.A. A Bio-Inspired Strategy for the Synthesis of Zinc Oxide Nanoparticles (ZnO NPs) Using the Cell Extract of Cyanobacterium: *Nostoc* Sp. EA03: From Biological Function to Toxicity Evaluation. *RSC Adv.* **2019**, *9*, 23508–23525. [[CrossRef](#)]
30. Mahdi, Z.S.; Talebnia Roshan, F.; Nikzad, M.; Ezoji, H. Biosynthesis of Zinc Oxide Nanoparticles Using Bacteria: A Study on the Characterization and Application for Electrochemical Determination of Bisphenol A. *Inorg. Nano-Met. Chem.* **2021**, *51*, 1249–1257. [[CrossRef](#)]
31. Kiani, A.; Dastafkan, K. Zinc Oxide Nanocubes as a Destructive Nanoadsorbent for the Neutralization Chemistry of 2-Chloroethyl Phenyl Sulfide: A Sulfur Mustard Simulant. *J. Colloid Interface Sci.* **2016**, *478*, 271–279. [[CrossRef](#)]
32. Mustapha, S.; Ndamitso, M.M.; Abdulkareem, A.S.; Tijani, J.O.; Shuaib, D.T.; Ajala, A.O.; Mohammed, A.K. Application of TiO₂ and ZnO Nanoparticles Immobilized on Clay in Wastewater Treatment: A Review. *Appl. Water Sci.* **2020**, *10*, 1–36. [[CrossRef](#)]
33. Saeed, M.; Siddique, M.; Ibrahim, M.; Akram, N.; Usman, M.; Aleem, M.A.; Baig, A. Calotropis Gigantea Leaves Assisted Biosynthesis of ZnO and Ag@ZnO Catalysts for Degradation of Rhodamine B Dye in Aqueous Medium. *Environ. Prog. Sustain. Energy* **2020**, *39*, e13408. [[CrossRef](#)]
34. Abdelhakim, H.K.; El-Sayed, E.R.; Rashidi, F.B. Biosynthesis of Zinc Oxide Nanoparticles with Antimicrobial, Anticancer, Antioxidant and Photocatalytic Activities by the Endophytic *Alternaria tenuissima*. *J. Appl. Microbiol.* **2020**, *128*, 1634–1646. [[CrossRef](#)] [[PubMed](#)]
35. Liu, Y.; Liu, H.; Zhang, Q.; Li, T. Adjusting the Proportions of {0001} Facets and High-Index Facets of ZnO Hexagonal Prisms and Their Photocatalytic Activity. *RSC Adv.* **2017**, *7*, 3515–3520. [[CrossRef](#)]
36. Zhang, J.; Zhao, B.; Pan, Z.; Gu, M.; Punnoose, A. Synthesis of ZnO Nanoparticles with Controlled Shapes, Sizes, Aggregations, and Surface Complex Compounds for Tuning or Switching the Photoluminescence. *Cryst. Growth Des.* **2015**, *15*, 3144–3149. [[CrossRef](#)]
37. Tănase, M.A.; Marinescu, M.; Oancea, P.; Răducan, A.; Mihaescu, C.I.; Alexandrescu, E.; Nistor, C.L.; Jînga, L.I.; Dițu, L.M.; Petcu, C.; et al. Antibacterial and Photocatalytic Properties of ZnO Nanoparticles Obtained from Chemical versus *Saponaria officinalis* Extract-Mediated Synthesis. *Molecules* **2021**, *26*, 2072. [[CrossRef](#)] [[PubMed](#)]
38. Ramirez-Vick, J.E. Nanostructured ZnO for Electrochemical Biosensors. *J. Biosens. Bioelectron.* **2012**, *3*, 1. [[CrossRef](#)]
39. Rambabu, K.; Bharath, G.; Banat, F.; Show, P.L. Green Synthesis of Zinc Oxide Nanoparticles Using *Phoenix dactylifera* Waste as Bioreductant for Effective Dye Degradation and Antibacterial Performance in Wastewater Treatment. *J. Hazard. Mater.* **2021**, *402*, 123560. [[CrossRef](#)] [[PubMed](#)]
40. Sharma, S.; Kumar, K.; Thakur, N.; Chauhan, M.S. *Ocimum tenuiflorum* Leaf Extract as a Green Mediator for the Synthesis of ZnO Nanocapsules Inactivating Bacterial Pathogens. *Chem. Pap.* **2020**, *74*, 3431–3444. [[CrossRef](#)]

41. Fazlzadeh, M.; Khosravi, R.; Zarei, A. Green Synthesis of Zinc Oxide Nanoparticles Using *Peganum harmala* Seed Extract, and Loaded on *Peganum harmala* Seed Powdered Activated Carbon as New Adsorbent for Removal of Cr(VI) from Aqueous Solution. *Ecol. Eng.* **2017**, *103*, 180–190. [[CrossRef](#)]
42. Bao, S.; Hou, T.; Tan, Q.; Kong, X.; Cao, H.; He, M.; Wu, G.; Xu, B. Immobilization of Zinc Oxide Nanoparticles on Graphene Sheets for Lithium Ion Storage and Electromagnetic Microwave Absorption. *Mater. Chem. Phys.* **2020**, *245*, 1–3. [[CrossRef](#)]
43. Ren, Q.; Cao, Y.-Q.; Arulraj, D.; Liu, C.; Wu, D.; Li, W.-M.; Li, A.-D. Review—Resistive-Type Hydrogen Sensors Based on Zinc Oxide Nanostructures. *J. Electrochem. Soc.* **2020**, *167*, 067528. [[CrossRef](#)]
44. Kim, K.B.; Kim, Y.W.; Lim, S.K.; Roh, T.H.; Bang, D.Y.; Choi, S.M.; Lim, D.S.; Kim, Y.J.; Baek, S.H.; Kim, M.K.; et al. Risk Assessment of Zinc Oxide, a Cosmetic Ingredient Used as a UV Filter of Sunscreens. *J. Toxicol. Environ. Heal.-Part B Crit. Rev.* **2017**, *20*, 155–182. [[CrossRef](#)] [[PubMed](#)]
45. Khashan, K.S.; Sulaiman, G.M.; Hussain, S.A.; Marzoog, T.R.; Jabir, M.S. Synthesis, Characterization and Evaluation of Anti-Bacterial, Anti-Parasitic and Anti-Cancer Activities of Aluminum-Doped Zinc Oxide Nanoparticles. *J. Inorg. Organomet. Polym. Mater.* **2020**, *30*, 3677–3693. [[CrossRef](#)]
46. Nakano, M.; Nakagawa, S.; Sato, F.; Shahiduzzaman, M.; Karakawa, M.; Taima, T.; Takahashi, K. Study on Properties of Low-Temperature-Prepared Zinc Oxide-Based Inverted Organic Solar Cells and Improvement of Their Photodurability. *ACS Appl. Energy Mater.* **2021**, *4*, 6385–6390. [[CrossRef](#)]
47. Rafique, M.; Tahir, R.; Gillani, S.S.A.; Tahir, M.B.; Shakil, M.; Iqbal, T.; Abdellahi, M.O. Plant-Mediated Green Synthesis of Zinc Oxide Nanoparticles from *Syzygium Cumini* for Seed Germination and Wastewater Purification. *Int. J. Environ. Anal. Chem.* **2020**, *102*, 23–28. [[CrossRef](#)]
48. Bandeira, M.; Chee, B.S.; Frassini, R.; Nugent, M.; Giovanela, M.; Roeschely, M.; Crespo, J. da S.; Devine, D.M. Antimicrobial Paa/Pah Electrospun Fiber Containing Green Synthesized Zinc Oxide Nanoparticles for Wound Healing. *Matreials* **2021**, *14*, 2889. [[CrossRef](#)]
49. Sirelkhatim, A.; Mahmud, S.; Seeni, A.; Kaus, N.H.M.; Ann, L.C.; Bakhori, S.K.M.; Hasan, H.; Mohamad, D. Review on Zinc Oxide Nanoparticles: Antibacterial Activity and Toxicity Mechanism. *Nano-Micro Lett.* **2015**, *7*, 219–242. [[CrossRef](#)]
50. Jamkhande, P.G.; Ghule, N.W.; Bamer, A.H.; Kalaskar, M.G. Metal Nanoparticles Synthesis: An Overview on Methods of Preparation, Advantages and Disadvantages, and Applications. *J. Drug Deliv. Sci. Technol.* **2019**, *53*, 101174. [[CrossRef](#)]
51. Srujana, S.; Bhagat, D. Chemical—Based Synthesis of ZnO Nanoparticles and Their Applications in Agriculture. *Nanotechnol. Environ. Eng.* **2022**, *7*, 269–275. [[CrossRef](#)]
52. Naveed Ul Haq, A.; Nadhman, A.; Ullah, I.; Mustafa, G.; Yasinza, M.; Khan, I. Synthesis Approaches of Zinc Oxide Nanoparticles: The Dilemma of Ecotoxicity. *J. Nanomater.* **2017**, 1–14. [[CrossRef](#)]
53. Jose Varghese, R.; Zikalala, N.; Sakho, E.H.M.; Oluwafemi, O.S. Green Synthesis Protocol on Metal Oxide Nanoparticles Using Plant Extracts. In *Colloidal Metal Oxide Nanoparticles—Synthesis, Characterization and Applications*; Thomas, S., Sani, A.T., Velayudhan, P., Eds.; Elsevier: Amsterdam, The Netherlands, 2020; pp. 67–82; ISBN 978-0-12-813357-6.
54. Jessop, P.G.; Trakhtenberg, S.; Warner, J. The Twelve Principles of Green Chemistry. *ACS Symp. Ser.* **2009**, *1000*, 401–436. [[CrossRef](#)]
55. Rubab, L.; Anum, A.; Al-hussain, S.A.; Irfan, A.; Ahmad, S.; Ullah, S.; Al-mutairi, A.A.; Zaki, M.E.A. Green Chemistry in Organic Synthesis: Recent Update on Green Catalytic Approaches in Synthesis of 1, 2, 4-Thiadiazoles. *Catalysts* **2022**, *12*, 1329. [[CrossRef](#)]
56. Mourdikoudis, S.; Liz-Marzán, L.M. Oleylamine in Nanoparticle Synthesis. *Chem. Mater.* **2013**, *25*, 1465–1476. [[CrossRef](#)]
57. Bandeira, M.; Giovanela, M.; Roesch-Ely, M.; Devine, D.M.; da Silva Crespo, J. Green Synthesis of Zinc Oxide Nanoparticles: A Review of the Synthesis Methodology and Mechanism of Formation. *Sustain. Chem. Pharm.* **2020**, *15*, 100223. [[CrossRef](#)]
58. Swati, Verma, R.; Chauhan, A.; Shandilya, M.; Li, X.; Kumar, R.; Kulshrestha, S. Antimicrobial Potential of Ag-Doped ZnO Nanostructure Synthesized by the Green Method Using *Moringa oleifera* Extract. *J. Environ. Chem. Eng.* **2020**, *8*, 103730. [[CrossRef](#)]
59. Jayaseelan, C.; Rahuman, A.A.; Kirthi, A.V.; Marimuthu, S.; Santhoshkumar, T.; Bagavan, A.; Gaurav, K.; Karthik, L.; Rao, K.V.B. Novel Microbial Route to Synthesize ZnO Nanoparticles Using *Aeromonas hydrophila* and Their Activity against Pathogenic Bacteria and Fungi. *Spectrochim. Acta-Part A Mol. Biomol. Spectrosc.* **2012**, *90*, 78–84. [[CrossRef](#)] [[PubMed](#)]
60. Jain, N.; Bhargava, A.; Tarafdar, J.C.; Singh, S.K.; Panwar, J. A Biomimetic Approach towards Synthesis of Zinc Oxide Nanoparticles. *Appl. Microbiol. Biotechnol.* **2013**, *97*, 859–869. [[CrossRef](#)]
61. Rao, M.D.; Gautam, D.P. Nanoflowers Using *Chlamydomonas reinhardtii*: A Green Approach. *Environ. Prog. Sustain. Energy* **2016**, *35*, 1020–1026. [[CrossRef](#)]
62. Divya, M.; Vaseeharan, B.; Abinaya, M.; Vijayakumar, S.; Govindarajan, M.; Alharbi, N.S.; Kadaikunnan, S.; Khaled, J.M.; Benelli, G. Biopolymer Gelatin-Coated Zinc Oxide Nanoparticles Showed High Antibacterial, Antibiofilm and Anti-Angiogenic Activity. *J. Photochem. Photobiol. B Biol.* **2018**, *178*, 211–218. [[CrossRef](#)] [[PubMed](#)]
63. Zikalala, N.; Matshetshe, K.; Parani, S.; Oluwafemi, O.S. Biosynthesis Protocols for Colloidal Metal Oxide Nanoparticles. *Nano-Struct. Nano-Objects* **2018**, *16*, 288–299. [[CrossRef](#)]
64. Vijayaraghavan, K.; Ashokkumar, T. Plant-Mediated Biosynthesis of Metallic Nanoparticles: A Review of Literature, Factors Affecting Synthesis, Characterization Techniques and Applications. *J. Environ. Chem. Eng.* **2017**, *5*, 4866–4883. [[CrossRef](#)]
65. Ahmed, S.; Annu; Chaudhry, S.A.; Ikram, S. A Review on Biogenic Synthesis of ZnO Nanoparticles Using Plant Extracts and Microbes: A Prospect towards Green Chemistry. *J. Photochem. Photobiol. B Biol.* **2017**, *166*, 272–284. [[CrossRef](#)]
66. Akbar, S.; Tauseef, I.; Subhan, F.; Sultana, N.; Khan, I.; Ahmed, U.; Haleem, K.S. An Overview of the Plant-Mediated Synthesis of Zinc Oxide Nanoparticles and Their Antimicrobial Potential. *Inorg. Nano-Met. Chem.* **2020**, *50*, 257–271. [[CrossRef](#)]

67. Prasad, A.R.; Anagha, M.; Shamsheera, K.O.; Joseph, A. Bio-Fabricated ZnO Nanoparticles: Direct Sunlight-Driven Selective Photodegradation, Antibacterial Activity, and Thermoluminescence-Emission Characteristics. *New J. Chem.* **2020**, *44*, 8273–8279. [[CrossRef](#)]
68. Verma, P.R.; Khan, F.; Banerjee, S. *Salvadora persica* Root Extract-Mediated Fabrication of ZnO Nanoparticles and Characterization. *Inorg. Nano-Met. Chem.* **2020**, *51*, 427–433. [[CrossRef](#)]
69. Fagier, M.A. Plant-Mediated Biosynthesis and Photocatalysis Activities of Zinc Oxide Nanoparticles: A Prospect towards Dyes Mineralization. *J. Nanotechnol.* **2021**, *2021*. [[CrossRef](#)]
70. Elumalai, K.; Velmurugan, S.; Ravi, S.; Kathiravan, V.; Adaikala Raj, G. Bio-Approach: Plant Mediated Synthesis of ZnO Nanoparticles and Their Catalytic Reduction of Methylene Blue and Antimicrobial Activity. *Adv. Powder Technol.* **2015**, *26*, 1639–1651. [[CrossRef](#)]
71. Gebre, S.H.; Sendeku, M.G. New Frontiers in the Biosynthesis of Metal Oxide Nanoparticles and Their Environmental Applications: An Overview. *SN Appl. Sci.* **2019**, *1*, 1–28. [[CrossRef](#)]
72. Nasrollahzadeh, M.; Sajjadi, M.; Irvani, S.; Varma, R.S. Green-Synthesized Nanocatalysts and Nanomaterials for Water Treatment: Current Challenges and Future Perspectives. *J. Hazard. Mater.* **2021**, *401*, 123401. [[CrossRef](#)]
73. Sharma, A.; Nagraik, R.; Sharma, S.; Sharma, G.; Pandey, S.; Azizov, S.; Chauhan, P.K.; Kumar, D. Green Synthesis of ZnO Nanoparticles Using *Ficus palmata*: Antioxidant, Antibacterial and Antidiabetic Studies. *Results Chem.* **2022**, *4*, 100509. [[CrossRef](#)]
74. Bala, N.; Saha, S.; Chakraborty, M.; Maiti, M.; Das, S.; Basu, R.; Nandy, P. Green Synthesis of Zinc Oxide Nanoparticles Using *Hibiscus subdariffa* Leaf Extract: Effect of Temperature on Synthesis, Anti-Bacterial Activity and Anti-Diabetic Activity. *RSC Adv.* **2015**, *5*, 4993–5003. [[CrossRef](#)]
75. Senthilkumar, N.; Nandhakumar, E.; Priya, P.; Soni, D.; Vimalan, M.; Vetha Potheher, I. Synthesis of ZnO Nanoparticles Using Leaf Extract of *Tectona grandis* (L.) and Their Anti-Bacterial, Anti-Arthritic, Anti-Oxidant and in Vitro Cytotoxicity Activities. *New J. Chem.* **2017**, *41*, 10347–10356.
76. Bowles, D.; Lim, E.K.; Poppenberger, B.; Vaistij, F.E. Glycosyltransferases of Lipophilic Small Molecules. *Annu. Rev. Plant Biol.* **2006**, *57*, 567–597. [[CrossRef](#)] [[PubMed](#)]
77. Król, A.; Railean-Plugaru, V.; Pomastowski, P.; Buszewski, B. Phytochemical Investigation of *Medicago sativa* L. Extract and Its Potential as a Safe Source for the Synthesis of ZnO Nanoparticles: The Proposed Mechanism of Formation and Antimicrobial Activity. *Phytochem. Lett.* **2019**, *31*, 170–180. [[CrossRef](#)]
78. Krężel, A.; Maret, W. The Biological Inorganic Chemistry of Zinc Ions. *Arch. Biochem. Biophys.* **2016**, *611*, 3–19. [[CrossRef](#)]
79. Kumar, B.; Smita, K.; Cumbal, L.; Debut, A. Green Approach for Fabrication and Applications of Zinc Oxide Nanoparticles. *Bioinorg. Chem. Appl.* **2014**, *2014*. [[CrossRef](#)] [[PubMed](#)]
80. Singh, P.; Kim, Y.J.; Zhang, D.; Yang, D.C. Biological Synthesis of Nanoparticles from Plants and Microorganisms. *Trends Biotechnol.* **2016**, *34*, 588–599. [[CrossRef](#)]
81. De Souza, R.F.V.; Giovani, W.F. De Synthesis, Spectral and Electrochemical Properties of Al (III) and Zn (II) Complexes with Flavonoids. *Spectrochim. Acta Part A Mol. Biomol. Spectrosc.* **2005**, *61*, 1985–1990. [[CrossRef](#)]
82. Mirgane, N.A.; Shivankar, V.S.; Kotwal, S.B.; Wadhawa, G.C.; Sonawale, M.C. Waste Pericarp of *Ananas comosus* in Green Synthesis Zinc Oxide Nanoparticles and Their Application in Waste Water Treatment. *Mater. Today Proc.* **2020**, *37*, 886–889. [[CrossRef](#)]
83. Madhumitha, G.; Fowsiya, J.; Gupta, N.; Kumar, A.; Singh, M. Green Synthesis, Characterization and Antifungal and Photocatalytic Activity of *Pithecellobium dulce* Peel-Mediated ZnO Nanoparticles. *J. Phys. Chem. Solids* **2019**, *127*, 43–51. [[CrossRef](#)]
84. Mohamad Sukri, S.N.A.; Shameli, K.; Mei-Theng Wong, M.; Teow, S.Y.; Chew, J.; Ismail, N.A. Cytotoxicity and Antibacterial Activities of Plant-Mediated Synthesized Zinc Oxide (ZnO) Nanoparticles Using *Punica granatum* (Pomegranate) Fruit Peels Extract. *J. Mol. Struct.* **2019**, *1189*, 57–65. [[CrossRef](#)]
85. Golmohammadi, M.; Honarmand, M.; Ghanbari, S. A Green Approach to Synthesis of ZnO Nanoparticles Using Jujube Fruit Extract and Their Application in Photocatalytic Degradation of Organic Dyes. *Spectrochim. Acta-Part A Mol. Biomol. Spectrosc.* **2020**, *229*, 117961. [[CrossRef](#)] [[PubMed](#)]
86. Faisal, S.; Jan, H.; Shah, S.A.; Shah, S.; Khan, A.; Akbar, M.T.; Rizwan, M.; Jan, F.; Wajidullah; Akhtar, N.; et al. Green Synthesis of Zinc Oxide (ZnO) Nanoparticles Using Aqueous Fruit Extracts of *Myristica fragrans*: Their Characterizations and Biological and Environmental Applications. *ACS Omega* **2021**, *6*, 9709–9722. [[CrossRef](#)] [[PubMed](#)]
87. Soto-Robles, C.A.; Luque, P.A.; Gómez-Gutiérrez, C.M.; Nava, O.; Vilchis-Nestor, A.R.; Lugo-Medina, E.; Ranjithkumar, R.; Castro-Beltrán, A. Study on the Effect of the Concentration of *Hibiscus sabdariffa* Extract on the Green Synthesis of ZnO Nanoparticles. *Results Phys.* **2019**, *15*, 102807. [[CrossRef](#)]
88. Khara, G.; Padalia, H.; Moteriya, P.; Chanda, S. *Peltophorum pterocarpum* Flower-Mediated Synthesis, Characterization, Antimicrobial and Cytotoxic Activities of ZnO Nanoparticles. *Arab. J. Sci. Eng.* **2018**, *43*, 3393–3401. [[CrossRef](#)]
89. Diallo, A.; Ngom, B.D.; Park, E.; Maaza, M. Green Synthesis of ZnO Nanoparticles by *Aspalathus linearis*: Structural & Optical Properties. *J. Alloys Compd.* **2015**, *646*, 425–430. [[CrossRef](#)]
90. Chauhan, A.K.; Kataria, N.; Garg, V.K. Green Fabrication of ZnO Nanoparticles Using *Eucalyptus* Spp. Leaves Extract and Their Application in Wastewater Remediation. *Chemosphere* **2020**, *247*, 125803. [[CrossRef](#)]
91. Nilavukkarasi, M.; Vijayakumar, S.; Prathipkumar, S. Capparis Zeylanica Mediated Bio-Synthesized ZnO Nanoparticles as Antimicrobial, Photocatalytic and Anti-Cancer Applications. *Mater. Sci. Energy Technol.* **2020**, *3*, 335–343. [[CrossRef](#)]

92. Bala Chennaiah, M.; Kumar, K.D.; Kumar, B.S.; Tanneeru, S.R. Characterisation of Zinc Oxide Nanoparticles–Herbal Synthesised Coated with *Ocimum tenuiflorum*. *Adv. Mater. Process. Technol.* **2021**, 1–12. [[CrossRef](#)]
93. Ekennia, A.C.; Uduagwu, D.N.; Nwaji, N.N.; Oje, O.O.; Emma-Uba, C.O.; Mgbii, S.I.; Olowo, O.J.; Nwanji, O.L. Green Synthesis of Biogenic Zinc Oxide Nanoflower as Dual Agent for Photodegradation of an Organic Dye and Tyrosinase Inhibitor. *J. Inorg. Organomet. Polym. Mater.* **2021**, *31*, 886–897. [[CrossRef](#)]
94. Tabrizi Hafez Moghaddas, S.M.; Elahi, B.; Javanbakht, V. Biosynthesis of Pure Zinc Oxide Nanoparticles Using Quince Seed Mucilage for Photocatalytic Dye Degradation. *J. Alloys Compd.* **2020**, *821*, 153519. [[CrossRef](#)]
95. Prasad, A.R.; Garvasis, J.; Oruvil, S.K.; Joseph, A. Bio-Inspired Green Synthesis of Zinc Oxide Nanoparticles Using *Abelmoschus esculentus* Mucilage and Selective Degradation of Cationic Dye Pollutants. *J. Phys. Chem. Solids* **2019**, *127*, 265–274. [[CrossRef](#)]
96. Kaliraj, L.; Ahn, J.C.; Rupa, E.J.; Abid, S.; Lu, J.; Yang, D.C. Synthesis of Panos Extract Mediated ZnO Nano-Flowers as Photocatalyst for Industrial Dye Degradation by UV Illumination. *J. Photochem. Photobiol. B Biol.* **2019**, *199*, 111588. [[CrossRef](#)] [[PubMed](#)]
97. Matinise, N.; Fuku, X.G.; Kaviyarasu, K.; Mayedwa, N.; Maaza, M. ZnO Nanoparticles via Moringa Oleifera Green Synthesis: Physical Properties & Mechanism of Formation. *Appl. Surf. Sci.* **2017**, *406*, 339–347. [[CrossRef](#)]
98. Thema, F.T.; Manikandan, E.; Dhlamini, M.S.; Maaza, M. Green Synthesis of ZnO Nanoparticles via *Agathosma betulina* Natural Extract. *Mater. Lett.* **2015**, *161*, 124–127. [[CrossRef](#)]
99. Ngom, I.; Ndiayea, N.M.; Bakayoko, A.F.M.; Ngom, B.D.; Maaza, M. On the Use of *Moringa oleifera* Leaves Extract for the Biosynthesis of NiO and ZnO Nanoparticles. *MRS Adv.* **2020**, *5*, 1145–1155. [[CrossRef](#)]
100. Rajendran, N.K.; George, B.P.; Houreld, N.N.; Abrahamse, H. Synthesis of Zinc Oxide Nanoparticles Using Rubus Fairholmianus Root Extract and Their Activity against Pathogenic Bacteria. *Molecules* **2021**, *26*, 3029. [[CrossRef](#)]
101. Zafar, Z.; Yi, S.; Li, J.; Li, C.; Zhu, Y.; Zada, A.; Yao, W.; Liu, Z.; Yue, X. Recent Development in Defects Engineered Photocatalysts: An Overview of the Experimental and Theoretical Strategies. *Energy Environ. Mater.* **2022**, *5*, 68–114. [[CrossRef](#)]
102. Noman, M.T.; Amor, N.; Petru, M.; Mahmood, A.; Kejzlar, P. Photocatalytic Behaviour of Zinc Oxide Nanostructures on Surface Activation of Polymeric Fibres. *Polymers* **2021**, *13*, 1227. [[CrossRef](#)] [[PubMed](#)]
103. Shelar, S.G.; Mahajan, V.K.; Patil, S.P.; Sonawane, G.H. Effect of Doping Parameters on Photocatalytic Degradation of Methylene Blue Using Ag Doped ZnO Nanocatalyst. *SN Appl. Sci.* **2020**, *2*, 1–10. [[CrossRef](#)]
104. Srivastava, A.K.; Gupta, V.K.; Lal, B.; Roy, S.; Yadav, S.K.; Gurjar, M.S.; Bag, T.K.; Pandey, N.K.; Singh, B.P. Assessment of the Level of Knowledge and Training Needs of Potato Growing Tribal Farmers of Meghalaya. *Int. J. Agric. Environ. Biotechnol.* **2012**, *5*, 483–487.
105. Jain, D.; Shivani; Bhojiya, A.A.; Singh, H.; Daima, H.K.; Singh, M.; Mohanty, S.R.; Stephen, B.J.; Singh, A. Microbial Fabrication of Zinc Oxide Nanoparticles and Evaluation of Their Antimicrobial and Photocatalytic Properties. *Front. Chem.* **2020**, *8*, 778. [[CrossRef](#)] [[PubMed](#)]
106. Panchal, P.; Paul, D.R.; Sharma, A.; Choudhary, P.; Meena, P.; Nehra, S.P. Biogenic Mediated Ag/ZnO Nanocomposites for Photocatalytic and Antibacterial Activities towards Disinfection of Water. *J. Colloid Interface Sci.* **2020**, *563*, 370–380. [[CrossRef](#)] [[PubMed](#)]
107. Khan, M.M.; Harunsani, M.H.; Tan, A.L.; Hojamberdiev, M.; Azamay, S.; Ahmad, N. Antibacterial Activities of Zinc Oxide and Mn-Doped Zinc Oxide Synthesized Using *Melastoma malabathricum* (L.) Leaf Extract. *Bioprocess Biosyst. Eng.* **2020**, *43*, 1499–1508. [[CrossRef](#)]
108. Akbar Jan, F.; Wajidullah; Ullah, R.; Ullah, N.; Salman; Usman, M. Exploring the Environmental and Potential Therapeutic Applications of *Myrtus communis* L. Assisted Synthesized Zinc Oxide (ZnO) and Iron Doped Zinc Oxide (Fe-ZnO) Nanoparticles. *J. Saudi Chem. Soc.* **2021**, *25*, 101278. [[CrossRef](#)]
109. Okeke, I.S.; Agwu, K.K.; Ubachukwu, A.A.; Madiba, I.G.; Maaza, M.; Whyte, G.M.; Ezema, F.I. Impact of Particle Size and Surface Defects on Antibacterial and Photocatalytic Activities of Undoped and Mg-Doped ZnO Nanoparticles, Biosynthesized Using One-Step Simple Process. *Vacuum* **2021**, *187*, 110110. [[CrossRef](#)]
110. Rahman, A.; Harunsani, M.H.; Tan, A.L.; Ahmad, N.; Min, B.K.; Khan, M.M. Influence of Mg and Cu Dual-Doping on Phytogenic Synthesized ZnO for Light Induced Antibacterial and Radical Scavenging Activities. *Mater. Sci. Semicond. Process.* **2021**, *128*, 105761. [[CrossRef](#)]
111. Nguyen, T.H.A.; Le, V.T.; Doan, V.D.; Tran, A.V.; Nguyen, V.C.; Nguyen, A.T.; Vasseghian, Y. Green Synthesis of Nb-Doped ZnO Nanocomposite for Photocatalytic Degradation of Tetracycline Antibiotic under Visible Light. *Mater. Lett.* **2022**, *308*, 131129. [[CrossRef](#)]
112. Kitching, M.; Ramani, M.; Marsili, E. Fungal Biosynthesis of Gold Nanoparticles: Mechanism and Scale Up. *Microb. Biotechnol.* **2015**, *8*, 904–917. [[CrossRef](#)] [[PubMed](#)]
113. Salvadori, M.R.; Ando, R.A.; Oller Do Nascimento, C.A.; Corrêa, B. Intracellular Biosynthesis and Removal of Copper Nanoparticles by Dead Biomass of Yeast Isolated from the Wastewater of a Mine in the Brazilian Amazonia. *PLoS ONE* **2014**, *9*, e87968. [[CrossRef](#)]
114. Thakkar, K.N.; Mhatre, S.S.; Parikh, R.Y. Biological Synthesis of Metallic Nanoparticles. *Nanomed. Nanotechnol. Biol. Med.* **2010**, *6*, 257–262. [[CrossRef](#)] [[PubMed](#)]
115. Velusamy, P.; Kumar, G.V.; Jeyanthi, V.; Das, J.; Pachaiappan, R. Bio-Inspired Green Nanoparticles: Synthesis, Mechanism, and Antibacterial Application. *Toxicol. Res.* **2016**, *32*, 95–102. [[CrossRef](#)] [[PubMed](#)]

116. Tripathi, R.M.; Bhadwal, A.S.; Gupta, R.K.; Singh, P.; Shrivastav, A.; Shrivastav, B.R. ZnO Nanoflowers: Novel Biogenic Synthesis and Enhanced Photocatalytic Activity. *J. Photochem. Photobiol. B Biol.* **2014**, *141*, 288–295. [[CrossRef](#)]
117. Slavin, Y.N.; Asnis, J.; Häfeli, U.O.; Bach, H. Metal Nanoparticles: Understanding the Mechanisms behind Antibacterial Activity. *J. Nanobiotechnol.* **2017**, *15*, 1–20. [[CrossRef](#)] [[PubMed](#)]
118. Sengani, M.; Grumezescu, A.M.; Rajeswari, V.D. Recent Trends and Methodologies in Gold Nanoparticle Synthesis – A Prospective Review on Drug Delivery Aspect. *OpenNano* **2017**, *2*, 37–46. [[CrossRef](#)]
119. Mohd Yusof, H.; Mohamad, R.; Zaidan, U.H.; Abdul Rahman, N.A. Microbial Synthesis of Zinc Oxide Nanoparticles and Their Potential Application as an Antimicrobial Agent and a Feed Supplement in Animal Industry: A Review. *J. Anim. Sci. Biotechnol.* **2019**, *10*, 1–22. [[CrossRef](#)]
120. Shedbalkar, U.; Singh, R.; Wadhvani, S.; Gaidhani, S.; Chopade, B.A. Microbial Synthesis of Gold Nanoparticles: Current Status and Future Prospects. *Adv. Colloid Interface Sci.* **2014**, *209*, 40–48. [[CrossRef](#)]
121. Jeevanandam, J.; Chan, Y.S.; Danquah, M.K. Biosynthesis of Metal and Metal Oxide Nanoparticles. *ChemBioEng Rev.* **2016**, *3*, 55–67. [[CrossRef](#)]
122. Molnár, Z.; Bódai, V.; Szakacs, G.; Erdélyi, B.; Fogarassy, Z.; Sáfrán, G.; Varga, T.; Kónya, Z.; Tóth-Szeles, E.; Szucs, R.; et al. Green Synthesis of Gold Nanoparticles by Thermophilic Filamentous Fungi. *Sci. Rep.* **2018**, *8*, 1–12. [[CrossRef](#)]
123. Hulkoti, N.I.; Taranath, T.C. Biosynthesis of Nanoparticles Using Microbes-A Review. *Colloids Surf. B Biointerfaces* **2014**, *121*, 474–483. [[CrossRef](#)]
124. Dhandapani, P.; Prakash, A.A.; AlSalhi, M.S.; Maruthamuthu, S.; Devanesan, S.; Rajasekar, A. Ureolytic Bacteria Mediated Synthesis of Hairy ZnO Nanostructure as Photocatalyst for Decolorization of Dyes. *Mater. Chem. Phys.* **2020**, *243*, 122619. [[CrossRef](#)]
125. Rehman, S.; Jermy, B.R.; Akhtar, S.; Borgio, J.F.; Abdul Azeez, S.; Ravinayagam, V.; Al Jindan, R.; Alsalem, Z.H.; Buhameid, A.; Gani, A. Isolation and Characterization of a Novel Thermophile; *Bacillus haynesii*, Applied for the Green Synthesis of ZnO Nanoparticles. *Artif. Cells Nanomed. Biotechnol.* **2019**, *47*, 2072–2082. [[CrossRef](#)] [[PubMed](#)]
126. Al-Kordy, H.M.H.; Sabry, S.A.; Mabrouk, M.E.M. Statistical Optimization of Experimental Parameters for Extracellular Synthesis of Zinc Oxide Nanoparticles by a Novel *Haloalaliphilic alkalibacillus* sp. W7. *Sci. Rep.* **2021**, *11*, 1–14. [[CrossRef](#)]
127. Jayabalan, J.; Mani, G.; Krishnan, N.; Pernabas, J.; Devadoss, J.M.; Jang, H.T. Green Biogenic Synthesis of Zinc Oxide Nanoparticles Using *Pseudomonas putida* Culture and Its In Vitro Antibacterial and Anti-Biofilm Activity. *Biocatal. Agric. Biotechnol.* **2019**, *21*, 101327. [[CrossRef](#)]
128. Taran, M.; Rad, M.; Alavi, M. Biosynthesis of TiO₂ and ZnO Nanoparticles by *Halomonas Elongata* IBRC-M 10214 in Different Conditions of Medium. *BiolImpacts* **2018**, *8*, 81–89. [[CrossRef](#)] [[PubMed](#)]
129. Mohd Yusof, H.; Abdul Rahman, N.A.; Mohamad, R.; Zaidan, U.H.; Samsudin, A.A. Biosynthesis of Zinc Oxide Nanoparticles by Cell-Biomass and Supernatant of *Lactobacillus plantarum* TA4 and Its Antibacterial and Biocompatibility Properties. *Sci. Rep.* **2020**, *10*, 1–13. [[CrossRef](#)]
130. Rajivgandhi, G.; Mythili Gnanamangai, B.; Heela Prabha, T.; Poornima, S.; Maruthupandy, M.; Alharbi, N.S.; Kadaikunnan, S.; Li, W.-J. Biosynthesized Zinc Oxide Nanoparticles (ZnO NPs) Using Actinomycetes Enhance the Anti-Bacterial Efficacy against *K. pneumoniae*. *J. King Saud Univ.-Sci.* **2022**, *34*, 101731. [[CrossRef](#)]
131. Raliya, R.; Tarafdar, J.C. ZnO Nanoparticle Biosynthesis and Its Effect on Phosphorous-Mobilizing Enzyme Secretion and Gum Contents in Clusterbean (*Cyamopsis tetragonoloba* L.). *Agric. Res.* **2013**, *2*, 48–57. [[CrossRef](#)]
132. Rajan, A.; Cherian, E.; Baskar, G. Biosynthesis of Zinc Oxide Nanoparticles Using *Aspergillus fumigatus* JCF and Its Antibacterial Activity. *Int. J. Mod. Sci. Technol.* **2016**, *1*, 52–57.
133. Kalpana, V.N.; Kataru, B.A.S.; Sravani, N.; Vigneshwari, T.; Panneerselvam, A.; Devi Rajeswari, V. Biosynthesis of Zinc Oxide Nanoparticles Using Culture Filtrates of *Aspergillus niger*: Antimicrobial Textiles and Dye Degradation Studies. *OpenNano* **2018**, *3*, 48–55. [[CrossRef](#)]
134. Mohana, S.; Sumathi, S. Synthesis of Zinc Oxide Using *Agaricus Bisporus* and Its In-Vitro Biological Activities. *J. Environ. Chem. Eng.* **2020**, *8*, 104192. [[CrossRef](#)]
135. Sumanth, B.; Lakshmeesha, T.R.; Ansari, M.A.; Alzohairy, M.A.; Udayashankar, A.C.; Shobha, B.; Niranjana, S.R.; Srinivas, C.; Almatroudi, A. Mycogenic Synthesis of Extracellular Zinc Oxide Nanoparticles from *Xylaria acuta* and Its Nanoantibiotic Potential. *Int. J. Nanomed.* **2020**, *15*, 8519–8536. [[CrossRef](#)]
136. Moghaddam, A.B.; Moniri, M.; Azizi, S.; Rahim, R.A.; Ariff, A.B.; Saad, W.Z.; Namvar, F.; Navaderi, M.; Mohamad, R. Biosynthesis of ZnO Nanoparticles by a New *Pichia kudriavzevii* Yeast Strain and Evaluation of Their Antimicrobial and Antioxidant Activities. *Molecules* **2017**, *22*, 872. [[CrossRef](#)] [[PubMed](#)]
137. Kadam, V.V.; Ettiappan, J.P.; Mohan Balakrishnan, R. Mechanistic Insight into the Endophytic Fungus Mediated Synthesis of Protein Capped ZnO Nanoparticles. *Mater. Sci. Eng. B Solid-State Mater. Adv. Technol.* **2019**, *243*, 214–221. [[CrossRef](#)]
138. Motazedi, R.; Rahaiee, S.; Zare, M. Efficient Biogenesis of ZnO Nanoparticles Using Extracellular Extract of *Saccharomyces cerevisiae*: Evaluation of Photocatalytic, Cytotoxic and Other Biological Activities. *Bioorg. Chem.* **2020**, *101*, 103998. [[CrossRef](#)]
139. Mani, V.M.; Nivetha, S.; Sabarathinam, S.; Barath, S.; Das, M.P.A.; Basha, S.; Elfasakhany, A.; Pugazhendhi, A. Multifunctionalities of Mycosynthesized Zinc Oxide Nanoparticles (ZnONPs) from *Cladosporium tenuissimum* FCBGr: Antimicrobial Additives for Paints Coating, Functionalized Fabrics and Biomedical Properties. *Prog. Org. Coat.* **2022**, *163*, 106650. [[CrossRef](#)]

140. Khalafi, T.; Buazar, F.; Ghanemi, K. Phycosynthesis and Enhanced Photocatalytic Activity of Zinc Oxide Nanoparticles Toward Organosulfur Pollutants. *Sci. Rep.* **2019**, *9*, 1–10. [[CrossRef](#)]
141. El-Belely, E.F.; Farag, M.M.S.; Said, H.A.; Amin, A.S.; Azab, E.; Gobouri, A.A.; Fouda, A. Green Synthesis of Zinc Oxide Nanoparticles (ZnO-Nps) Using *Arthrospira platensis* (Class: Cyanophyceae) and Evaluation of Their Biomedical Activities. *Nanomaterials* **2021**, *11*, 95. [[CrossRef](#)] [[PubMed](#)]
142. Rajaboopathi, S.; Thambidurai, S. Enhanced Photocatalytic Activity of Ag-ZnO Nanoparticles Synthesized by Using *Padina gymnospora* Seaweed Extract. *J. Mol. Liq.* **2018**, *262*, 148–160. [[CrossRef](#)]
143. Rabie, A.M.; Abukhadra, M.R.; Rady, A.M.; Ahmed, S.A.; Labena, A.; Mohamed, H.S.H.; Betiha, M.A.; Shim, J.J. Instantaneous Photocatalytic Degradation of Malachite Green Dye under Visible Light Using Novel Green Co-ZnO/Algae Composites. *Res. Chem. Intermed.* **2020**, *46*, 1955–1973. [[CrossRef](#)]
144. Syed, A.; Ahmad, A. Extracellular Biosynthesis of Platinum Nanoparticles Using the Fungus *Fusarium oxysporum*. *Colloids Surf. B Biointerfaces* **2012**, *97*, 27–31. [[CrossRef](#)] [[PubMed](#)]
145. Zielonka, A.; Klimek-Ochab, M. Fungal Synthesis of Size-Defined Nanoparticles. *Adv. Nat. Sci. Nanosci. Nanotechnol.* **2017**, *8*, 043001. [[CrossRef](#)]
146. Azizi, S.; Ahmad, M.B.; Namvar, F.; Mohamad, R. Green Biosynthesis and Characterization of Zinc Oxide Nanoparticles Using Brown Marine Macroalga *Sargassum muticum* Aqueous Extract. *Mater. Lett.* **2014**, *116*, 275–277. [[CrossRef](#)]
147. Mohamed Isa, E.D.; Shameli, K.; Ch'ng, H.J.; Che Jusoh, N.W.; Hazan, R. Photocatalytic Degradation of Selected Pharmaceuticals Using Green Fabricated Zinc Oxide Nanoparticles. *Adv. Powder Technol.* **2021**, *32*, 2398–2409. [[CrossRef](#)]
148. El-Saied, H.A.A.; Ibrahim, A.M. Effective Fabrication and Characterization of Eco-Friendly Nano Chitosan Capped Zinc Oxide Nanoparticles for Effective Marine Fouling Inhibition. *J. Environ. Chem. Eng.* **2020**, *8*, 103949. [[CrossRef](#)]
149. Vijayakumar, T.S.; Mahboob, S.; Bupesh, G.; Vasanth, S.; Al-Ghanim, K.A.; Al-Misned, F.; Govindarajan, M. Facile Synthesis and Biophysical Characterization of Egg Albumen-Wrapped Zinc Oxide Nanoparticles: A Potential Drug Delivery Vehicles for Anticancer Therapy. *J. Drug Deliv. Sci. Technol.* **2020**, *60*, 102015. [[CrossRef](#)]
150. Qian, C.; Yin, J.; Zhao, J.; Li, X.; Wang, S.; Bai, Z.; Jiao, T. Facile Preparation and Highly Efficient Photodegradation Performances of Self-Assembled Artemia Eggshell-ZnO Nanocomposites for Wastewater Treatment. *Colloids Surf. A Physicochem. Eng. Asp.* **2021**, *610*, 125752. [[CrossRef](#)]
151. Rekha, R.; Mahboob, S.; Ramya, A.K.; Kerthekeyan, S.; Govindarajan, M.; Al-Ghanim, K.A.; Al-Misned, F.; Ahmed, Z.; Vaseeharan, B. Synthesis and Bio-Physical Characterization of Crustin Capped Zinc Oxide Nanoparticles, and Their Photocatalytic, Antibacterial, Antifungal and Antibiofilm Activity. *J. Clust. Sci.* **2021**, *32*, 843–855. [[CrossRef](#)]
152. Almhazia, A.A.; Al-Omar, M.A.; Naglah, A.M.; Bhat, M.A.; Al-Shakliah, N.S. Facile Synthesis and Characterization of ZnO Nanoparticles for Studying Their Biological Activities and Photocatalytic Degradation Properties toward Methylene Blue Dye. *Alex. Eng. J.* **2021**, *61*, 2386–2395. [[CrossRef](#)]
153. Kamaruzaman, A.; Lah, N.A.C. Formation of ZnO Nanoparticles in the Presence of Tannic Acid. *Mater. Today Proc.* **2020**, *41*, 61–64. [[CrossRef](#)]
154. Ranjithkumar, B.; Ramalingam, H.B.; Kumar, E.R.; Srinivas, C.; Magesh, G.; Rahale, C.S.; El-Metwaly, N.M.; Shekar, B.C. Natural Fuels (Honey and Cow Urine) Assisted Combustion Synthesis of Zinc Oxide Nanoparticles for Antimicrobial Activities. *Ceram. Int.* **2021**, *47*, 14475–14481. [[CrossRef](#)]
155. Motshekg, S.C.; Sinha Ray, S.; Maity, A. Synthesis and Characterization of Alginate Beads Encapsulated Zinc Oxide Nanoparticles for Bacteria Disinfection in Water. *J. Colloid Interface Sci.* **2018**, *512*, 686–692. [[CrossRef](#)] [[PubMed](#)]
156. Peychev, B.; Vasileva, P. Novel Starch-Mediated Synthesis of Au/ZnO Nanocrystals and Their Photocatalytic Properties. *Heliyon* **2021**, *7*, e07402. [[CrossRef](#)] [[PubMed](#)]
157. Wang, Y.; Wang, H.; Li, Z.; Yang, D.; Qiu, X.; Liu, Y.; Yan, M.; Li, Q. Fabrication of Litchi-like Lignin/Zinc Oxide Composites with Enhanced Antibacterial Activity and Their Application in Polyurethane Films. *J. Colloid Interface Sci.* **2021**, *594*, 316–325. [[CrossRef](#)]
158. Das, R.K.; Gogoi, N.; Babu, P.J.; Sharma, P.; Mahanta, C.; Bora, U. The Synthesis of Gold Nanoparticles Using *Amaranthus spinosus* Leaf Extract and Study of Their Optical Properties. *Adv. Mater. Phys. Chem.* **2012**, *2*, 275–281. [[CrossRef](#)]
159. Umar, H.; Kavaz, D.; Rizaner, N. Biosynthesis of Zinc Oxide Nanoparticles Using *Albizia Lebbeck* Stem Bark, and Evaluation of Its Antimicrobial, Antioxidant, and Cytotoxic Activities on Human Breast Cancer Cell Lines. *Int. J. Nanomed.* **2019**, *14*, 87–100. [[CrossRef](#)] [[PubMed](#)]
160. Barabadi, H.; Honary, S.; Ebrahimi, P.; Mohammadi, M.A.; Alizadeh, A.; Naghibi, F. Microbial Mediated Preparation, Characterization and Optimization of Gold Nanoparticles. *Braz. J. Microbiol.* **2014**, *45*, 1493–1501. [[CrossRef](#)]
161. Guan, Y.; Yu, H.Y.; Abdalkarim, S.Y.H.; Wang, C.; Tang, F.; Marek, J.; Chen, W.L.; Militky, J.; Yao, J.M. Green One-Step Synthesis of ZnO/Cellulose Nanocrystal Hybrids with Modulated Morphologies and Superfast Absorption of Cationic Dyes. *Int. J. Biol. Macromol.* **2019**, *132*, 51–62. [[CrossRef](#)]
162. Zheng, B.; Kong, T.; Jing, X.; Odoom-Wubah, T.; Li, X.; Sun, D.; Lu, F.; Zheng, Y.; Huang, J.; Li, Q. Plant-Mediated Synthesis of Platinum Nanoparticles and Its Bioreductive Mechanism. *J. Colloid Interface Sci.* **2013**, *396*, 138–145. [[CrossRef](#)]
163. Vanaja, M. Kinetic Study on Green Synthesis of Silver Nanoparticles Using *Coleus aromaticus* Leaf Extract. *Adv. Appl. Sci. Res.* **2013**, *4*, 50–55.

164. Jamdagni, P.; Khatri, P.; Rana, J.S. Green Synthesis of Zinc Oxide Nanoparticles Using Flower Extract of *Nyctanthes arbor-tristis* and Their Antifungal Activity. *J. King Saud Univ.-Sci.* **2018**, *30*, 168–175. [[CrossRef](#)]
165. Dhandapani, P.; Siddarth, A.S.; Kamalasekaran, S.; Maruthamuthu, S.; Rajagopal, G. Bio-Approach: Ureolytic Bacteria Mediated Synthesis of ZnO Nanocrystals on Cotton Fabric and Evaluation of Their Antibacterial Properties. *Carbohydr. Polym.* **2014**, *103*, 448–455. [[CrossRef](#)] [[PubMed](#)]
166. Shaziman, S.; Ismailrosdi, A.S.; Mamat, M.H.; Zoolfakar, A.S. Influence of Growth Time and Temperature on the Morphology of ZnO Nanorods via Hydrothermal. *IOP Conf. Ser. Mater. Sci. Eng.* **2015**, *99*, 1–2. [[CrossRef](#)]
167. Mohamed, A.A.; Fouda, A.; Abdel-Rahman, M.A.; Hassan, S.E.D.; El-Gamal, M.S.; Salem, S.S.; Shaheen, T.I. Fungal Strain Impacts the Shape, Bioactivity and Multifunctional Properties of Green Synthesized Zinc Oxide Nanoparticles. *Biocatal. Agric. Biotechnol.* **2019**, *19*, 101103. [[CrossRef](#)]
168. Zak, K.; Razali, R.; Majid, W.A.; Darround, M. Synthesis and Characterization of a Narrow Size Distribution of Zinc Oxide Nanoparticles. *Int. J. Nanomed.* **2011**, *6*, 1399–1403. [[CrossRef](#)]
169. Aldeen, T.S.; Ahmed Mohamed, H.E.; Maaza, M. ZnO Nanoparticles Prepared via a Green Synthesis Approach: Physical Properties, Photocatalytic and Antibacterial Activity. *J. Phys. Chem. Solids* **2022**, *160*, 110313. [[CrossRef](#)]
170. Gabriel Kaningini, A.; Azizi, S.; Sintwa, N.; Mokalan, K.; Cecilia Mohale, K.; Nixwell Mudau, F.; Maaza, M. Effect of Optimized Precursor Concentration, Temperature, and Doping on Optical Properties of ZnO Nanoparticles Synthesized via a Green Route Using Bush Tea (*Athrixia phylicoides* DC.) Leaf Extracts. *ACS Omega* **2022**, *7*, 31658–31666. [[CrossRef](#)]
171. Bharathi, D.; Ranjithkumar, R.; Chandarshekar, B.; Bhuvaneshwari, V. Preparation of Chitosan Coated Zinc Oxide Nanocomposite for Enhanced Antibacterial and Photocatalytic Activity: As a Bionanocomposite. *Int. J. Biol. Macromol.* **2019**, *129*, 989–996. [[CrossRef](#)]
172. Ayoub, I.; Kumar, V.; Abolhassani, R.; Sehgal, R.R.; Sharma, V.; Sehgal, R.R.; Swart, H.C.; Mishra, Y.K.; Chen, D.; Wang, Z.; et al. Enhanced Photocatalytic Performance for the BiPO_{4-x} Nanorod Induced by Surface Oxygen Vacancy. *J. Phys. Chem. C* **2022**, *5*, 18520–18528. [[CrossRef](#)]
173. Hafiz, M.; Iã, M.; Khusaimi, Z.; Zahidi, M.M.; Abu Bakar, S.; Siran, Y.M.; Anuar, S.; Rejab, M.; Asis, A.J.; Tahiruddin, S.; et al. Controllable Growth of Vertically Aligned Aluminum-Doped Zinc Oxide Nanorod Arrays by Sonicated Sol-Gel Immersion Method Depending on Precursor Solution Volumes. *Jpn. J. Appl. Phys.* **2011**, *50*, 06GH04. [[CrossRef](#)]
174. Chen, W.; Liu, Q.; Tian, S.; Zhao, X. Exposed Facet Dependent Stability of ZnO Micro/Nano Crystals as a Photocatalyst. *Appl. Surf. Sci.* **2019**, *470*, 807–816. [[CrossRef](#)]
175. Debroye, E.; Van Loon, J.; Yuan, H.; Janssen, K.P.F.; Lou, Z.; Kim, S.; Majima, T.; Roeffaers, M.B.J. Facet-Dependent Photoreduction on Single ZnO Crystals. *J. Phys. Chem. Lett.* **2017**, *8*, 340–346. [[CrossRef](#)] [[PubMed](#)]
176. Adhikari, S.; Sarkar, D.; Madras, G. Synthesis and Photocatalytic Performance of Quasi-Fibrous ZnO. *RSC Adv.* **2014**, *4*, 55807–55814. [[CrossRef](#)]
177. Zhao, Y.; Cui, T.; Wu, T.; Jin, C.; Qiao, R.; Qian, Y.; Tong, G. Polymorphous ZnO Nanostructures: Zn Polar Surface-Guided Size and Shape Evolution Mechanism and Enhanced Photocatalytic Activity. *ChemCatChem* **2017**, *9*, 3180–3190. [[CrossRef](#)]
178. Naderi, M. Surface Area: Brunauer–Emmett–Teller (BET). In *Progress in Filtration and Separation*; Tarleton, S., Ed.; Elsevier & Academic Press: London, UK, 2015; pp. 585–608. ISBN 9780123983077.
179. Salvadori, M.R.; Ando, R.A.; Nascimento, C.A.O.; Corrêa, B. Extra and Intracellular Synthesis of Nickel Oxide Nanoparticles Mediated by Dead Fungal Biomass. *PLoS ONE* **2015**, *10*, e0129799. [[CrossRef](#)] [[PubMed](#)]
180. Dimapilis, E.A.S.; Hsu, C.S.; Mendoza, R.M.O.; Lu, M.C. Zinc Oxide Nanoparticles for Water Disinfection. *Sustain. Environ. Res.* **2018**, *28*, 47–56. [[CrossRef](#)]
181. Gnanaprakasam, A.; Sivakumar, V.M.; Thirumarimurugan, M. Influencing Parameters in the Photocatalytic Degradation of Organic Effluent via Nanometal Oxide Catalyst: A Review. *Indian J. Mater. Sci.* **2015**, *2015*, 1–16. [[CrossRef](#)]
182. Rathnasamy, R.; Thangasamy, P.; Thangamuthu, R.; Sampath, S.; Alagan, V. Green Synthesis of ZnO Nanoparticles Using *Carica papaya* Leaf Extracts for Photocatalytic and Photovoltaic Applications. *J. Mater. Sci. Mater. Electron.* **2017**, *28*, 10374–10381. [[CrossRef](#)]
183. Ahmed, W.; Chantes, P.; Jarusutthirak, C.; Danwittayakul, S. A Comparison Study of Photocatalytic Activity of TiO₂ and ZnO on the Degradation of Real Batik Wastewater. *Int. Conf. Biol. Environ. Food Eng.* **2015**, *16*. [[CrossRef](#)]
184. Gonçalves, R.A.; Toledo, R.P.; Joshi, N.; Berengue, O.M. Green Synthesis and Applications of ZnO and TiO₂ Nanostructures. *Molecules* **2021**, *26*, 2236. [[CrossRef](#)]
185. Sin, J.C.; Lam, S.M.; Satoshi, I.; Lee, K.T.; Mohamed, A.R. Sunlight Photocatalytic Activity Enhancement and Mechanism of Novel Europium-Doped ZnO Hierarchical Micro/Nanospheres for Degradation of Phenol. *Appl. Catal. B Environ.* **2014**, *148–149*, 258–268. [[CrossRef](#)]
186. Nava, O.J.; Soto-Robles, C.A.; Gómez-Gutiérrez, C.M.; Vilchis-Nestor, A.R.; Castro-Beltrán, A.; Olivas, A.; Luque, P.A. Fruit Peel Extract Mediated Green Synthesis of Zinc Oxide Nanoparticles. *J. Mol. Struct.* **2017**, *1147*, 1–6. [[CrossRef](#)]
187. Vinayagam, R.; Selvaraj, R.; Arivalagan, P.; Varadavenkatesan, T. Synthesis, Characterization and Photocatalytic Dye Degradation Capability of *Calliandra haematocephala*-Mediated Zinc Oxide Nanoflowers. *J. Photochem. Photobiol. B Biol.* **2020**, *203*, 111760. [[CrossRef](#)] [[PubMed](#)]
188. Mirgane, N.A.; Shivankar, V.S.; Kotwal, S.B.; Wadhawa, G.C.; Sonawale, M.C. Degradation of Dyes Using Biologically Synthesized Zinc Oxide Nanoparticles. *Mater. Today Proc.* **2020**, *37*, 849–853. [[CrossRef](#)]

189. Nava, O.J.; Luque, P.A.; Gómez-Gutiérrez, C.M.; Vilchis-Nestor, A.R.; Castro-Beltrán, A.; Mota-González, M.L.; Olivás, A. Influence of *Camellia sinensis* Extract on Zinc Oxide Nanoparticle Green Synthesis. *J. Mol. Struct.* **2017**, *1134*, 121–125. [CrossRef]
190. Vidya, C.; Manjunatha, C.; Chandraprabha, M.N.; Rajshekar, M.; Antony Raj, M.A.L. Hazard Free Green Synthesis of ZnO Nano-Photo-Catalyst Using *Artocarpus heterophyllus* Leaf Extract for the Degradation of Congo Red Dye in Water Treatment Applications. *J. Environ. Chem. Eng.* **2017**, *5*, 3172–3180. [CrossRef]
191. Razanamahandry, L.C.; Sackey, J.; Furqan, C.M.; Ntwampe, S.K.O.; Fosso-Kankeu, E.; Manikandan, E.; Maaza, M. Removal of Free Cyanide by a Green Photocatalyst ZnO Nanoparticle Synthesized via *Eucalyptus globulus* Leaves. In *Photocatalysts in Advanced Oxidation Processes for Wastewater Treatment*; Elvis Fosso-Kankeu, Pandey, S., Ray, S.S., Eds.; Srinevener Publishing, Wiley: Beverley, UK, 2020; pp. 271–288. ISBN 9781119631422.
192. Patil, S.S.; Mali, M.G.; Tamboli, M.S.; Patil, D.R.; Kulkarni, M.V.; Yoon, H.; Kim, H.; Al-Deyab, S.S.; Yoon, S.S.; Kolekar, S.S.; et al. Green Approach for Hierarchical Nanostructured Ag-ZnO and Their Photocatalytic Performance under Sunlight. *Catal. Today* **2016**, *260*, 126–134. [CrossRef]
193. Noukelag, S.K.; Razanamahandry, L.C.; Ntwampe, S.K.O.; Arendse, C.J.; Maaza, M. Industrial Dye Removal Using Bio-Synthesized Ag-Doped ZnO Nanoparticles. *Environ. Nanotechnol. Monit. Manag.* **2021**, *16*, 100463. [CrossRef]
194. Karthik, K.V.; Raghu, A.V.; Reddy, K.R.; Ravishankar, R.; Sangeeta, M.; Shetti, N.P.; Reddy, C.V. Green Synthesis of Cu-Doped ZnO Nanoparticles and Its Application for the Photocatalytic Degradation of Hazardous Organic Pollutants. *Chemosphere* **2022**, *287*, 132081. [CrossRef]
195. Li, J.F.; Rupa, E.J.; Hurh, J.; Huo, Y.; Chen, L.; Han, Y.; Ahn, J.C.; Park, J.K.; Lee, H.A.; Mathiyalagan, R.; et al. *Cordyceps militaris* Fungus Mediated Zinc Oxide Nanoparticles for the Photocatalytic Degradation of Methylene Blue Dye. *Optik* **2019**, *183*, 691–697. [CrossRef]
196. Kumar, N.; Bhadwal, A.S.; Garg, M.; Sharma, R.; Singh, S.; Mizaikoff, B. Photocatalytic and Antibacterial Biomimetic ZnO Nanoparticles. *Anal. Methods* **2017**, *9*, 4776–4782. [CrossRef]
197. Deyab, M.; Elkatomy, T.; Ward, F. Qualitative and Quantitative Analysis of Phytochemical Studies on Brown Seaweed, *Dictyota dichotoma*. *Int. J. Eng. Dev. Res.* **2016**, *4*, 2321–9939.
198. Preethi, J.; Farzana, M.H.; Meenakshi, S. Photo-Reduction of Cr(VI) Using Chitosan Supported Zinc Oxide Materials. *Int. J. Biol. Macromol.* **2017**, *104*, 1783–1793. [CrossRef] [PubMed]
199. Li, X.; Zhang, L.; Wang, Z.; Wu, S.; Ma, J. Cellulose Controlled Zinc Oxide Nanoparticles with Adjustable Morphology and Their Photocatalytic Performances. *Carbohydr. Polym.* **2021**, *259*, 117752. [CrossRef] [PubMed]
200. Rashbari, Y.; Hazrati, S.; Azari, A.; Afshin, S.; Fazlzadeh, M.; Vosoughi, M. A Novel, Eco-Friendly and Green Synthesis of PPAC-ZnO and PPAC-NZVI Nanocomposite Using Pomegranate Peel: Cephalexin Adsorption Experiments, Mechanisms, Isotherms and Kinetics. *Adv. Powder Technol.* **2020**, *31*, 1612–1623. [CrossRef]
201. Yokwana, K.; Kuvarega, A.T.; Mhlanga, S.D.; Nxumalo, E.N. Mechanistic Aspects for the Removal of Congo Red Dye from Aqueous Media through Adsorption over N-Doped Graphene Oxide Nano-adsorbents Prepared from Graphite Flakes and Powders. *Phys. Chem. Earth* **2018**, *107*, 58–70. [CrossRef]
202. Nagar, N.; Devra, V. A Kinetic Study on the Degradation and Biodegradability of Silver Nanoparticles Catalyzed Methyl Orange and Textile Effluents. *Heliyon* **2019**, *5*, e01356. [CrossRef]
203. Mahdavi, S.; Jalali, M.; Afkhami, A. Removal of Heavy Metals from Aqueous Solutions Using Fe₃O₄, ZnO, and CuO Nanoparticles. *Nanotechnol. Sustain. Dev.* **2014**, *846*, 171–188. [CrossRef]
204. Kim, K.M.; Choi, M.H.; Lee, J.K.; Jeong, J.; Kim, Y.R.; Kim, M.K.; Paek, S.M.; Oh, J.M. Physicochemical Properties of Surface Charge-Modified ZnO Nanoparticles with Different Particle Sizes. *Int. J. Nanomed.* **2014**, *9*, 41–56. [CrossRef]
205. Nayak, A.; Sahoo, J.K.; Sahoo, S.K.; Sahu, D. Removal of Congo Red Dye from Aqueous Solution Using Zinc Oxide Nanoparticles Synthesised from *Ocimum sanctum* (Tulsi Leaf): A Green Approach. *Int. J. Environ. Anal. Chem.* **2020**, 1–22. [CrossRef]
206. Muthukumar, P.; Babu, P.S.; Shyamalagowri, S.; Kamaraj, M.; Manikandan, A.; Aravind, J. Nanotechnological Approaches as a Promising Way for Heavy Metal Mitigation in an Aqueous System. *J. Basic Microbiol.* **2021**, *62*, 376–394. [CrossRef] [PubMed]
207. Le, A.T.; Pung, S.Y.; Sreekantan, S.; Matsuda, A.; Huynh, D.P. Mechanisms of Removal of Heavy Metal Ions by ZnO Particles. *Heliyon* **2019**, *5*, e01440. [CrossRef] [PubMed]
208. Joshi, N.; Singh, A. Adsorptive Performances and Characterisations of Biologically Synthesised Zinc Oxide Based Nanosorbent (ZOBN). *Groundw. Sustain. Dev.* **2020**, *10*, 100325. [CrossRef]
209. Tshangana, C.; Chabalala, M.; Muleja, A.; Nxumalo, E.; Mamba, B. Shape-Dependant Photocatalytic and Antimicrobial Activity of ZnO Nanostructures When Conjugated to Graphene Quantum Dots. *J. Environ. Chem. Eng.* **2020**, *8*, 103930. [CrossRef]
210. Sun, H.; Brocato, J.; Costa, M. Oral Chromium Exposure and Toxicity. *Curr. Environ. Health Rep.* **2015**, *2*, 295–303. [CrossRef]
211. Khan, T.A.; Nazir, M.; Ali, I.; Kumar, A. Removal of Chromium(VI) from Aqueous Solution Using Guar Gum–Nano Zinc Oxide Biocomposite Adsorbent. *Arab. J. Chem.* **2017**, *10*, S2388–S2398. [CrossRef]
212. Kamaraj, M.; Srinivasan, N.R.; Assefa, G.; Adugna, A.T.; Kebede, M. Facile Development of Sunlit ZnO Nanoparticles-Activated Carbon Hybrid from Pernicious Weed as an Operative Nano-Adsorbent for Removal of Methylene Blue and Chromium from Aqueous Solution: Extended Application in Tannery Industrial Wastewater. *Environ. Technol. Innov.* **2020**, *17*, 100540. [CrossRef]
213. Wani, A.L.; Ara, A.; Usmani, J.A. Lead Toxicity: A Review. *Interdiscip. Toxicol.* **2015**, *8*, 55–64. [CrossRef]
214. Gordon, B.; Callan, P.; Vickers, C. WHO Guidelines for Drinking-Water Quality. *WHO Chron.* **2008**, *38*, 564. [CrossRef]

215. Somu, P.; Paul, S. Casein Based Biogenic-Synthesized Zinc Oxide Nanoparticles Simultaneously Decontaminate Heavy Metals, Dyes, and Pathogenic Microbes: A Rational Strategy for Wastewater Treatment. *J. Chem. Technol. Biotechnol.* **2018**, *93*, 2962–2976. [[CrossRef](#)]
216. Joshi, N.; Malik, S.; Gururani, P. Utilization of Polypyrrole/ZnO Nanocomposite in the Adsorptive Removal of Cu²⁺, Pb²⁺ and Cd²⁺ Ions from Wastewater. *Lett. Appl. NanoBioScience* **2020**, *10*, 2339–2351. [[CrossRef](#)]
217. Nel, L.; Strydom, N.A.; Bouwman, H. Preliminary Assessment of Contaminants in the Sediment and Organisms of the Swartkops Estuary, South Africa. *Mar. Pollut. Bull.* **2015**, *101*, 878–885. [[CrossRef](#)] [[PubMed](#)]
218. Debnath, P.; Mondal, N.K. Effective Removal of Congo Red Dye from Aqueous Solution Using Biosynthesized Zinc Oxide Nanoparticles. *Environ. Nanotechnol. Monit. Manag.* **2020**, *14*, 100320. [[CrossRef](#)]
219. Arab, C.; El Kurdi, R.; Patra, D. Efficient Removal of Congo Red Using Curcumin Conjugated Zinc Oxide Nanoparticles as New Adsorbent Complex. *Chemosphere* **2021**, *276*, 1–3. [[CrossRef](#)]
220. Jose, L.M.; Raj, R.S.A.; Sajan, D.; Aravind, A. Adsorption and Photocatalytic Activity of Biosynthesised ZnO Nanoparticles Using *Aloe vera* Leaf Extract. *Nano Express* **2021**, *2*, 010039. [[CrossRef](#)]
221. Mittal, H.; Morajkar, P.P.; Al Alili, A.; Alhassan, S.M. In-Situ Synthesis of ZnO Nanoparticles Using Gum Arabic Based Hydrogels as a Self-Template for Effective Malachite Green Dye Adsorption. *J. Polym. Environ.* **2020**, *28*, 1637–1653. [[CrossRef](#)]
222. Kahsay, M.H. Synthesis and Characterization of ZnO Nanoparticles Using Aqueous Extract of *Becium grandiflorum* for Antimicrobial Activity and Adsorption of Methylene Blue. *Appl. Water Sci.* **2021**, *11*, 1–12. [[CrossRef](#)]
223. Oyewo, O.A.; Adeniyi, A.; Sithole, B.B.; Onyango, M.S. Sawdust-Based Cellulose Nanocrystals Incorporated with ZnO Nanoparticles as Efficient Adsorption Media in the Removal of Methylene Blue Dye. *ACS Omega* **2020**, *5*, 18798–18807. [[CrossRef](#)]
224. Akpomie, K.G.; Conradie, J. Synthesis, Characterization, and Regeneration of an Inorganic–Organic Nanocomposite (ZnO@biomass) and Its Application in the Capture of Cationic Dye. *Sci. Rep.* **2020**, *10*, 1–12. [[CrossRef](#)]
225. Singh, J.; Vishwakarma, K.; Ramawat, N.; Rai, P.; Singh, V.K.; Mishra, R.K.; Kumar, V.; Tripathi, D.K.; Sharma, S. Nanomaterials and Microbes' Interactions: A Contemporary Overview. *3 Biotech* **2019**, *9*, 1–14. [[CrossRef](#)]
226. Soren, S.; Kumar, S.; Mishra, S.; Jena, P.K.; Verma, S.K.; Parhi, P. Evaluation of Antibacterial and Antioxidant Potential of the Zinc Oxide Nanoparticles Synthesized by Aqueous and Polyol Method. *Microb. Pathog.* **2018**, *119*, 145–151. [[CrossRef](#)] [[PubMed](#)]
227. Padmavathy, N.; Vijayaraghavan, R. Enhanced Bioactivity of ZnO Nanoparticles—An Antimicrobial Study. *Sci. Technol. Adv. Mater.* **2008**, *9*, 035004. [[CrossRef](#)] [[PubMed](#)]
228. Stoimenov, P.K.; Klinger, R.L.; Marchin, G.L.; Klabunde, K.J. Metal Oxide Nanoparticles as Bactericidal Agents. *Langmuir* **2002**, *18*, 6679–6686. [[CrossRef](#)]
229. Mahendra, C.; Murali, M.; Manasa, G.; Ponnamma, P.; Abhilash, M.R.; Lakshmeesha, T.R.; Satish, A.; Amruthesh, K.N.; Sudarshana, M.S. Antibacterial and Antimitotic Potential of Bio-Fabricated Zinc Oxide Nanoparticles of *Cochlospermum religiosum* (L.). *Microb. Pathog.* **2017**, *110*, 620–629. [[CrossRef](#)]
230. Agarwal, H.; Menon, S.; Shanmugam, V.K. Functionalization of Zinc Oxide Nanoparticles Using *Mucuna pruriens* and Its Antibacterial Activity. *Surf. Interfaces* **2020**, *19*, 100521. [[CrossRef](#)]
231. Theophil Anand, G.; Renuka, D.; Ramesh, R.; Anandaraj, L.; John Sundaram, S.; Ramalingam, G.; Magdalane, C.M.; Bashir, A.K.H.; Maaza, M.; Kaviyarasu, K. Green Synthesis of ZnO Nanoparticle Using *Prunus dulcis* (Almond Gum) for Antimicrobial and Supercapacitor Applications. *Surf. Interfaces* **2019**, *17*, 100376. [[CrossRef](#)]
232. Kokabi, M.; Yousefzadi, M.; Nejad Ebrahimi, S.; Zarei, M. Green Synthesis of Zinc Oxide Nanoparticles Using Seaweed Aqueous Extract and Evaluation of Antibacterial and Ecotoxicological Activity. *J. Persian Gulf (Mar. Sci.)* **2017**, *8*, 61–72. [[CrossRef](#)]
233. Jamil, Z.; Naqvi, S.T.Q.; Rasul, S.; Hussain, S.B.; Fatima, N.; Qadir, M.I.; Muhammad, S.A. Antibacterial Activity and Characterization of Zinc Oxide Nanoparticles Synthesized by Microalgae. *Pak. J. Pharm. Sci.* **2020**, *33*, 2497–2504. [[CrossRef](#)]
234. Subramanian, H.; Krishnan, M.; Mahalingam, A. Photocatalytic Dye Degradation and Photoexcited Anti-Microbial Activities of Green Zinc Oxide Nanoparticles Synthesized via *Sargassum muticum* Extracts. *RSC Adv.* **2022**, *12*, 985–997. [[CrossRef](#)]
235. Gharpure, S.; Yadwade, R.; Ankamwar, B. Non-Antimicrobial and Non-Anticancer Properties of ZnO Nanoparticles Biosynthesized Using Different Plant Parts of *Bixa orellana*. *ACS Omega* **2022**, *7*, 1914–1933. [[CrossRef](#)]
236. Mocanu, A.; Isopencu, G.; Busuioc, C.; Popa, O.M.; Dietrich, P.; Socaciu-Siebert, L. Bacterial Cellulose Films with ZnO Nanoparticles and Propolis Extracts: Synergistic Antimicrobial Effect. *Sci. Rep.* **2019**, *9*, 1–10. [[CrossRef](#)]